Mechanosensing for Directional Migration in Fast-Crawling Cells

高速アメーバ運動する細胞が移動方向を決めるメカノセンシング

December 2019

Chika OKIMURA

沖村　千夏

Mechanosensing for Directional Migration in Fast-Crawling Cells

高速アメーバ運動する細胞が移動方向を決めるメカノセンシング

December 2019

Waseda University

Graduate School of Advanced Science and Engineering

Chika OKIMURA

沖村　千夏

Contents

Chapter 1

General Introduction

The life of an individual multicellular organism begins when an egg is fertilized by a sperm. The single cell in the fertilized egg then begins to divide and differentiate. During this process of development and growth to the adult form of the organism, the differentiated cells move to the appropriate sites to form new tissues and organs. Even in adult organisms, various cell types including neutrophils during immune system activation, epithelial cells during wound healing, and cancer cells during metastasis continuously move around (Stroka and Konstantopoulos, 2014; Weninger et al., 2014). Cell movement plays an essential role in various biological phenomena throughout the lifetime of organisms (Lauffenburger and Horwitz, 1996; Raftopoulou and Hall, 2004; Ridley et al., 2003).

One of the modes of cell movement is "crawling," in which cells adhere to substrates and migrate by the frontal expansion and the rear retraction. Crawling cells generally sense the concentration gradient of chemoattractants and migrate toward the center of them. For instance, neutrophils migrate towards bacteria-derived N-formyl-methionyl-leucyl-phenylalanine (fMLP) when pathogens invade the body (Kamakura et al., 2013; Marshall and Lichtman, 1984; Wang et al., 2014; Wu et al., 2015), and *Dictyostelium* cells migrate toward cAMP when they form multicellular structures (Nichols et al., 2015; Okimura and Iwadate, 2017; Sowers, 1984). However, even when crawling cells cannot sense the gradient of the chemoattractants in a medium in which a chemoattractant is absent or uniformly present, they can migrate, although their direction is random. In media containing a uniform concentration of fMLP, neutrophil-like HL-60 cells localize actin filaments and myosin IIA at the opposite portions in the cell (Shin et al., 2010; Xu et al., 2003). In the case of *Dictyostelium* cells, it is generally considered that the localization of phosphatidylinositol 3,4,5-trisphosphate (PIP3) to the front determines the polarity for cell migration. The localization of PIP3 takes place not only in the presence of extracellular cAMP (Kölsch et al., 2008; Van Haastert and Devreotes, 2004), but also in its absence (Arai et al., 2010; Nishikawa et al., 2014; Sasaki et al., 2007; Shibata et al., 2013). The frontal localization of PIP3 has been attributed to anterior localization of phosphoinositide 3-kinase (PI3K), and posterior localization of phosphatase and tensin homolog deleted from chromosome 10 (PTEN) (Comer and Parent, 2002; Iijima and Devreotes, 2002; Matsuoka et al., 2013; Sasaki et al., 2007). Mutually exclusive localization of PI3K and PTEN takes place even in the floating cells without adhesion to the substrate. Interestingly, even the cells that lack both PI3K and PTEN can migrate without localization of PIP3, albeit at slower velocities (Hoeller and Kay, 2007).

This fact suggests that crawling cells may have primitive mechanisms that generate polarity for migration, with chemotaxis being a highly sophisticated version. In general, crawling cells adhere to their substrate via focal adhesions. It therefore seems that, under physiological conditions, the cells receive mechanical stimuli from the substrates. It is already known that rigidity of the substrate plays an

important role during cell differentiation. Mesenchymal stem cells differentiate into osteogenic-like cells on a rigid substrate, into neurons on a soft gel or into myogenic cells on an intermediately rigid surface (Deng et al., 2006; Engler et al., 2006; Hofstetter et al., 2002; Kondo et al., 2005; Pittenger et al., 1999). Not only stem cells but also other crawling cells may sense the rigidity of the substrate and use it as an exogenous fundamental signal to generate polarity for migration without the need for a concentration gradient of chemoattractants.

Although it has not been strictly determined, many investigators accept that migrating cells can be roughly classified into slow-crawling cell types and fast-crawling cell types according to their migration velocities (Entschladen and Zänker, 2010; Jurado et al., 2005; Morin et al., 2014; Vargas et al., 2017; Wang and Discher, 2007). Characteristics of them are summarized in Table 1.

The durotaxis of fibroblasts, which are slow-crawling cells, is based on their ability to acquire dynamic information from the substrate (Lo et al., 2000). It has been demonstrated, in the crawling fibroblasts, that at the boundary between rigid area and soft area of a substrate, cells can move only from the soft to the rigid part and cannot in the opposite direction (Kawano and Kidoaki, 2011; Lo et al., 2000; Ueki and Kidoaki, 2015). Durotaxis is seen in other slow-crawling cells, such as mesenchymal stem cells (Raab et al., 2012; Tse and Engler, 2011; Vincent et al., 2013), human adipose-derived stem cells (Raab et al., 2012), pancreatic stellate cells (Lachowski et al., 2017), microglial cells (Hadden et al., 2017), and vascular smooth muscle cells (Bollmann et al., 2015; Hadden et al., 2017). *Dictyostelium* cells (Li et al., 2008) and HL-60 cells are, on the other hand, fast-crawling cell types that are widely used in research into chemotaxis (Chen et al., 2012; Li et al., 2008; Wong et al., 2003).

Since the immune response of leucocytes, a typical fast-crawling cell type, functions throughout the human lifespan, it is evident that both slow-crawling cells and fast-crawling types play important roles in the human body. Thus, we believe that in order to understand the whole picture of cell migration, it is essential to understand the mechanosensing response not only in slow-crawling cell types but also in fast-crawling ones. However, to our knowledge, rigidity sensing like durotaxis has not been hitherto detected in these fast-crawling cell types. Thus, we decided to elucidate the mechanosensing mechanism of fast-crawling cell types. A technology that enables artificial control of the migration of fast-crawling cell types based on their mechanosensing response would contribute to future medical care as a non-invasive, drug-independent method to control their migration. Consequently, in this study, we found that fast-crawling cell types generate their migration polarity based on mechanical interaction with the substrate to which they are adhering. Furthermore, we have clarified a part of this polarity generation mechanism.

In Chapter 2, we describe a novel mode of rigidity sensing seen in fast-crawling cell types such as *Dictyostelium* cells and HL-60 cells. These cell types migrate in the "soft" direction on an anisotropic substrate whose rigidity along the x-axis is larger than that along the y-axis.

Cells receive mechanical stimuli chiefly from the substrate under normal physiological conditions, (Giannone and Sheetz, 2006; Vogel and Sheetz, 2006). To model this situation, one of the most suitable techniques for artificially applying mechanical stimuli is cyclic stretching of a substrate to which cells

are adhered (Crosby et al., 2011; Desai et al., 2010; Iwadate and Yumura, 2009a; Naruse et al., 1998a; Naruse et al., 1998c). Stress fibers are a characteristic cytoskeleton in slow-crawling cell types. It is known that intracellular stress fibers in slow-crawling cell types rearrange themselves to the direction perpendicular to the direction of stretch in response to cyclic substrate stretching, then the shape of the cells extends in the same direction (Birukov et al., 2003; Kaunas et al., 2005; Lee et al., 2010; Morioka et al., 2011; Sato et al., 2005; Tondon et al., 2012; Zhao et al., 2011). In contrast, fast-crawling cell types have no stress fibers (Bretschneider et al., 2004; Iwadate and Yumura, 2008b). The migration properties of fast-crawling cell types under cyclic substrate stretching are described in the following three chapters. In Chapters 3 and 4, we describe how *Dictyostelium* cells and HL-60 cells migrate perpendicular to the direction of stretch. It seems that they do not advance faster in the direction they want to go, but advance in a way that avoids directions in which they do not want to travel.

In Chapter 5, we characterized the migration of fish epidermal keratocytes in response to cyclic substrate stretching (Bretschneider et al., 2004). Keratocytes show fast-crawling cell type behavior similar to that of HL-60 cells and *Dictyostelium* cells. However, they have stress fibers, which are typical in slow-crawling cell types, in their cell body. Keratocytes are unique cells that combine the features of both fast- and slow-crawling cell types. In response to cyclic substrate stretching, intact keratocytes migrate parallel to the direction of stretching, unlike fast-crawling cell types, and oriented their stress fibers perpendicular to the direction of stretch, like the slow-crawling cell types. However, stress fiber-less keratocytes treated with blebbistatin (Okeyo et al., 2009) advance perpendicular to the direction of stretch like seen in fast-crawling cell types.

Stress fibers should play a unique role in their preference of directional migration. The leading edge of slow-crawling cell is expanded by polymerization of actin (Okeyo et al., 2009; Svitkina et al., 1997), and the rear-retraction is induced by the stress fiber-contraction (Kolega, 2003). To retract the rear efficiently, ventral stress fibers need to be arranged parallel to the migration-direction in the cell body (Burridge and Guilluy, 2016). Surprisingly, the stress fibers in the cell body of a keratocyte are aligned almost perpendicularly to the direction of migration. It would initially appear that stress fibers configured in this way would be unable to retract the cell-rear. In Chapter 6, we describe how the stress fibers in keratocytes, which are not directly involved in retraction of the rear, play a unique role in their crawling migration.

In this study, we found that the fast-crawling cell types sense the rigidity of their substrates and migrate in the soft direction. However, we were unable to fully elucidate the underlying molecular mechanism. Thus, in Chapter 7, we describe our hypothesis of the mechanism for future experimental examination.

Table 1. Characteristics of crawling cells.

Cell types	Slow		Fast		
	Fibroblasts	Endothelial cells	*Dictyostelium discoideum*	Neutrophils or HL-60 cells	Keratocytes
Size (μm)	~100 [1)],	~100 [2)]	~10 [3)]	~10 [3)]	~10 (longitudinal) ~50 (lateral) [3)]
Velocity (μm/min)	0.827 ± 0.175 [1)]	~0.3 [2)]	7.1 ± 0.17 [4)]	9.95 ± 3.37 [5)]	10.1 ± 0.64 [6)]
Adhesion strength [Shear stress (Pa)]	73 ± 3 [7)]	-	<1 [8)]	-	-
Stress fiber	Yes [9)]	Yes [10)]	No*	No*	Yes [11)]
Peak traction force (kPa)	~10 [12)]	~10 [13)]	~0.66 [14)]	0.638 ± 0.102 [15)]	0.66 ± 0.29 [6)]

The numbers on the right shoulder of each value refer to the following papers; 1) Wang et al., 2001, 2) Matsusaka and Wakabayashi, 2005, 3) Tsugiyama et al., 2013, 4) Iwadate et al., 2013, 5) Chen et al., 2012, 6) Nakashima et al., 2015, 7) Engler et al., 2006, 8) Tarantola et al., 2014, 9) Hotulainen and Lappalainen, 2006, 10) Kaunas et al., 2005, 11) Svitkina et al., 1997, 12) Munevar et al., 2001, 13) Reinhart-King et al., 2003, 14) Iwadate and Yumura, 2008, 15) Shin et al., 2010. *To our knowledge, no paper has indicated the existence of stress fibers.

Chapter 2

Rigidity Sensing for Directional Migration in Fast-Crawling Cell Types

2-1 Abstract

Living cells sense the mechanical properties of the surrounding environment and react accordingly. Crawling cells often detect the rigidity of their substrate and modify the migration directions. They can be classified into two categories: slow-crawling and fast-crawling cell types. On a substrate with a rigidity gradient, slow-crawling cell types, such as fibroblasts, mesenchymal stem cells and smooth muscle cells, move toward rigid areas. However, whether fast-crawling cell types, whose size is ~10 μm and migration velocity is ~10 μm/min, show rigidity sensing or not has hitherto not been recorded. In the experiments of this chapter, we used not only isotropic substrates with different rigidities but also anisotropic substrates that are rigid along the *x*-axis but soft along the *y*-axis in order to show rigidity sensing by fast-crawling cell types such as *Dictyostelium* cells and neutrophil-like differentiated HL-60 cells. In the experiments using anisotropic substrates, *Dictyostelium* cells and HL-60 cells moved in the "soft" direction. On the other hand, myosin II-null *Dictyostelium* cells moved in the "soft" or "rigid" direction at the same frequency. Further detailed experiments were performed with *Dictyostelium* cells using isotropic substrate. The more rigid the substrate, the larger traction forces *Dictyostelium* cells exerted on the substrate. These results indicate that rigidity sensing of fast-crawling cell types is different from that of slow types and is mediated by a myosin II-related process.

2-2 Introduction

It has been demonstrated that, at the boundary between rigid and soft areas of a substrate, fibroblasts move only from the soft part to the rigid part and never in the opposite direction (Kawano and Kidoaki, 2011; Lo et al., 2000; Ueki and Kidoaki, 2015). This characteristic of cell migration was named durotaxis (Lo et al., 2000). To date durotaxis has been found in various cell types. For example, on a substrate of graded rigidity, smooth muscle cells (Isenberg et al., 2009; Wong et al., 2003), mesenchymal stem cells (Raab et al., 2012; Tse and Engler, 2011; Vincent et al., 2013), human adipose-derived stem cells (Hadden et al., 2017), pancreatic stellate cells (Lachowski et al., 2017), and microglial cells (Bollmann et al., 2015) sense the rigidity gradient and migrate toward the more rigid areas.

Crawling cells can be classified into two different categories depending on their migration velocities. All of the above-mentioned cells that move toward rigid areas are classified as slow-crawling cell types. Their migration velocities (~1 μm/min or slower) (Isenberg et al., 2009; Vincent et al., 2013; Wang et al., 2001a) are much slower than those of fast-crawling cell types, such as neutrophils and *Dictyostelium* cells (~10 μm/min) (Chen et al., 2012; Iwadate et al., 2013; Maeda et al., 2008; Okimura et al., 2016; Tanimoto and Sano, 2014). To our knowledge, directional migration of these fast-crawling cell types depending on the rigidity of their substrate has not been reported.

The size of neutrophils and *Dictyostelium* cells (~10 μm) (Iwadate and Yumura, 2008a; Shin et al., 2010) are typically smaller than fibroblasts (maximum ~100 μm) (Wang et al., 2001a). This makes it very difficult to prepare a substrate with a clear boundary of rigidity for such small cells. This may be the reason why the preferential migration of fast-crawling cell types at the boundary between the rigid area and soft area of a substrate has not been reported. Similarly, preferential migration of fast-crawling cells on a substrate with a rigidity gradient has not been reported in any investigation. This is probably because difference in rigidity of the substrate between the front and the rear of single cells may be too small for the cells to sense it due to their small size.

Liu et al. developed an unique anisotropic substrate, rigid along the *x*-axis and soft along the *y*-axis, by stretching an elastic substrate, made from polydimethylsiloxane (PDMS), in the *x*-direction (Liu et al., 2014). Using this substrate, they showed that mesenchymal stem cells, one of the slow-crawling cell types, elongated parallel to the *x*-direction. This type of anisotropic substrate may be useful to investigate the preferential migration of fast-crawling cell types.

In this chapter, we first observed the crawling migration of *Dictyostelium* cells on isotropic substrates with different rigidities. The more rigid the substrate, the larger the traction force they exerted. Next, we made new anisotropic substrates optimized for fast-crawling cell types such as *Dictyostelium* and HL-60 cells. Then, we observed the crawling migration of *Dictyostelium* and HL-60 cells on those substrates. Both cell types moved parallel to the “soft” direction. This shows that rigidity sensing of fast-crawling cell types is different from durotaxis. Myosin II-knock-out *Dictyostelium* cells moved with the same frequency in the soft and the rigid directions, indicating that the rigidity sensing of fast-crawling cell types is myosin II dependent.

2-3 Materials and Methods

***Dictyostelium* cell lines**

Dictyostelium discoideum cell lines were developed in Bonner's standard saline (BSS, 10 mM NaCl, 10 mM KCl, 3 mM $CaCl_2$) until they became aggregation-competent as described previously (Iwadate and Yumura, 2008a). The *Dictyostelium* cell lines used were wild type AX2 cells (an axenic derivative of the wild-type NC4 strain); myosin II heavy chain-knockout *mhcA*$^-$ cells; and *mhcA*$^-$ cells restoring GFP-myosin II, GFP-3×ALA myosin II (Egelhoff et al., 1993), GFP-3×ASP myosin II (Egelhoff et al., 1993), or GFP-E476K myosin II (Ruppel and Spudich, 1996; Yumura and Uyeda, 1997). Formation of myosin II-bipolar thick-filaments in *Dictyostelium* cells is regulated by the phosphorylation of three threonine residues (Egelhoff et al., 1993). In 3×ALA, the three threonine phosphorylation sites are replaced with alanine, so that the protein retains the unphosphorylated state and constitutively forms bipolar thick filaments. In 3×ASP, the three threonine phosphorylation sites are replaced with aspartate residues. Thus, the protein retains the phosphorylated state and cannot form thick filaments. The E476K mutant of myosin II cannot hydrolyze ATP (Ruppel and Spudich, 1996; Yumura and Uyeda, 1997). The monomers and the filaments of E476K myosin II are in equilibrium as in the wild type myosin II.

The HL-60 cell line

Leukemia cell line HL-60 was obtained from Riken Cell Bank (Cell No. RCB0041, Tsukuba, Japan) and cultivated in RPMI 1640 medium (189-02145; Wako, Osaka, Japan) supplemented with 10% FBS (Nichirei, Tokyo, Japan), 100 U/ml streptomycin, 100 U/ml penicillin G and 0.25 mg/ml amphotericin B (09366-44, Nacalai Tesque, Kyoto, Japan). Differentiation into neutrophil-like cells was induced by transfer into culture medium containing 1.3% DMSO. After 3 days in 5% CO_2 at 37 ˚C, cells showed neutrophil-like crawling migration.

Traction force microscopy

Elastic substrates were prepared as follows. Two-component PDMS CY52-276A and B (Dow Corning Toray, Tokyo, Japan) were mixed at ratios of 10:7, 10:8, and 10:9 in weight to make substrates of different Young's moduli. The mixture was spread on a 22 x 22 mm cover slip (No. 0, Matsunami, Osaka, Japan). The thickness of the spread was about 100 μm. The mixture on the cover slip was solidified by keeping at room temperature (~23 ºC) for 2 days. Then, 3-aminopropyl triethoxysilane was attached to the surface of the solidified substrate by vapor deposition in order to attach the 100 nm carboxylate-modified microspheres (F-8800, Life Technologies, Carlsbad, CA, USA) to the surface.

Young's moduli of the elastic substrates were measured by the method of Lo et al. (Lo et al., 2000). A small steel ball (0.5 mm diameter, 7.8 kg/m^3) was placed on the substrate. The indentation-depth of the sheet due to the weight of the ball was measured by observing the fluorescence of the microsphere. Young's modulus was calculated from the indentation-depth as $3(1–p^2)w/4d^{3/2}r^{1/2}$, where w is the weight of the ball, d is the indentation-depth, r is the radius of the ball, and p is the Poisson ratio which was assumed to be 0.5 (Dembo et al., 1996). Calculated Young's modulus of each substrate with different

mixture ratio of CY52-276A and B were shown in Figure 2-1A. They were estimated as 101, 281 and 463 Pa (Figures 2-2A – 2-2F) for the mixture ratio of 10:7, 10:8, and 10:9, respectively.

Preparation of anisotropic and isotropic substrates

Flexible substrates with elastic anisotropy were constructed from two kinds of PDMS (CY52-276A and B, and Sylgard 184, Dow Corning Toray). The rigid PDMS, Sylgard 184, with a Young's modulus of 2.2 ± 0.1 MPa (Mark, 1999), was used as a base for the soft PDMS, CY52-276A and B. A 300-mg of Sylgard 184 was poured into a mold (40 mm in length × 22 mm in width × 1 mm in depth, Figure 2-1C and G) and allowed to solidify at room temperature (23 ˚C) for two days. Then, a 300-mg of 1:1 mixture of CY52-276A and B was poured on the solidified Sylgard 184 (Figure 2-1D and H). After an additional two days to solidify at room temperature, the two-layered sheet was carefully peeled off from the mold. Both short, 22 mm, sides were held by a stretching device (Figure 2-1E and I), and the sheet was stretched to double its initial length (Figure 2-1F and J). In this situation, shortening of the sheet perpendicular to the axis of stretch (Poisson's effect) took place (white arrow in H). This stretched sheet and the other non-stretched sheet were used as the "anisotropic substrate" and isotropic "control substrate", respectively. When we dispersed HL-60 cells on the substrates, the surfaces of both substrates were coated with fibronectin (354008, BD Japan, Tokyo, Japan).

Young's moduli of the anisotropic substrates cannot be defined because the elasticity of them is different dependent on the direction. Thus, to estimate the apparent Young's moduli of the control and the anisotropic substrates, the indentations of the same steel ball placed on the substrates were measured in the same way as for the elastic substrate for traction microscopy. Apparent Young's moduli of the control and the anisotropic substrates were estimated as 267 and 542 Pa, respectively (Figure 2-1A).

Evaluation of the elasticities in the *x*- and the y-directions of the anisotropic substrate

The difference of the elasticities in the *x*- and the y-directions of the anisotropic substrate was evaluated by the following two measurements. First, a steel ball (0.3 mm diameter, 0.52 mg) was placed at the center of the sheet's surface (Figure 2-3A). A fine magnetic rod with a sharpened tip was positioned so that the direction of the magnetic field at the position where the steel ball was placed was horizontal to the surface of the substrate. The distance between the tip of the rod and the edge of the ball of the original position was adjusted to 265 μm (Figure 2-3B). The ball was pulled horizontally to the surface of substrate in parallel to the direction of stretch of the sheet (*x* in Figure 2-3A) by the magnetic force and stopped where the magnetic force and elastic force of the sheet were balanced. The displacement of the ball was measured (*L* in Figure 2-3B). The same measurement was then performed using an identical ball perpendicular to the direction of stretch of the sheet (*y* in Figure 2-3A). In all the measurements, after removal of the magnetic rod, the ball returned to its original position.

Next, a flexible glass micro needle (Figure 2-3E) was made from a glass capillary (Microcaps 30, Drummond, Broomall, Pa, USA). Hooke's elastic constant of the needle (Figure 2-3G and H) was estimated from the deflection by applying weight to the tip (Figure 2-3F). The anisotropic substrate was

pulled in parallel (x in Figure 2-3A) and perpendicular (y in Figure 2-3A) to the stretched direction with the needle whose tip adhered to the surface of the substrate. Apparent spring constants of the anisotropic substrate in x- and y-directions were calculated from the displacement of the tip.

The flatness of the sheet-surface was confirmed by electron microscopy. The surface of the anisotropic sheet was sputter-coated with platinum/palladium and then observed using a scanning electron microscope (JSM-7600F, JEOL, Tokyo, Japan).

Statistical analysis of cell migration

On the stage of a phase-contrast inverted microscope (TS100, Nikon, Tokyo, Japan) with a 20× objective lens (LWD ADL 20xF; Nikon), migrations of crawling cells were observed and the images were recorded at 30-s intervals for 30 min at room temperature (23 ˚C). The line parallel to the rigid direction of the anisotropic substrate and the other straight line from the starting and ending points of the migrating cell were respectively drawn. The angle (θ) between the two lines were measured (inset in Figure 2-4A). Next, $|\sin\theta|$ was calculated to quantitate and compare directional preference of migration. In the case when all cells move parallel to the rigid direction (0 or 180˚), averaged $|\sin\theta|$ should be 0. In contrast, when cells move perpendicularly (90 or 270˚), $|\sin\theta|$ should be 1. When cells move with the same probability in all directions, the value should be 0.64 (= $2/\pi$). The interior angle of each column in histograms of Figures 2-4, 2-5, 2-7 and 2-8 was 66.0˚.

Velocities of crawling migration in the rigid and soft directions, and the probabilities of the directional change from rigid to soft and vice versa, were estimated as follows. The migration vector from the initial location of a cell ($t = T$) to that in the next time frame ($t = T + 30$ s) was recorded (thick arrow in Figure 2-6A). Then, the angle (θ) between the migration vector and the horizontal x-axis (x in Figure 2-6A) was calculated. In the case when θ was between 315 and 45˚ or between 135 and 225˚ (gray in Figure 2-6A), the migration-direction at $t = T$ was defined as the “rigid” direction. Otherwise, the migration-direction was labeled as the “soft” one.

The probability of a directional change of crawling migration from “rigid” to “soft” was calculated by dividing the number of label changes from “rigid” to “soft” by the total number of vectors throughout the 30-min migration period. Each transition to the same direction was regarded as a discrete event. In the case when cells stop their migration, the vector was regarded as zero vector and it was not included in the total number of vectors. The probability of switching from “soft” to “rigid” was also calculated as the same manner.

From the images during migration period of 30 min, images of the cell crawling migration only in the rigid directions were picked-up. Then, the average velocity of the cell crawling migration in the rigid direction was calculated. The average velocity in the soft direction was calculated in the same manner.

2-4 Results

Traction forces exerted by *Dictyostelium* cells depending on the substrate rigidity

The relationship between the traction forces exerted by *Dictyostelium* cells and the rigidity of the substrate on which the cells migrated was first examined (Figure 2-2). Traction forces exerted by wild-type *Dictyostelium* cells on each substrate with different elasticities are shown (Figures 2-2A – C). "Maximum" and "mean" forces on the different Young's moduli were compared (Figures 2-2G and H). The "mean" force was calculated by averaging the forces over the projected single cell area for one-minute recording time. The "maximum" force was determined as maximum value in the projected cell area for one minute. The more rigid substrate, the larger traction forces wild-type cells exerted. In contrast, the cells did not change migration velocity depending on the Young's moduli of the substrates (Figures 2-2K).

Next, we measured the traction forces exerted by *mhcA*$^{-}$ *Dictyostelium* cells expressing GFP-E476K myosin II, which cannot hydrolyze ATP, and actomyosin consisting of E476K myosin II cannot contract. This strain is referred to as E476K cells in the following. The more rigid substrate, the larger traction forces E476K cells exerted just like wild-type cells (Figures 2-2D – F, 2-2I and J), indicating that contraction of actomyosin is not essential for this rigidity sensing. Moreover, the cells did not change migration velocity depending on the Young's moduli of the substrate. This situation is also the same as the case of wild-type cells. However, E476K cells migrated much slower than wild-type cells. It is unclear whether the slow speed is due to the GFP fusion or to the mutation (Figure 2-2L).

Substrate with anisotropic elasticity

To test whether the fast-crawling cell types sense the rigidity of the substrate in order to decide their subsequent migration-direction, a new anisotropic substrate optimized for fast-crawling cell types was prepared by stretching the elastic sheet twice the original length (Figure 2-3) with reference to the method of Liu et al. (Liu et al., 2014).

The elasticities of the sheet in the *x*-direction and *y*-direction (Figure 2-3A) were estimated by pulling a steel ball, which adhered to the surface of the sheet, using a thin magnetic rod ("Magnet" in Figure 2-3A and B). The displacement of the steel ball on the stretched PDMS sheet in the *x*-direction was significantly smaller than that in the *y*-direction (Figure 2-3C), whereas there was no significant difference before stretching (Figure 2-3D).

Next, the elasticities of the sheet in both directions (Figure 2-3A) were estimated using a different method, by pulling the sheet with a flexible glass needle (Figure 2-3E – H). Hooke's elastic constant for deflection of the needle was defined as 271 nN/μm beforehand (Figure 2-1B). From the deflection of the needle, pulling force was calculated (Figure 2-3C and D). The values obtained by dividing the pulling force by the displacement of the tip of the needle (*L* in Figure 2-3F) were regarded as apparent spring constants of the sheet in the pulling direction. The values of the stretched sheet in the *y*-direction was significantly smaller than that in the *x*-direction (Figure 2-3G), whereas there was no significant difference before stretching (Figure 2-3H). From the above two experiments, we concluded that the

stretched PDMS sheet can be regarded as an anisotropic substrate whose rigidity in the stretched *x*-direction is significantly larger than the *y*-direction.

We then ascertained the flatness of the surface of the stretched PDMS sheet by the observation with scanning electron microscopy (Figure 2-3I and J). A part of a dust particle on the surface of the sheet is included in the left side of the white square in Figure 2-3I. The whole area of Figure 2-3J is identical to the area in the white square in Figure 2-3J. As shown in the Figure 2-3J, there are no wrinkles and irregularities on the surface of the sheet. This indicates that there is no geometric anisotropy in our new anisotropic substrate.

Hereinafter, the stretched and un-stretched PDMS sheets are called as an anisotropic and an isotropic control substrate, respectively. In the un-stretched "control" substrate, the directions identical to the "rigid" and the "soft" ones in the stretched "anisotropic" sheet are called the "horizontal" and the "perpendicular" directions, respectively.

Migration of fast-crawling cell types in the "soft" directions

We observed the crawling migration of wild-type *Dictyostelium* cells on the anisotropic and the isotropic substrates. From the trajectories (Figure 2-4A) and frequencies of migration directions (Figure 2-4B), the cells tended to migrate in the "soft" direction (90 and 270˚ in Figure 2-4B). In contrast, they migrated equally frequently in the horizontal and the perpendicular directions on the control substrate (Figure 2-4C and D). The average $|\sin\theta|$ value calculated from the data of the cell migration on the anisotropic substrate (Figure 2-4A) was used as the index of polarized migration (left column in Figure 2-4E), was significantly higher than that from the data of the cell migration on the control substrate (Figure 2-4C) and higher than 0.64, the value when cells migrate equally frequently in all directions (right column in Figure 2-4E). These results indicate that *Dictyostelium* cells decide their migration direction by sensing the rigidity of the substrate, and tend to move in the "soft" direction.

Next, in order to test whether migration in the soft direction is typical only in *Dictyostelium* cells or if it is common in other fast-crawling cell types, we observed the migration of HL-60 cells on the anisotropic and the control substrates. From the trajectories of cell migrations on the anisotropic substrate (Figure 2-5A) and frequencies of migration directions on it (Figure 2-5B), HL-60 cells also tended to migrate in the "soft" direction (90 and 270˚ in Figure 2-5B). In contrast, they migrated equally frequently in the horizontal and the perpendicular directions on the control substrate (Figure 2-5C and D). The $|\sin\theta|$ value calculated from the data of the cell migration on the anisotropic substrate in Figure 2-5A (left column in Figure 2-5E) was significantly higher than that from the data of the cell migration on the control substrate in Figure 2-5C and 0.64 (right column in Figure 2-5E).

Directional change from the rigid to the soft direction

There are two possible mechanisms to achieve directional preference of migration in the soft direction. One is that the probability of directional change of migration from the rigid to the soft direction is greater than that vice versa. The other possibility is that the cells can move faster in the soft direction than in

the rigid direction. Thus, we next investigated how the *Dictyostelium* cells and the HL-60 cells move more frequently in the soft direction by carrying out a detailed analysis of their trajectories.

As shown in Figure 2-6, migration direction at each time point of the trajectories was defined (rigid direction; gray region, soft direction; white region in Figure 2-6). First, the migration velocity of *Dictyostelium* cells in the soft direction and that in rigid direction were compared (Figure 2-6B) from the trajectories of migration on the anisotropic substrate (Figure 2-4A). The migration velocity in the soft direction was the same as, rather than faster than, that in the rigid direction (Figure 2-6B). As expected, migration velocity in the perpendicular direction calculated from the trajectories on the control substrate (Figure 2-4C) was the same as that in the horizontal direction (Figure 2-6C).

Next, the probability of a directional change of migration from the soft to the rigid (left column in Figure 2-6D) and that from the rigid to the soft (right columns in Figure 2-6D) were calculated from the trajectories on the anisotropic substrate (Figure 2-4A). The probability of a directional change from the rigid to the soft direction was significantly higher than that in the other way around. The probability of a directional change was calculated also from the trajectories on the control substrate (Figure 2-4C). The probability of change from the perpendicular to horizontal direction was not different from that in the other way around (Figure 2-6E).

The migration velocity of HL-60 cells, calculated from the trajectories on the anisotropic substrate, was the same between the soft and the rigid directions (Figure 2-5A and 2-6F). As expected, HL-60 cells migrated in the same velocities in the perpendicular direction and the horizontal direction (Figure 2-6G), as calculated from the trajectories on the control substrate (Figure 2-5C). The probability of a directional change from the rigid to the soft direction was significantly higher than that in the other way around (Figure 2-6H). On the control substrate, however, there was no significant difference in the probability of a directional change from perpendicular to horizontal or that in the other way around (Figure 2-6I), as was the case in *Dictyostelium* cells. These results strongly suggest that preferential migration in the soft direction of fast-crawling cell types is due to a bias in the directional change of crawling migration from the rigid to the soft.

Myosin II dependent directional preference of migration in the soft direction

The next question is to what kind of intracellular signals the fast-crawling cell types transform the substrate rigidity. It was recently revealed that myosin II motors prefer to bind to tightly stretched actin filaments (Chi et al., 2014; Fernandez-Gonzalez et al., 2009; Luo et al., 2012; Ren et al., 2009; Uyeda et al., 2011). Thus, myosin II is one of the potential mediators for substrate-rigidity sensing for directional preference of migration in *Dictyostelium* cells.

We dispersed myosin II heavy chain-knock-out (*mhcA*$^{-}$) *Dictyostelium* cells on the anisotropic substrate. The cells seemed to migrate equally frequently in all directions, although small fluctuations were seen (Figure 2-7A and B). There was no significant difference in $|\sin\theta|$ (Figure 2-7E) between the anisotropic (Figure 2-7A and B) and control substrates (Figure 2-7C and D). Both $|\sin\theta|$ values were very close to 0.64, indicating the necessity of myosin II for the substrate-rigidity sensing by *Dictyostelium* cells.

Function of myosin II required for the substrate-rigidity sensing by *Dictyostelium* cells

To determine what function of myosin II is required for substrate-rigidity sensing, we examined *mhcA*$^{-}$ *Dictyostelium* cells expressing either of the three variants of myosin II; GFP-3×ASP myosin II; GFP-3×ALA myosin II and GFP-E476K myosin II. These three strains are referred to below respectively as 3×ASP, 3×ALA and E476K cells.

Migration directions of 3×ASP, 3×ALA and E476K cells on the anisotropic and control substrates are summarized in Figure 2-8. The 3×ALA and E476K cells migrated more frequently in the soft direction on the anisotropic substrate (arrows in Figure 2-8A and C), whereas they migrated equally frequently in all directions on the control substrate (Figure 2-8D and F). The $|\sin\theta|$ values of 3×ALA and E476K cells on the anisotropic substrate (left columns in Figure 2-8G and I) calculated from the trajectories of them on the anisotropic substrate were significantly higher than those from the trajectories on the control substrate and than 0.64, respectively (right columns in Figure 2-8G and I). On the other hand, 3×ASP cells migrated equally frequently in all directions, regardless of the substrate (Figure 2-8B and E). $|\sin\theta|$ of 3×ASP cells on the anisotropic substrate was almost the same as that on the control substrate (Figure 2-8H). Both $|\sin\theta|$ values were very close to 0.64.

To summarize the above results, the myosin II-knock-out cells never showed rigidity sensing, indicating myosin II is required for rigidity sensing. 3×ALA cells restored the production of myosin II as thick filaments, and rigidity sensing was also restored (positive control). 3×ASP cells restored the production of myosin II as monomers, and rigidity sensing was not restored (negative control). Finally, E476K cells restored the production of myosin II, which cannot contract actomyosin. The monomers and the thick filaments of GFP-E476K myosin II are in equilibrium like the wild type myosin II. Notably, rigidity sensing was restored in the E476K cells. These results suggest that preferential migration in the soft direction does not require the contraction of actomyosin, but requires the assembly of myosin II molecules into filaments.

Directional change from the rigid to the soft direction in 3×ALA and E476K cells

Next question is whether the characteristics of preferential migration in the soft direction exhibited by E476K and 3×ALA cells is the same as that by wild-type *Dictyostelium* cells. To answer this question, their trajectories were analyzed in detail. In the migrations of E476K and 3×ALA cells on the anisotropic or the control substrate (Figure 2-9A, B, E and F), velocities of only E476K cells in the soft direction on the anisotropic substrate were slightly slower than those in the rigid direction (Figure 2-9E). On the control substrate, the migration velocities of 3×ALA and E476K cells in the perpendicular direction were almost the same as those in the horizontal direction (Figure 2-9B and F).

The probability of a directional change from the soft to the rigid direction in both the E476K and 3×ALA cells was significantly lower than that in the other way around (Figure 2-9C and G). In contrast, the probability of a directional change on the control substrate from the horizontal to the perpendicular direction was the same as that from the perpendicular to the horizontal direction (Figure 2-9D and H). These results suggest that the E476K and 3×ALA cells possess the ability of substrate-rigidity sensing, which is similar to that of wild-type *Dictyostelium* cells.

2-5 Discussion

In the study presented in this chapter, we demonstrated that, fast-crawling cell types, such as *Dictyostelium* cells and HL-60 cells, prefer to migrate in the soft direction on the anisotropic substrate. Rigidity sensing of these cells appears to be different from "durotaxis" seen in slow-crawling cell types.

In our experiments, the range of the substrate-rigidity that fast-crawling cells were able to sense was less than about <1 kPa. In contrast, the range of the substrate-rigidity for slow-crawling cell types is reported to be about several ten kPa (for example 14 to 30 kPa for fibroblast (Lo et al., 2000) and 1 to 30-40 kPa for mesenchymal stem cells (Raab et al., 2012). The range of the substrate-rigidity for slow-crawling cell types to sense may be smaller than that for fast-crawling cell types, and the difference may be due to the difference in the magnitude of their traction forces. Traction forces exerted by slow-crawling cell types (~10 kPa exerted by fibroblasts (Munevar et al., 2001) and by endothelial cells (Reinhart-King et al., 2003) are larger than those by fast-crawling *Dictyostelium* cells (<100 Pa; Figure 2-2).

The more rigid isotropic substrate on which slow-crawling cell types adhere, the larger traction forces the cells exerted. This situation is the same as that in fast-crawling cell types, although the range of the substrate rigidities are different between slow- and fast-crawling cell types. In our experiments, traction forces generated by *Dictyostelium* cells on a substrate with the Young's modules of 101 Pa were smaller than those on a substrate with the Young's modules of 281 Pa (Figure 2-2). In contrast, traction forces generated by 3T3 fibroblasts on a substrate with the Young's modules of 14 kPa were smaller than those on a substrate with the Young's modules of 30 kPa (Lo et al., 2000).

In all cells which preferred to migrate in the soft direction on the anisotropic substrate, such as HL-60 cells, and wild-type, E476K and 3×ALA *Dictyostelium* cells, cells changed the migration-direction from the rigid to the soft directions more frequently than in the other way around (Figures 2-6 D, H, 2-9 C and G). Thus, the main cause of the preferential migration of the fast-crawling cell types to the soft direction should not be the difference in migration velocity in each direction, but a bias in the directional change of migration from the rigid to the soft direction.

Stress fiber is well known as a characteristic cytoskeleton in slow-crawling cell types (Cramer et al., 1997). When the stretched stress fibers are relaxed, cofilin binds to them and depolymerize them (Hayakawa et al., 2011; Hayakawa et al., 2014). Fast-crawling cell types do not have stress fibers. Mechanical reaction such as stretch and relax of the cytoskeletal structure like stress fiber may be necessary for durotaxis in which the slow-crawling cell types migrate towards the stiff region. Ni and Chiang theoretically predicted that cells migrate so that the free energy of the cell-substrate system is minimized(Ni and Chiang, 2007). They claimed that the cells on anisotropic substrate should migrate to the area whose stiffness is the same as that of the cell. Thus, when the cell stiffness is higher than that of their substrate the cell would move towards the soft region. Their theory may be able to explain the mechanism how the fast-crawling cell types prefer to move in the soft direction.

A molecular sensor on the cell cortex to sense the substrate-rigidity, and the subsequent intracellular signal transduction cascade including modulation of the myosin II-dynamics, were not considered in

this study. Both slow- and fast-crawling cells receive the reaction forces of their own traction at the adherent sites. Thus, the possible candidates for the molecular sensor include focal adhesion proteins, such as integrin, vinculin, talin, paxillin, focal adhesion kinase (FAK) and etc. (Case and Waterman, 2015; Elosegui-Artola et al., 2016; Gupta et al., 2016; Jiang et al., 2006; Kobayashi and Sokabe, 2010; Kuo, 2013; Naruse et al., 1998c; Plotnikov et al., 2012; Sun et al., 2016; Trichet et al., 2012; Wang et al., 2001a). Myosin II also plays important roles in the mechano-signal transduction cascade (Raab et al., 2012; Vicente-Manzanares, 2013). Rise in the substrate-rigidity prevents phosphorylation of Ser1943 in myosin IIA. Decrease in the Ser1943 phosphorylation enhances myosin IIA assembly (Dulyaninova et al., 2007). Thus, assembly of myosin IIA increases in the oriented stress fibers on the rigid substrates. To reveal the molecular dynamics and mechanisms of rigidity sensing not only in fast- but also in slow-crawling cell types is one of the interesting future research issues.

Figures

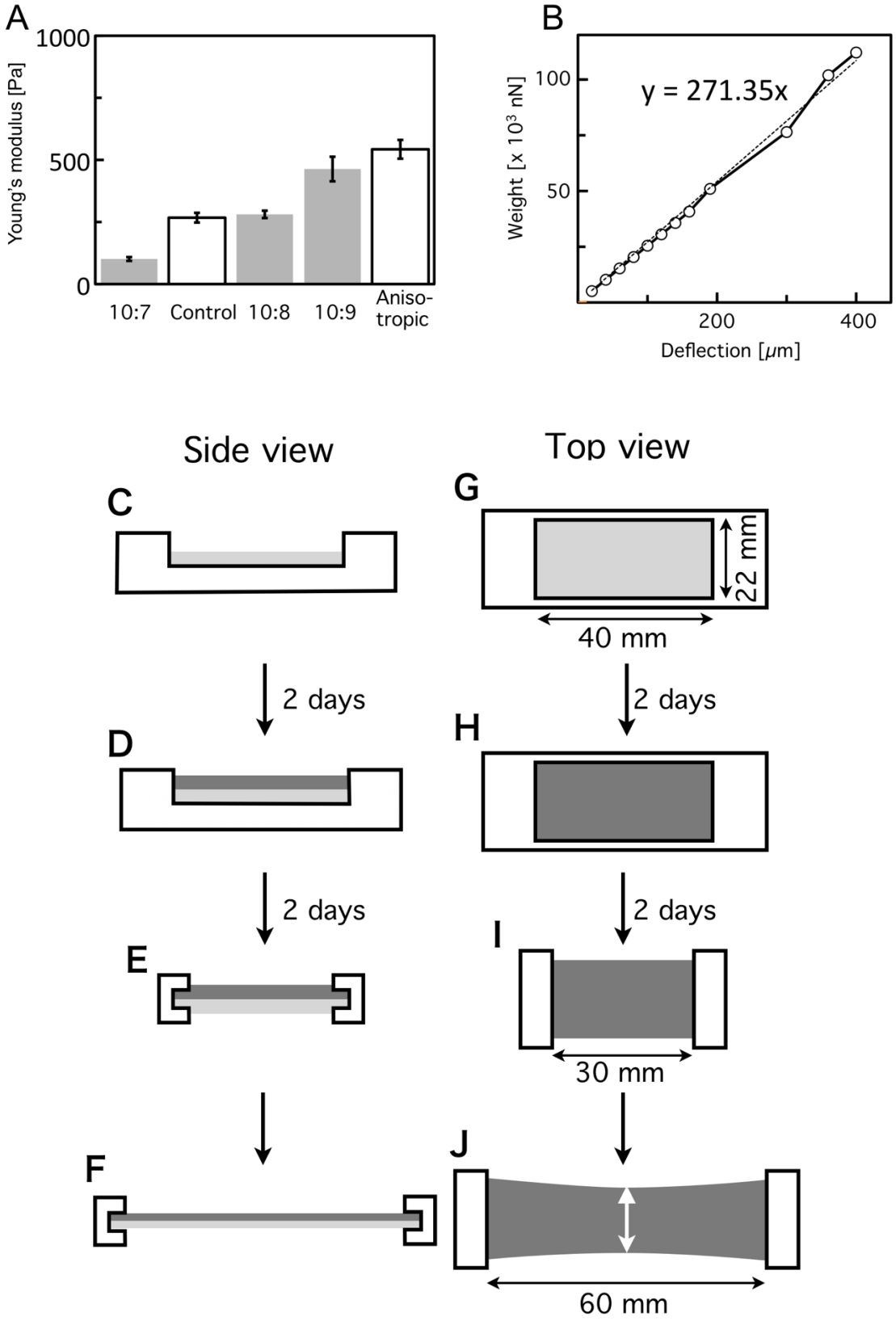
A
1000
500
0
Young's modulus [Pa]
10:7
Control
10:8
10:9
Aniso-
tropic
B
100
50
Weight [x 10³ nN]
y = 271.35x
200
400
Deflection [μm]
Side view
Top view
C
G
22 mm
40 mm
2 days
2 days
D
H
2 days
2 days
E
I
30 mm
F
J
60 mm

Figure 2-1. Young's moduli of our substrates and deflection of a flexible needle. (A) Young's moduli of isotropic substrates (gray columns) and apparent Young's moduli of the control and the anisotropic substrates (white columns). The isotropic substrates for traction force microscopy were made by mixing CY52-276A and B at different ratios of 10:7, 10:8 and 10:9 in weight. Bars mean SEM. n = 30 for each column. (B) Relationship between applied weight to the tip of a flexible glass needle and the deflection of it. A dotted straight regression line obtained by the least-squares method and the equation for the line is shown in the figure. Hooke's elastic constant was determined as the slope of the dotted line. (C – G) Procedure for preparing flexible substrata with elastic anisotropy. (C and G) A 300 mg of rigid PDMS (light gray) was poured into a mold and allowed to solidify for 2 days at room temperature. (D and H) A 300 mg of soft PDMS (dark gray) was poured onto the solidified rigid PDMS and allowed to solidify for an additional 2 days at room temperature. (E and I) The solidified two-layered sheet was peeled off carefully, and then both short sides were held by a stretching device. (F and J) The sheet was stretched to double the initial length. White arrow in H means the shortening of the sheet perpendicular to the axis of stretch (Poisson's effect). C – F, side view; G – J, top view.

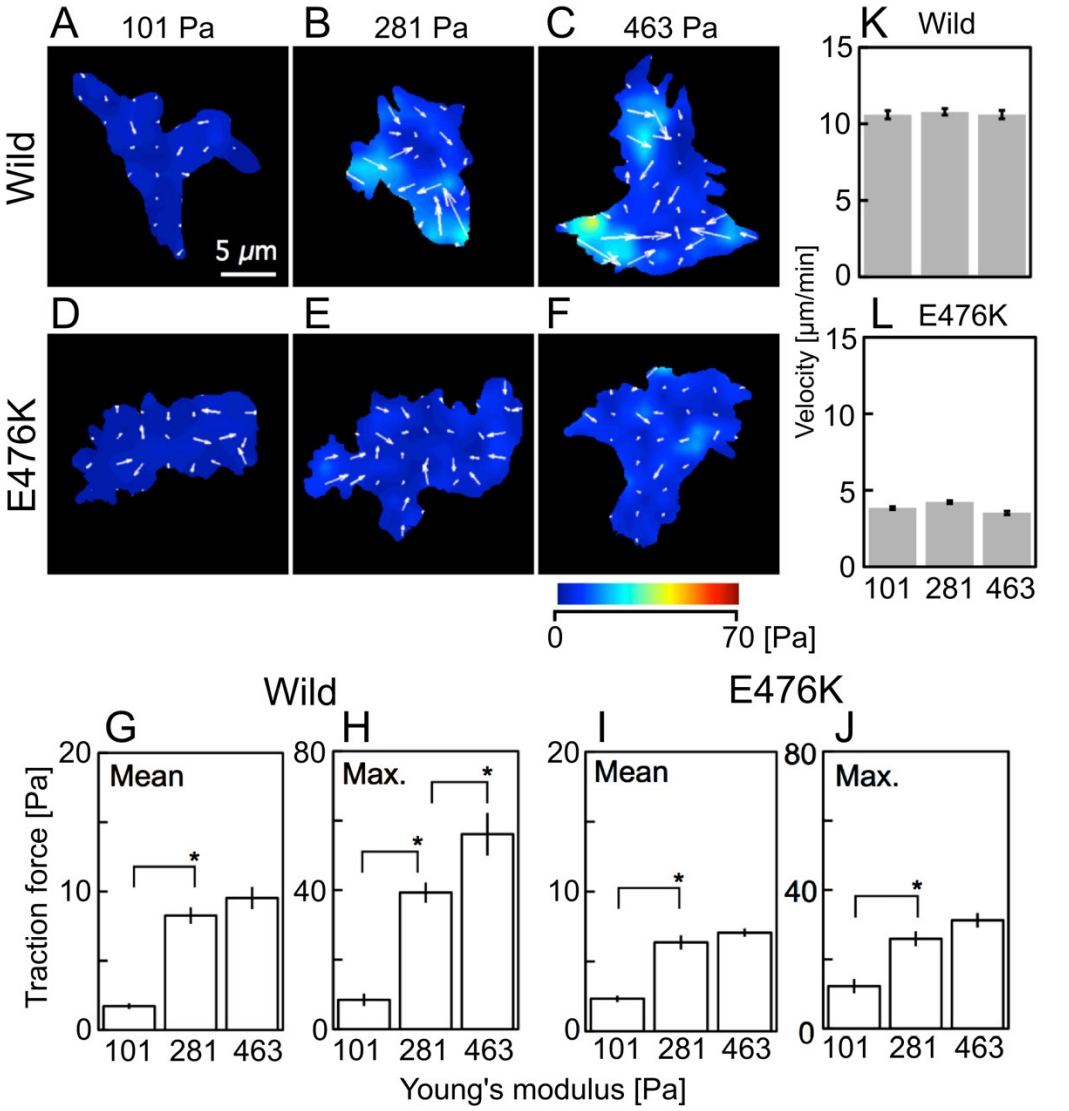

Figure 2-2. Traction forces exerted by *Dictyostelium* cells on substrates with different elasticities. (A – C) Wild-type cells. (D – F) E476K cells. Young's moduli in A and D, B and E, and C and F were 101, 281 and 463 Pa, respectively. Cells in A - F are typical of 20, 27, 24, 20, 21 and 25 cells, respectively. (G – J) Maximum and mean traction forces by wild-type and E476K cells on each substrate. (K and L) Migration velocities of wild-type and E476K cells on each substrate. K and L show data averaged from 30, 31 and 29 cells, and 20, 21 and 25 cells from the left, respectively. Bars mean SEM. The *p*-values were calculated using Student's t-test in G – I and one-way ANOVA in K and L. *$p < 0.01$.

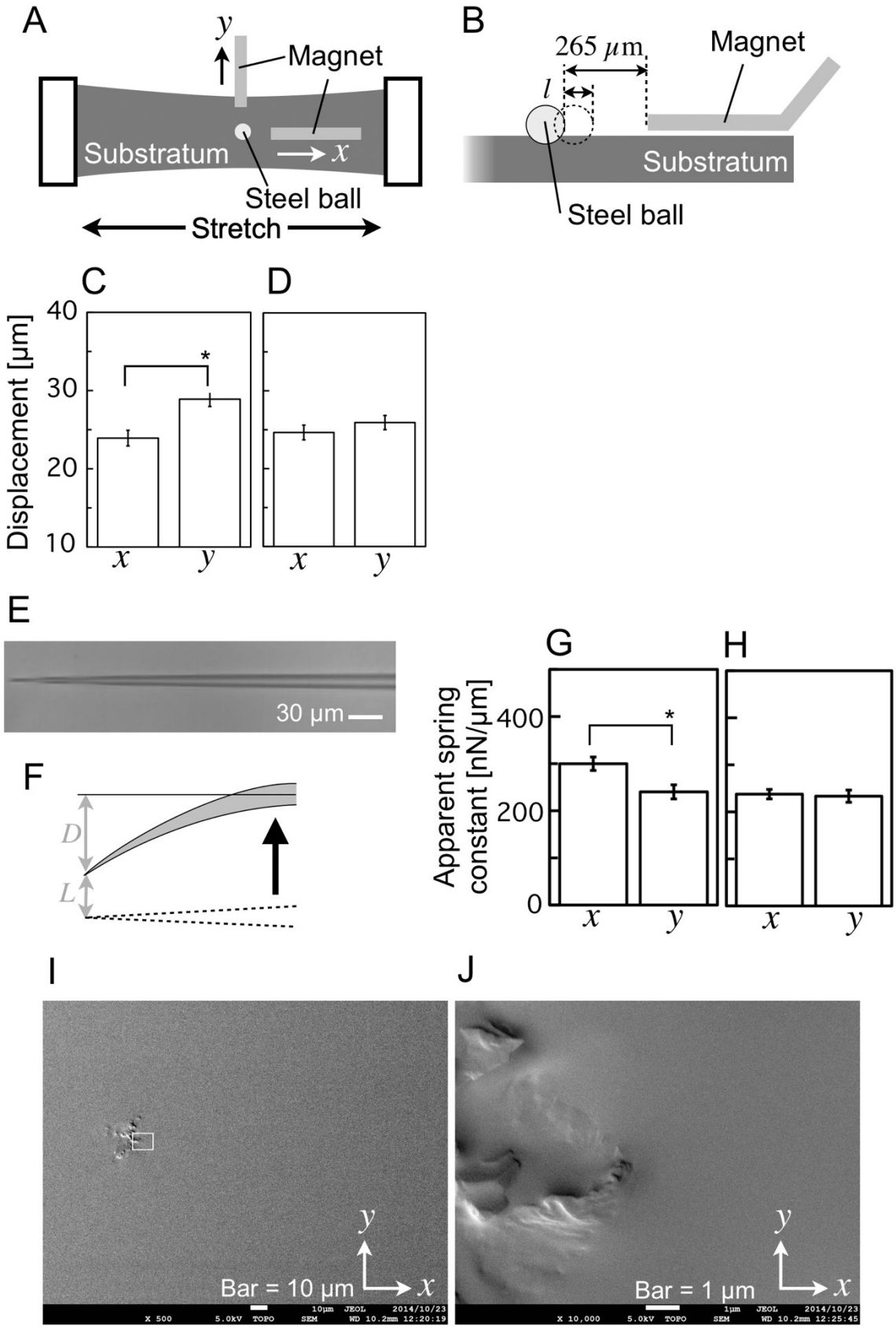
A
y
Magnet
Substratum
x
Steel ball
Stretch
B
265 μm
Magnet
l
Substratum
Steel ball
C
D
Displacement [μm]
40
30
20
10
*
x
y
x
y
E
30 μm
F
D
L
G
H
Apparent spring constant [nN/μm]
400
200
0
*
x
y
x
y
I
J
y
x
Bar = 10 μm
X 500 5.0kV TOPO SEM WD 10.2mm 12:20:19
y
x
Bar = 1 μm
X 10,000 5.0kV TOPO SEM WD 10.2mm 12:25:45

Figure 2-3. Evaluation of the new anisotropic substrate. (A and B) Estimation of elasticity of the substrate; top view (A) and side view (B). The two-layered PDMS sheet was stretched such that its length doubled. Displacements (l in B) of a steel ball (0.3 mm diameter, 0.52 mg) pulled by a fine magnetic rod (Magnet in A and B), whose tip was originally positioned 265 μm from the edge of the ball, were measured in the x and y directions, respectively. (C and D) Displacement of a steel ball after (C) and before (D) the stretching of the sheet. The x in C and D; n = 75 from 10 beads and y in C and D; n = 77 from 10 beads. (E) Glass micro needle to evaluate the elasticities of the substrate. (F) Method of measurement. The tip of the needle was adhered to the surface of the substrate. Then, the substrate was pulled in x or y direction in A by moving the needle (arrow). Deflection of the needle and displacement of the needle-tip are indicated as D and L, respectively. (G and H) Apparent spring constants of the substrate in x or y direction after (G) and before (H) the stretching of the sheet. G and H show data averaged from 14 (x in G) and 12 (y in G) cells, and 12 (x in H) and 11 (y in H) cells, respectively. (I and J) Image of the anisotropic substrate taken by scanning electron microscope. G is an enlarged view of the white square in I. Bars mean SEM. The p-values were calculated using Student's t-test. *$p < 0.01$.

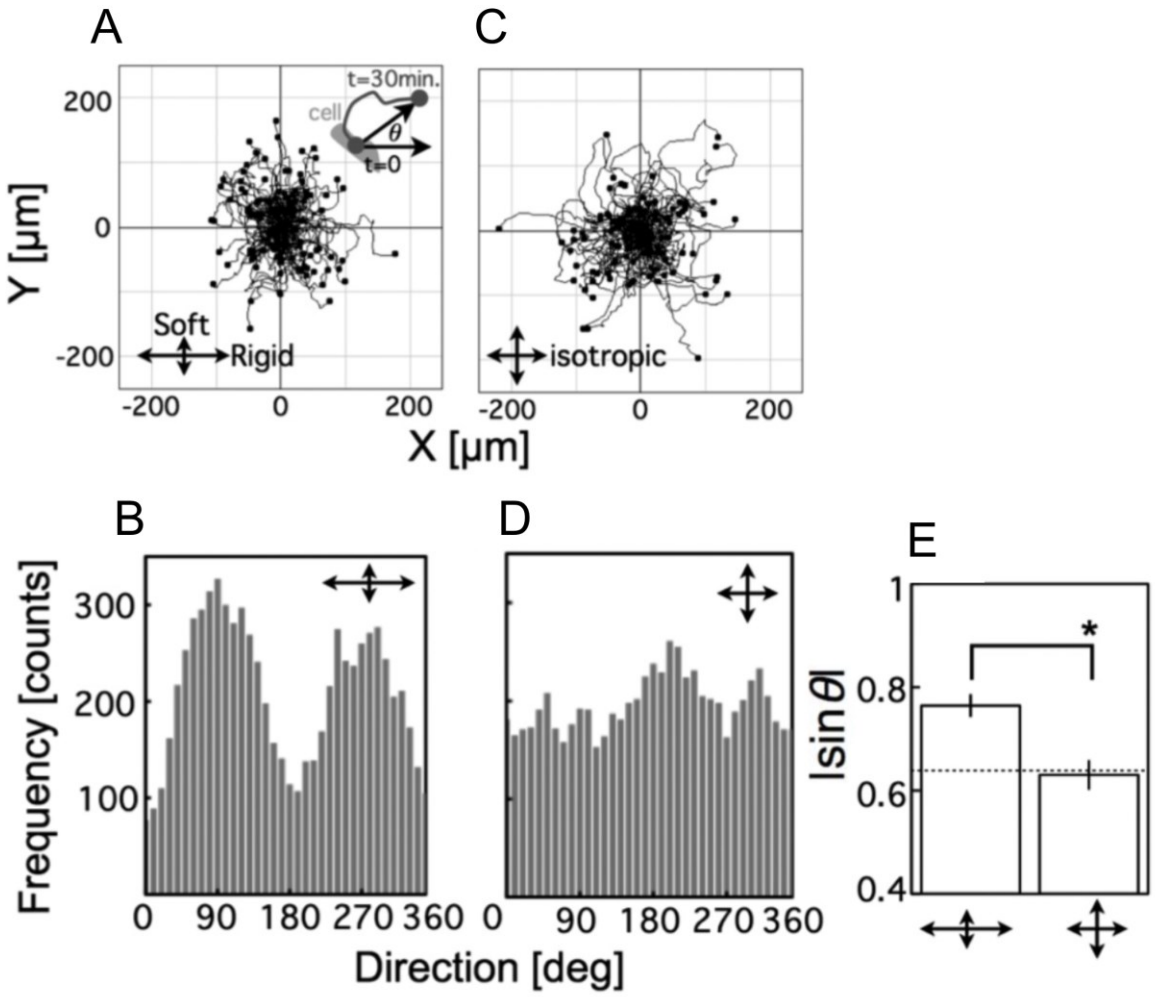

Figure 2-4. Movements of wild-type *Dictyostelium* cells. (A) Trajectories of 114 cells for 30 min on the anisotropic substrate, rigid in *x*- and soft in *y*-direction, from 6 experiments. (B) Frequencies of migration-directions (θ) from the data in A. The value θ (inset in A) is defined as the angle between the vector from the starting to the ending point of each trajectory and the vector in the 0° direction. (C) Trajectories of 107 cells on the control substrate from 10 experiments. (D) Frequencies of migration-directions (θ) from the data in C. (E) Average $|\sin\theta|$ values on the anisotropic and the control substrates. Dashed line means 0.64, the value when cells migrate equally in all directions. Bars mean SEM. The *p*-values were calculated using Student's t-test. $*p < 0.01$.

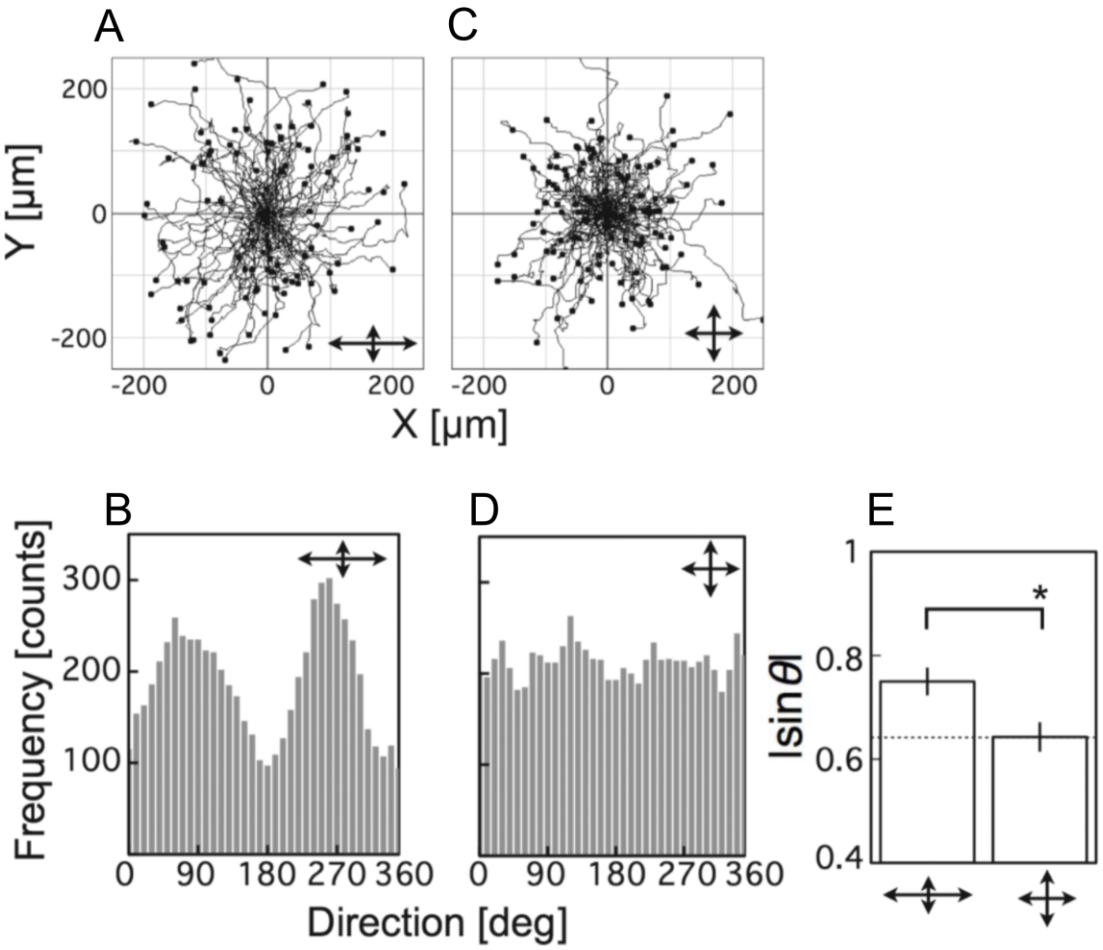

Figure 2-5. Movements of HL-60 cells. (A) Trajectories of 102 cells for 30 min on the anisotropic substrate from 5 experiments. (B) Frequencies of migration-directions from the data in A. (C) Trajectories of 116 cells for 30 min on the control substrate from 10 experiments. (D) Frequencies of migration-directions from the data in C. (E) Average $|\sin\theta|$ values on the anisotropic and the control substrates. Dashed line means 0.64. Bars mean SEM. The *p*-values were calculated using Student's t-test. $*p < 0.01$.

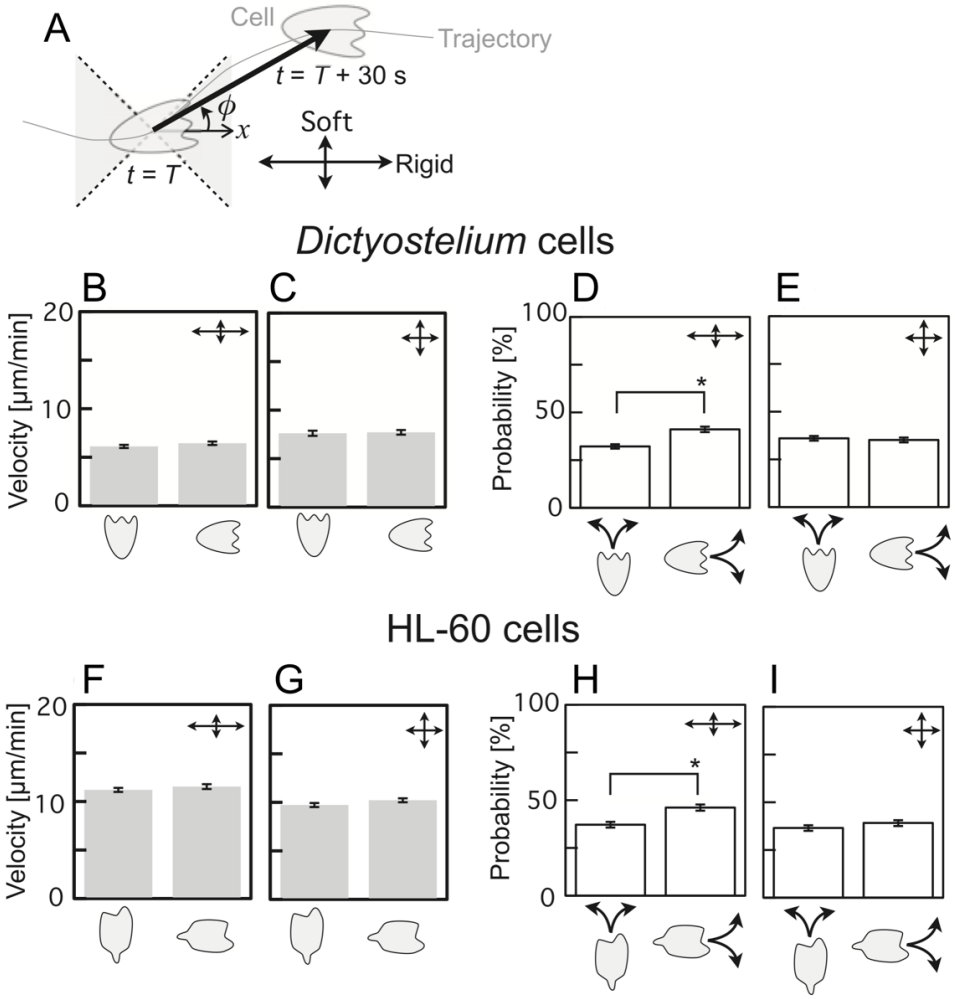

Figure 2-6. Property of crawling migration of *Dictyostelium* and HL-60 cells. (A) Definition of the directions. Thick arrow means a vector from a location of a cell to that after 30 s. The angle (ϕ) between the vector and the x-axis (x) means the migration-direction at each time point. Gray region between 315 and 45˚ or between 135 and 225˚ means the rigid direction. On the other hand, white region between 45 and 135˚ or between 225 and 315˚ means soft direction. (B) Velocities of *Dictyostelium* cells on the anisotropic substrate. (C) Velocities of *Dictyostelium* cells on control substrate. (D) Probabilities of directional change of *Dictyostelium* cells on the anisotropic substrate. (E) Probabilities of directional change of *Dictyostelium* on the control substrate. (F) Velocities of HL-60 cells on the anisotropic substrate. (G) Velocities of HL-60 cells on the control substrate. (H) Probabilities of directional change of HL-60 cells on the anisotropic substrate. (I) Probabilities of directional change of HL-60 cells on the control substrate. Bars mean SEM. The p-values were calculated using Student's t-test. *$p < 0.01$.

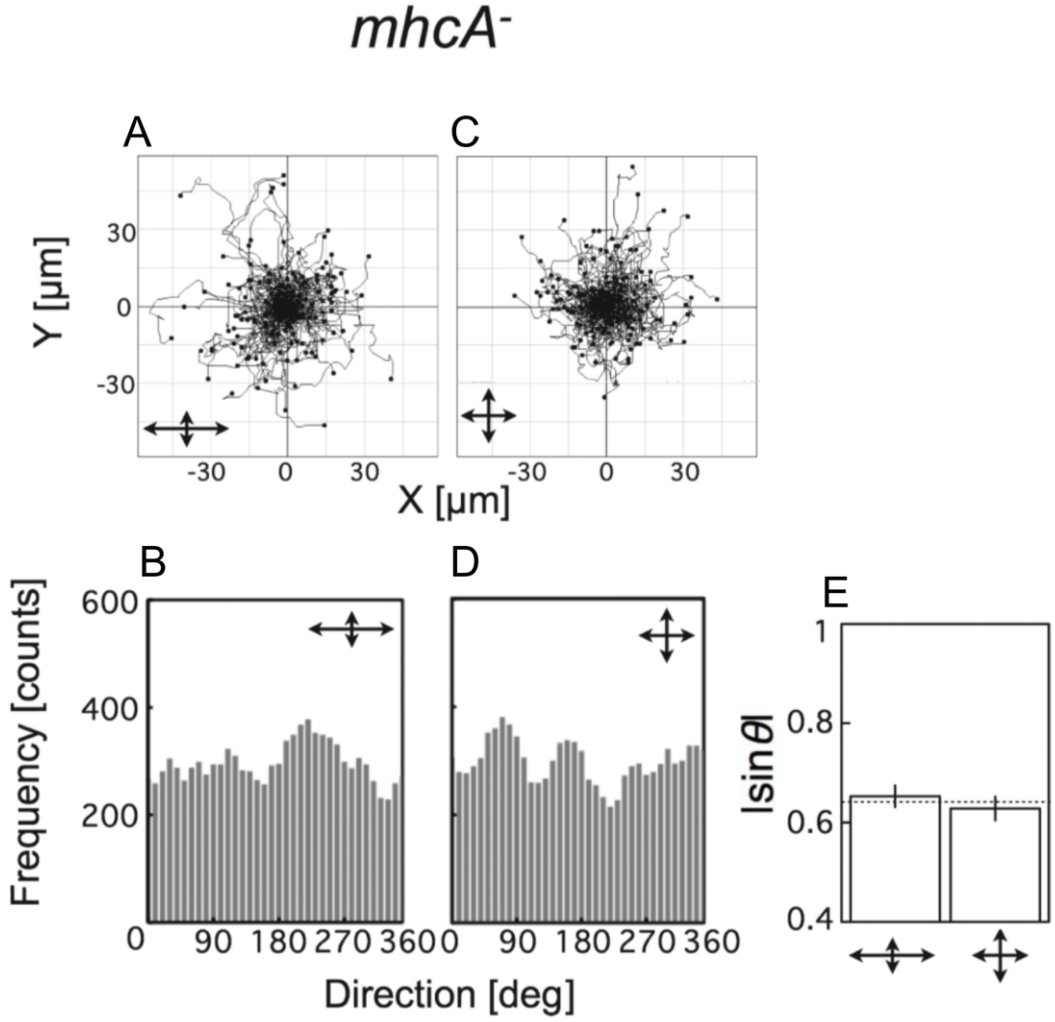

Figure 2-7. Movements of *mhcA*⁻ *Dictyostelium* cells. (A) Trajectories of 157 cells for 30 min on the anisotropic substrate from 6 experiments. (B) Frequencies of migration-directions from the data in A. (C) Trajectories of 163 cells on the control substrate from 6 experiments. (D) Frequencies of migration-directions from the data in C. (E) Average $|\sin\theta|$ values on the anisotropic and the control substrates. Dashed line means 0.64. Bars mean SEM. The *p*-values were calculated using Student's t-test. $*p < 0.01$.

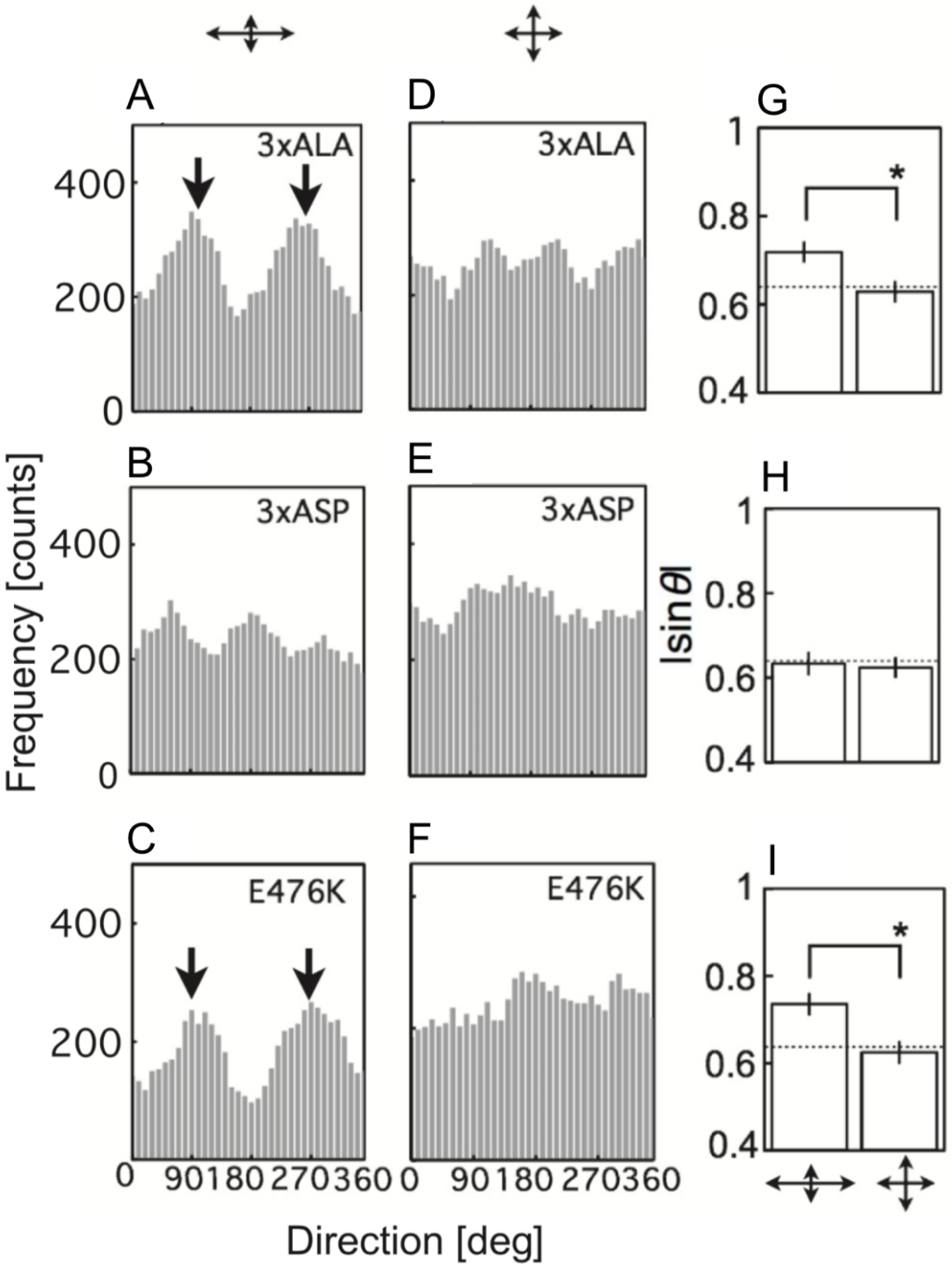

Figure 2-8. Movements of *mhcA*⁻ *Dictyostelium* cells expressing myosin II variants. (A – C) Frequencies of the migration-direction (θ) of 3×ALA, 3×ASP and E476K cells on the anisotropic substrate. The data in A – C are compilation of 138 cells from 5 experiments, 128 cells from 6 experiments and 101 cells from 5 experiments, respectively. Peaks at 90 and 270˚ are indicated by arrows in A and C. (D – F) Frequencies of the migration-direction of 3×ALA, 3×ASP and E476K cells on the control substrate. The data in D – F are compilation of 141 cells from 6 experiments, 160 cells from 6 experiments and 130 cells from 5 experiments, respectively. (G – I) Average $|\sin\theta|$ values on the anisotropic and the control substrates. Dashed line means 0.64. Bars mean SEM. The *p*-values were calculated using Student's t-test. *$p < 0.01$.

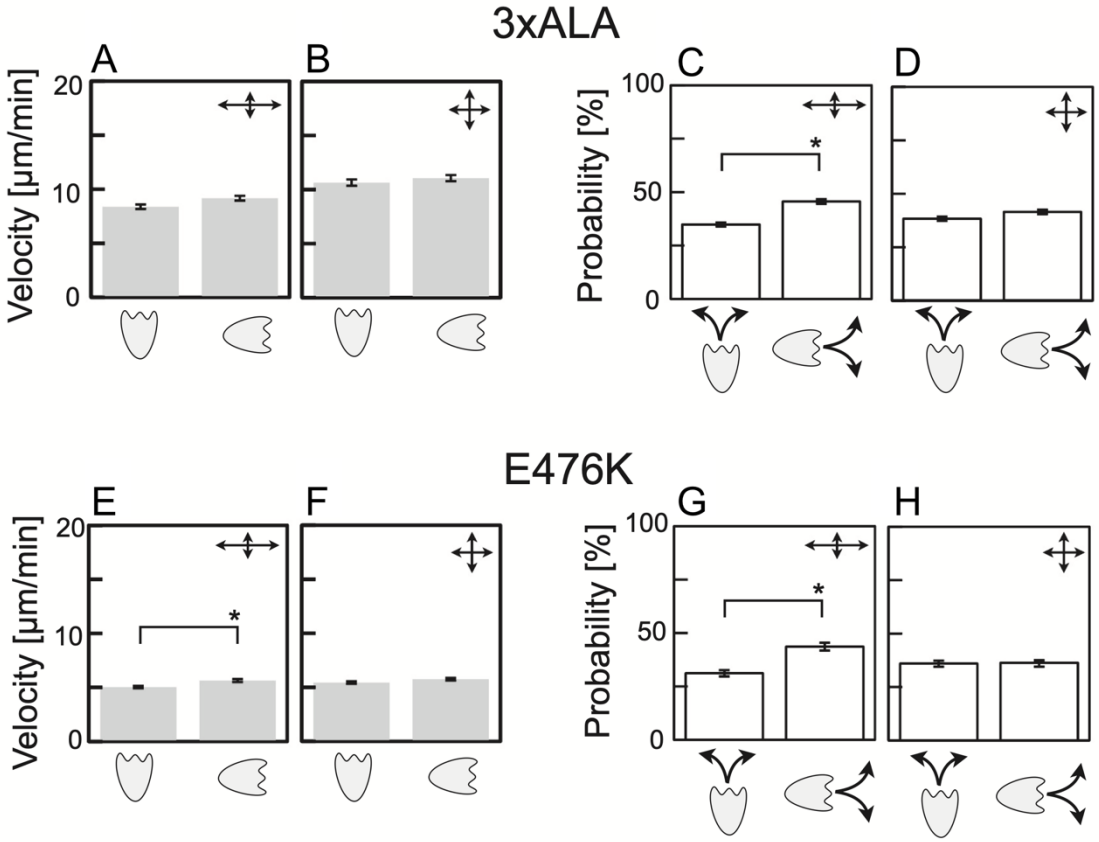

Figure 2-9. Property of crawling migration of 3×ALA and E476K *Dictyostelium* cells. (A) Velocities of 3×ALA cells on the anisotropic substrate. (B) Velocities of 3×ALA cells on the control substrate. (C) Probabilities of directional change of 3×ALA cells on the anisotropic substrate. (D) Probabilities of directional change of 3×ALA cells on the control substrate. (E) Velocities of E476K cells on the anisotropic substrate. (F) Velocities of E476K cells on the control substrate. (G) Probabilities of directional change of E476K cells on the anisotropic substrate. (H) Probabilities of directional change of E476K cells on the control substrate. Bars mean SEM. The *p*-values were calculated using Student's t-test. *$p < 0.01$.

Chapter 3

Cyclic Substrate Stretching Induces Directional Migration in *Dictyostelium* Cells

3-1 Abstract

Cells adhering to substrates should receive and respond to mechanical stimuli from the substrates and change their shape and decide migration-direction. Intracellular stress fibers in slow-crawling cell types are rearranged to the direction perpendicular to the stretching direction in response to cyclic stretching of the elastic substrate, and then the shape of those cells extend in the perpendicular direction. In the case of *Dictyostelium* cells, one of the typical fast crawling cell types, the cyclic stretching of elastic substrate controls not their shape but their migration-direction. The cyclic stretching biases *Dictyostelium* cells to move in the direction perpendicular to the stretching, although the underlying molecular mechanisms have been unknown. In this chapter, GFP-myosin II dynamics in *Dictyostelium* cells in response to the cyclic substrate stretching are demonstrated using a microstretching device. In response to the cyclic substrate stretching in the left and right direction, myosin II was localized equally along the left and the right edges in the cell body. In contrast, myosin II-knock-out cells, having no myosin II for localization, moved equally frequently in all directions under the cyclic substrate stretching. In the case when the cyclic substrate stretching was applied to myosin II-knock-out cells expressing a variant of myosin II that cannot hydrolyze ATP, the variant myosin II localized equally along the left and the right edges in the cell body, and the cell moved perpendicular to the stretch, in a manner similar to wild-type cells. These results indicate that the cyclic substrate stretching induces *Dictyostelium* cells to migrate in the direction perpendicular to the stretching via a myosin II related process, which is independent on the contraction as actomyosin.

3-2 Introduction

Living cells receive various mechanical stimuli such as substrate strain, shear flow and pressure from adjacent cells. It seems that crawling cells incessantly receive mechanical stimuli from substrates in physiological conditions (Giannone and Sheetz, 2006; Vogel and Sheetz, 2006). To test the role of the mechano-signal from the substrate, one of the most useful techniques to apply mechanical stimuli is artificial stretching of the elastic substrate to which cells adhere (Crosby et al., 2011; Desai et al., 2010; Naruse et al., 1998b; Naruse et al., 1998c).

In response to the cyclic substrate stretching, intracellular stress fibers in slow-crawling cell types such as smooth muscle, osteosarcoma, endothelial cells and fibroblasts, are rearranged to the direction perpendicular to the direction of stretching, and the cell shape extends in the perpendicular direction. A potential candidate of molecular mechanism in slow-crawling cell types for the stress fiber rearrangement has been proposed. Binding of cofilin to the actin filaments when the stretched stress fibers are relaxed should cause stress fiber disassembly (Birukov et al., 2003; Hayakawa et al., 2011; Hayakawa et al., 2014; Kaunas et al., 2005; Lee et al., 2010; Morioka et al., 2011; Sato et al., 2005; Tondon et al., 2012; Zhao et al., 2011).

It is known that the cyclic substrate stretching affects also fast-crawling cell types. It make *Dictyostelium* cells migrate perpendicular to the stretching direction (Iwadate and Yumura, 2009a). However, intracellular mechanotransduction that begins with the cyclic stretching stimuli in fast-crawling cell has remained unknown. A dense actin filament meshwork is shown throughout the cortex of *Dictyostelium* cells instead of the stress fibers (Bretschneider et al., 2004; Iwadate and Yumura, 2008b). Thus, the molecular dynamics of *Dictyostelium* cells in response to cyclic substrate-stretching should be different from that in slow-crawling cell types.

It is widely accepted in crawling cells that extension of the front and retraction of the rear are induced by actin polymerization (Svitkina et al., 1997; Wang, 1985) and contraction via myosin II-dependent processes (Chen, 1981; Jay et al., 1995), respectively. By sucking of a part of the cell surface with a micropipette, myosin II accumulates at the tip of the sucked cell lobe (Merkel et al., 2000; Ren et al., 2009), indicating that myosin II-accumulation is regulated by the mechanical stimuli. Myosin II accumulated at the lateral sides of the cell suppress the extension of the extra pseudopods (Chung et al., 2001; Wessels et al., 1988). Not only migration speed but also path linearity of myosin II-knock-out *Dictyostelium* cells are significantly lower than those of wild-type cells under chemotactic conditions (Clow and McNally, 1999; Eliott et al., 1993). Thus, cyclic substrate-stretching may induce directional preference of migration via a myosin II related mechanotransduction process.

In the study of this chapter, we show that cyclic substrate stretching in the left and right direction induces myosin II localization equally along the left and the right edges in the wild-type *Dictyostelium* cell. They migrated perpendicular to the stretching. In contrast, myosin II-knock-out cells, having no myosin II for localization, moved equally frequently in all directions under the cyclic substrate stretching. In the case when the cyclic substrate stretching was applied to myosin II-knock-out cells expressing a variant of myosin II that cannot hydrolyze ATP, the variant myosin II localized equally along the left

and the right edges in the cell body, and the cell moved perpendicular to the stretch direction, in a manner similar to wild-type cells. These results suggest that the mechanical stimuli from the substrate regulate the migration-direction of *Dictyostelium* cells via a myosin II related mechanosignal transduction cascade that is independent of the contraction as actomyosin.

3-3 Materials and Methods

***Dictyostelium* cell lines**

Preparation of *Dictyostelium discoideum* cells was described in Chapter 2. Similar to the study in Chapter 2, AX2 cells, *mhcA*$^{-}$ cells, E476K cells, 3×ASP cells and 3×ALA cells were used. In addition to the above cells, AX2 cells expressing GFP-ABD120k, *mhcA*$^{-}$ cells expressing GFP-myosin II, and SibA-null cells were also used in this chapter. ABP120 is a protein that crosslinks actin filaments (Pang et al., 1998). ABD120k is the actin-binding domain of ABP120 and can bind only to filamentous actin. Thus, the distribution of actin filaments can be detected by the observation of GFP-ABD120k. The GFP-ABD120k gene was kindly provided by D.A. Knecht (University of Connecticut). This fusion gene was inserted into the pBIG expression vector (Ruppel et al., 1994) by T.Q.P. Uyeda (Waseda University). SibA is a integrin β-like substrate adhesion protein in *Dictyostelium* cells (Cornillon et al., 2006; Tsujioka et al., 2012).

Cyclic substrate stretching

Elastic sheets (40 mm in length × 22 mm in width) were made from Sylgard 184 by using a mold described in Chapter 2 (Iwadate and Yumura, 2009a). One 22 mm side of the sheet was fixed and the other connected to 4 coils made from shape-memory alloy (BMX150; Toki, Japan). The coil contracts when electric current is passed through. Cyclic substrate stretching of the sheet was induced by the application of square voltage pulses sequentially to the 4 coils. The cycle time, duty ratio and stretching ratio of stretching were adjusted to 20%, 5 s and 1:1, respectively, in all experiments in this chapter. In our device, shrinkage of the sheet in the direction perpendicular to the stretching by Poisson's effect was <5%. *Dictyostelium* cells move equally frequently in all directions in response to the cyclic substrate stretching of 10% stretching ratio (Iwadate and Yumura, 2009a).

Trajectory analysis

Crawling cells on cyclically stretched substrate were observed using a phase-contrast inverted microscope (TS100; Nikon) with a 20× objective lens (LWD ADL 20xF; Nikon). Images were recorded at 30-s intervals for 30 min at room temperature (23 ˚C). Migration-direction was analyzed in the same way as described in Chapter 2. Directionality of the trajectory, expressed as the linear distance between the start and end points divided by the path length between the same two points, was also calculated.

Fluorescence observation

To observe fluorescence images, an inverted microscope (Ti; Nikon) equipped with a laser confocal scanner unit (CSU-X1; Yokogawa, Japan) was used. The fluorescence images through a 100x objective lens (CFI Apo TIRF 100xH/1.49; Nikon) were recorded with an EM CCD camera (DU897; Andor, Belfast, UK).

Analysis of myosin II accumulation and dynamics of pseudopods in free moving cells with no substrate stretching

From the sequential images, an image and another one 40 s after were arbitrarily selected (Figure 3-1A and B). In the former image ($t = t_0$ in Figure 3-1A), a dotted line was drawn from the centroid of the cell to the cell boundary. The length of the dotted line was defined as l_1. The cortical region is defined as 2 μm wide orbital area inside the cell boundary (gray area in Figure 3-1A), and the maximum GFP fluorescence value in the cortical region along the dotted line (black bar in Figure 3-1A) was defined as F. In the latter image ($t = t_0 + 40$ s in Figure 3-1B) too, a dotted line was drawn from the centroid at $t = t_0$ in the same direction as in the former image to the cell boundary. The length of the dotted line was defined as l_2. F and l_2/l_1 were calculated along the 12 dotted lines at intervals of 30º (Figure 3-1C).

Cyclic substrate stretching with microstretching device

A microstretching device (Figure 3-2) (Sato et al., 2010) was used for observing GFP fluorescence under the cyclic substrate stretching. Cells were plated onto the 100 μm × 400 μm substrate indicated as Chamber in Figure 3-2A. Prior to the experiments, strain distribution of the substrate was measured by stretching the substrate by 26%. Strain field was a roughly homogeneous (Figure 3-2B). Compressing strain along the rectangular axis to stretch was only 0.8%. In all experiments, the substrate was stretched 20% laterally by pushing the switch part of the device using a glass microneedle.

Evaluation of myosin II distribution

The cell area was divided into 4 portions by the 4 dotted lines drawn from the centroid of a cell to the angles of 45, 135, 225 and 315 degrees from the horizontal line (Figure 3-5B). Areas, a - d in each portion are defined as the areas within 2 μm from the cell boundary. F_a – F_d are the maximum GFP fluorescence values in a – d, respectively. $F_i|F_j$, is defined as the larger one of F_i and F_j divided by the smaller, and used as an index of the symmetrical distribution of myosin II.

Analysis of myosin II accumulation and dynamics of pseudopods in response to the substrate stretching

Before and after four repeats of 20% stretching with microstretching device, two images were taken (Figure 3-1D and E). In the first images (Figure 3-1D), a dotted line was drawn from the centroid to the boundary of a cell. The length of the dotted line was defined as l_1. The cortical region is defined as 2 μm wide orbital area inside the cell boundary (gray area in Figure 3-1D), and the maximum GFP fluorescence value in the cortical region along the dotted line (black bar in Figure 3-1D) was defined as F_1. In the second image (Figure 3-1E) too, a dotted line was drawn from the centroid of the first image in the same direction as in the first image to the cell boundary. The length of the dotted line was defined as l_2. F_2 (black bar in Figure 3-1E) was also defined in the same manner as F_1. The values of l_2/l_1 and F_2/F_1 were calculated at the 6 areas on the dotted lines (black bars in Figure 3-1F).

3-4 Results

Cyclic substrate stretching induces directional preference in wild-type cells

An elastic substrate on which wild-type *Dictyostelium* cells were dispersed was stretched and relaxed repeatedly. Trajectories of crawling cells are shown in Figure 3-3A. Frequencies of migration directions (Figure 3-3C) were calculated from the trajectories. Apparently the cells under cyclic substrate stretching stimuli tended to move perpendicular to the stretching direction (arrows in Figure 3-3C) whereas the cells under no stretching stimuli move equally frequently in all directions (Figure 3-3B and D). Average $|\sin\theta|$ value (θ: inset in Figure 3-3A) of the cells under stretching stimuli was significantly higher than that of the cells under no stimuli (compare left and right columns in Figure 3-3E). These results agree well with the previous experiment using the cAMP receptors-knockout *Dictyostelium* cell line RI9 (Iwadate and Yumura, 2009a).

Cyclic substrate stretching-induced directional preference requires myosin II

Next, crawling migration of *mhcA*$^-$ cells under cyclic substrate stretching was observed. Unlike wild-type cells, *mhcA*$^-$ cells moved equally frequently in all directions under cyclic substrate stretching (Figure 3-4A and C), which was the same as the case under no stimuli (Figure 3-4B and D). There was no statistical difference in $|\sin\theta|$ (Figure 3-4E) between the case under cyclic substrate stretching and that under no stimuli, indicating that myosin II is required for the directional preference of crawling migration of *Dictyostelium* cells in response to cyclic substrate stretching.

To test role of cell-substrate adhesion as a path to transmit the mechanical stimuli from the substrate to the cell, cyclic substrate stretching was applied to *SibA*$^-$ cells. SibA in known as one of the adhesion molecules in *Dictyostelium* (Cornillon et al., 2006). *SibA*$^-$ cells moved in a direction perpendicular to the stretching direction (arrows in Figure 3-4F), while they moved equally frequently in all directions under no stretching stimuli (Figure 3-4G, H). These results indicate that the mechanical signal is transmitted through some path other than the SibA-related adhesion.

To clarify the role of myosin II for the directional preference in response to cyclic substrate stretching, myosin II localization was observed using a microstretching device (Figure 3-2A). After the 4 repeats of substrate-stretching in the left-right direction, GFP-myosin II seemed to accumulate equally along the left and the right edges in the cell body (dotted oval in Figure 3-5A). Fluorescence intensities of GFP-myosin II along the left (F_c in Figure 3-5C and D) and the right sides (F_a in Figure 3-5C and D) significantly increased after the substrate stretching ($p = 0.001$ for F_a and 0.001 for F_c,). The ratio of the greater to the smaller fluorescence intensity of GFP-myosin II in the left-right direction dramatically decreased after the stretching (compare $F_a|F_c$ values in Figure 3-5E and F, $p = 9.06 \times 10^{-5}$), although that in the top-bottom direction did not change (compare $F_b|F_d$ values in Figure 3-5E and F, $p = 0.933$), suggesting that the left-right symmetrical stretching forces induce the same symmetrical localization of myosin II.

To reveal whether the arrangement of actin meshwork was also changed by the cyclic substrate stretching, we next observed the fluorescence image of GFP-ABD120k in wild-type cells before and

after 4 repeats of stretching (Figure 3G). Even after the 4 repeats, actin filaments did not show noticeable alignment in a particular direction. Distribution of actin filaments along the boundary of the cell was statistically analyzed. The ratio of the greater to the smaller fluorescence intensity of GFP-ABD120k in the left-right direction slightly increased after the stretching, but the difference was not significant (compare $F_a|F_c$ values in Figure 3-5H and I, $p = 0.209$). Similarly, the ratio in the top-bottom direction did not change (compare $F_b|F_d$ values in Figure 3-5H and I, $p = 0.945$),

Myosin II-function essential directional preference of migration

To determine what function of myosin II is essential for directional preference of migration in response to the cyclic stretching, E476K cells, 3×ASP cells and 3×ALA cells were used. After 4 repeats of substrate stretching in the left-right direction, GFP-E476K and -3×ALA myosin II localized equally along the left and the right edges in the cell body (dotted oval in Figure 3-6A and C, and white columns in D, F, G, and I). However, the distribution of GFP-3×ASP myosin II was not affected (Figure 3-6B, E and H).

The migration trajectories of the myosin II-mutant cells under cyclic substrate stretching were also analyzed. E476K and 3×ALA cells under cyclic substrate stretching moved perpendicular to the stretching direction (arrows in Figure 3-7A and C), and the cells under no stretching stimuli moved equally frequently in all directions (Figure 3-7D and F). Average $|\sin\theta|$ values of the cells under cyclic substrate stretching condition was significantly higher than those of the cells under no stimuli (compare left and right columns in Figure 3-7G and I). In contrast, 3×ASP cells moved equally frequently in all directions with or without cyclic substrate stretching stimuli (Figure 3-7B, E and H).

Relationship between myosin II accumulation and pseudopod dynamics

Images of free migration of E476K cells and *mhcA*$^-$ cells expressing GFP-myosin II under no stretching stimuli were recorded sequentially. Then, the values of F, l_1 and l_2 in Figure 3-1A and B were measured along the twelve directions in Figure 3-1C from the sequential images. In *mhcA*$^-$ cells expressing GFP-myosin II (Figure 3-8A), the l_2/l_1 values at high F values were lower than 1, suggesting that spontaneous myosin II accumulation triggered the pseudopod retraction. In contrast, in E476K cells (Figure 3-8B), the l_2/l_1 values at high F values were almost 1 although those at low F values were higher than 1, suggesting that the spontaneous localization of E476K myosin II did not trigger the pseudopod retraction but prevented their expansion.

Next, to reveal the relationship between myosin II accumulation and pseudopod dynamics under cyclic substrate stretching, the values of F_1, F_2, l_1 and l_2 in Figure 3-1D and E were measured along the six stretching directions in Figure 3-1F. The data presented in Figures 3-5 and 3-6 were used for this analysis. In all cases of wild-type, E476K and 3×ALA myosin II, the F_2/F_1 values were larger than 1 (Figure 3-8C, D and E), indicating that the cyclic substrate stretching in the left and right direction accumulated all of wild-type, E476K and 3×ALA myosin II along the edges of the cell in the left and right sides. In contrast, the l_2/l_1 values in E476K cells ranged around 1 (Figure 3-8E), although those in

mhcA^{-} cells expressing GFP-myosin II and 3×ALA cells were lower than 1 (Figure 3-8C and D). These results suggest that accumulation of myosin II and 3×ALA myosin II along the edges of the cell in the stretching direction induces the retraction of the pseudopods there. However, when E476K myosin II accumulated (F_2/F_1 values were larger than 2), the pseudopods neither retracted nor expanded there (l_2/l_1 values were almost 1).

3-5 Discussion

In this chapter, we observed actin filaments in *Dictyostelium* cells under cyclic substrate stretching. In the middle of the cell body, actin filaments did not align in a particular direction (Figure 3-5G). On the other hand, the density of actin filaments at any portion on the boundary of the cell continuously changed regardless of the stretching stimuli (Figure 3-5G). In contrast, myosin II accumulated "equally" along the two edges of the cell body (Figure 3-5A). In the case of slow-crawling cell types, it is well known that stress fibers are rearranged to the direction perpendicular to the stretching direction (Birukov et al., 2003; Morioka et al., 2011). Thus, the molecular dynamics in *Dictyostelium* cells in response to cyclic substrate stretching should differ from that in slow-crawling cells.

In fibroblasts, a typical slow-crawling cell, their adhesion sites receive mechanical stimuli from the substrate as deformation of focal adhesion proteins, such as focal adhesion kinase and p130Cas (Jiang et al., 2006; Sawada et al., 2006; Wang et al., 2001a). *SibA*$^{-}$ *Dictyostelium* cells respond to the cyclic substrate stretching stimuli and moved normally in a direction perpendicular to the stretching (Figure 3-4F), suggesting that *Dictyostelium* cells may receive mechanical stimuli from the substrate via their adhesion sites configured without SibA.

There may be several possibilities how myosin II accumulates in response to the cyclic substrate stretching. (1) Mechanical forces from the substrate are transmitted through their adhesion sites and deform some intracellular structures such as the actin cytoskeleton or (2) Mechanical forces induce activation of unknown mechanosensitive ion channels.

Deformation of actin filaments is one of the possible candidates to induce the myosin II accumulation, because filamentous actin meshwork is required for myosin II accumulation (Bosgraaf and van, 2006; Uyeda et al., 2011). The affinity of myosin II to actin filaments may be regulated by the tension, just as the affinity of cofilin to actin filaments increase by the relaxation of stretched actin filaments (Galkin et al., 2001). Recently, it was reported using *Dictyostelium* cells that stretching actin filaments enhances their affinity for myosin II (Uyeda et al., 2011). During cytokinesis, GFP-E476K myosin II accumulates in the equatorial region where the strain of the cell cortex should be maximum (Yumura and Uyeda, 1997). Myosin II is accumulated at the tip of the cell lobe formed by sucking using a micropipette (Merkel et al., 2000; Ren et al., 2009). These results suggest that the affinity of myosin II to actin filaments increases by the stretching of actin filaments. Unfortunately, the experiments in this chapter cannot distinguish which of the stretching or relaxation of the substrate induces the accumulation of myosin II.

Accumulation of GFP-E476K myosin II and directional preference of migration of E476K cells under cyclic substrate stretching indicate that actomyosin contraction is not required for those functions (Figures 3-6C and 3-7C). E476K myosin cannot hydrolyze ATP (Ruppel and Spudich, 1996). Majority of the heads of the mutants carry bound ATP and interact only weakly with actin filaments. Thus, the probability of the binding of an E476K myosin II monomer to actin is low. That of the thick filaments of E476K myosin II should be high enough to keep binding to the actin filaments, not only in migrating cells as in this chapter but also in dividing cells (Yumura and Uyeda, 1997). Accumulated E476K myosin II filaments seemed to locally prevent elongation of pseudopods (Figure 3-8), suggesting that accumulated myosin II thick filaments may cross-link actin filaments and stabilize the cell cortex.

Figures

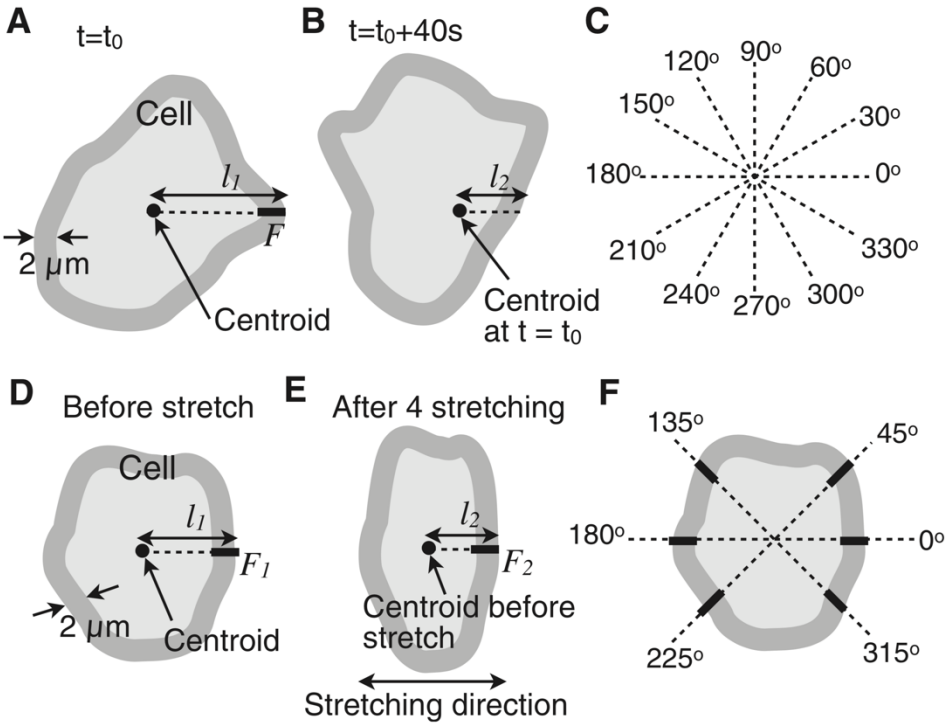

Figure 3-1. Evaluation of pseudopod dynamics and myosin II accumulation. (A – C) On a cover slip. The values l_1, l_2 and F were measured from two sequential images of A and B along the 12 dotted lines in C. F refers to the degree of spontaneous accumulation of myosin II. The value l_2/l_1 means the contraction or expansion of pseudopods. (D – F) Under cyclic substrate-stretching. The values l_1, l_2, F_1 and F_2 were measured from two images before and after four repeats of stretching using the microstretching device as shown in D and E along the 6 dotted lines in F. F_2/F_1 means the accumulation of myosin II in response to the four repeats of substrate-stretching.

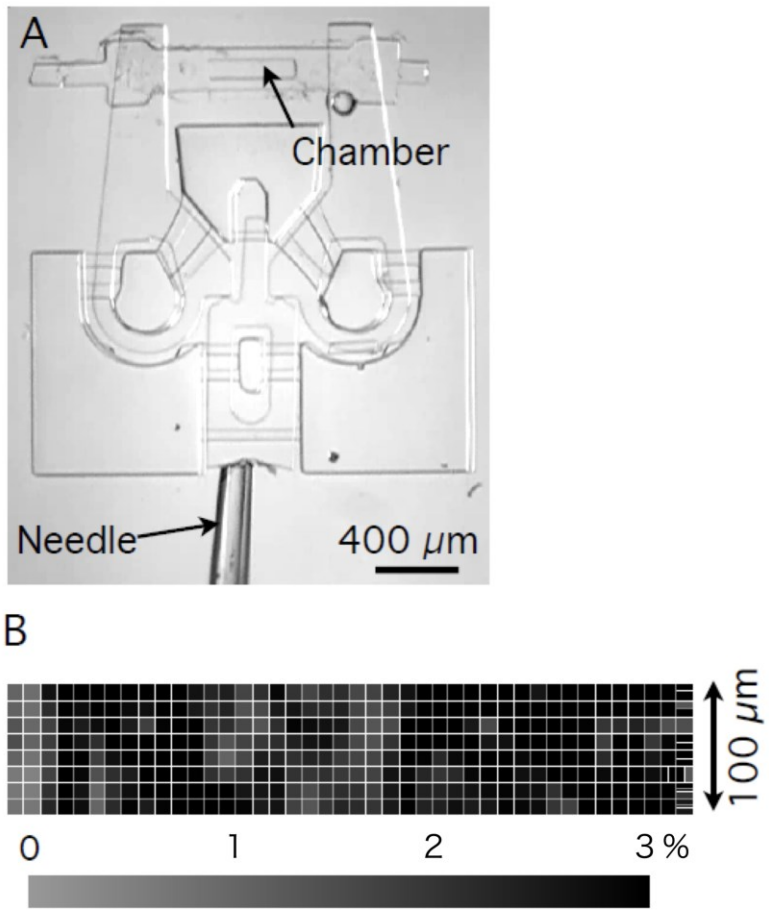

Figure 3-2. Microstretching device to detect the GFP fluorescence. (A) Overview. By pushing a bottom part of the device with a needle, the chamber is stretched in the left-right direction. Cells were plated onto the chamber area. (B) Strain distribution of the chamber are in A when left-right direction of the chamber is stretched by 26%.

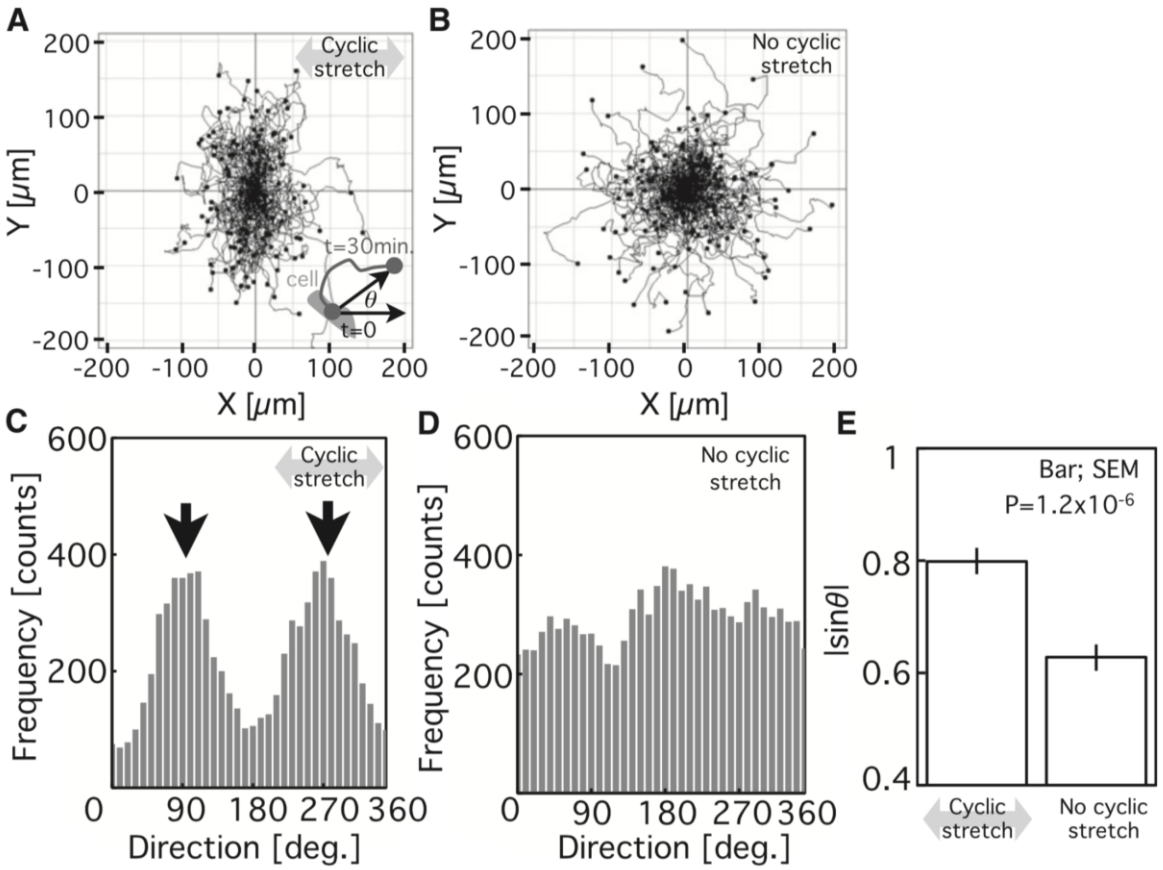

Figure 3-3. Movements of wild-type cells. (A) Trajectories of 120 cells under cyclic substrate stretching in the left-right direction obtained from 5 experiments. (B) Trajectories of 161 cells without cyclic substrate-stretching from 6 experiments. (C and D) Frequencies of migration-direction (θ) from the data in A and B, respectively. The value θ is defined as indicated in the inset in A. Peaks at 90 and 270˚ are indicated by arrows in C. (E) Average $|\sin\theta|$ values. The *p*-values were calculated using Student's t-test.

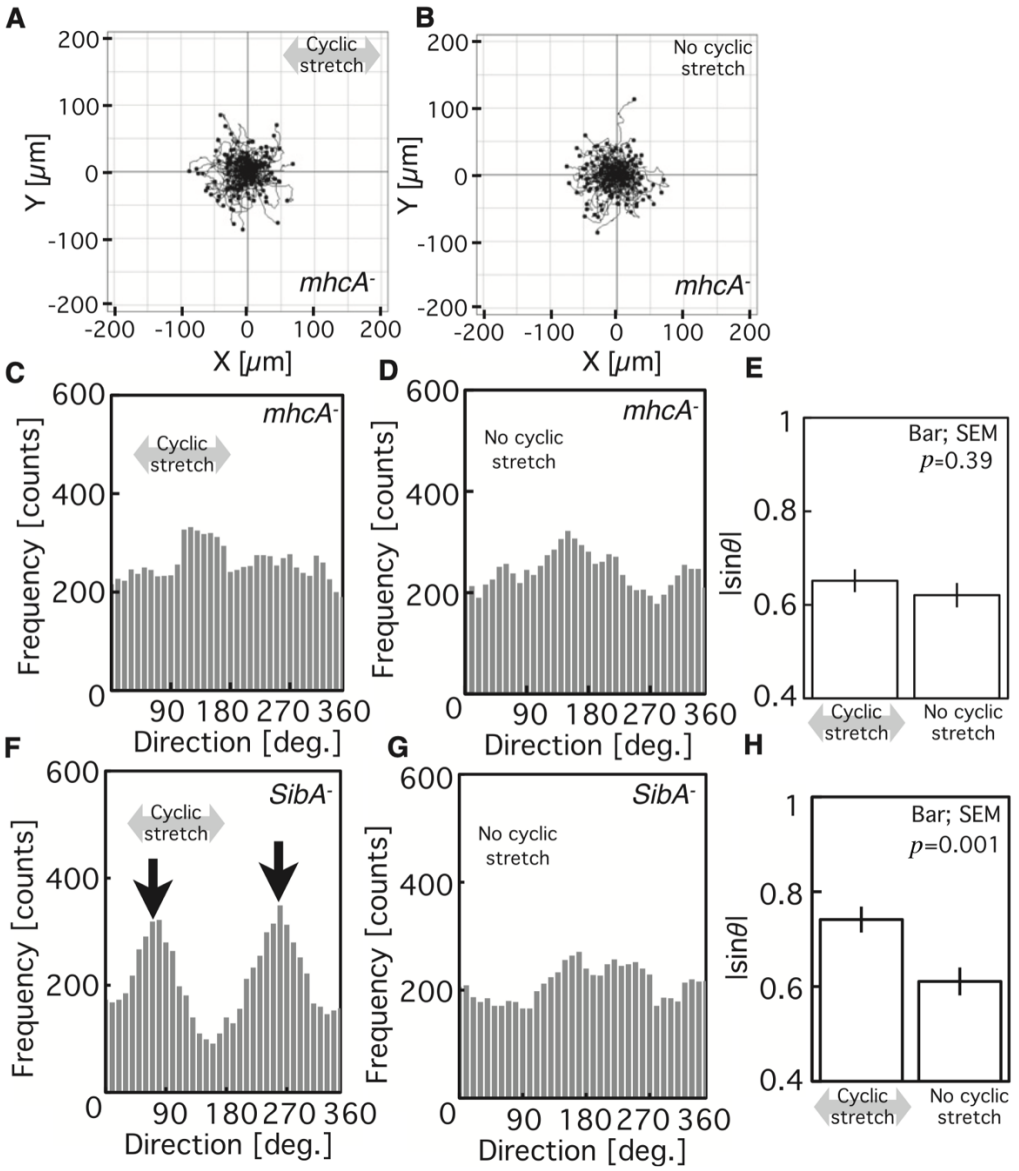

Figure 3-4. Movements of mutant cells. (A) Trajectories of 141 *mhcA*$^{-}$ cells under cyclic substrate stretching in the left-right direction from 5 experiments. (B) Trajectories of 132 *mhcA*$^{-}$ cells without cyclic substrate stretching, from 6 experiments. (C and D) Frequencies of migration-direction (θ) from the data in A and B. (E) Average $|\sin\theta|$ values from the data in C and D. (F) Frequencies of θ of 114 *SibA*$^{-}$ cells under cyclic substrate stretching from 6 experiments. (G) Frequencies of θ of 116 *SibA*$^{-}$ cells under cyclic substrate stretching from 6 experiments. (H) Average $|\sin\theta|$ values calculated from the data in F and G. The *p*-values were calculated using Student's t-test.

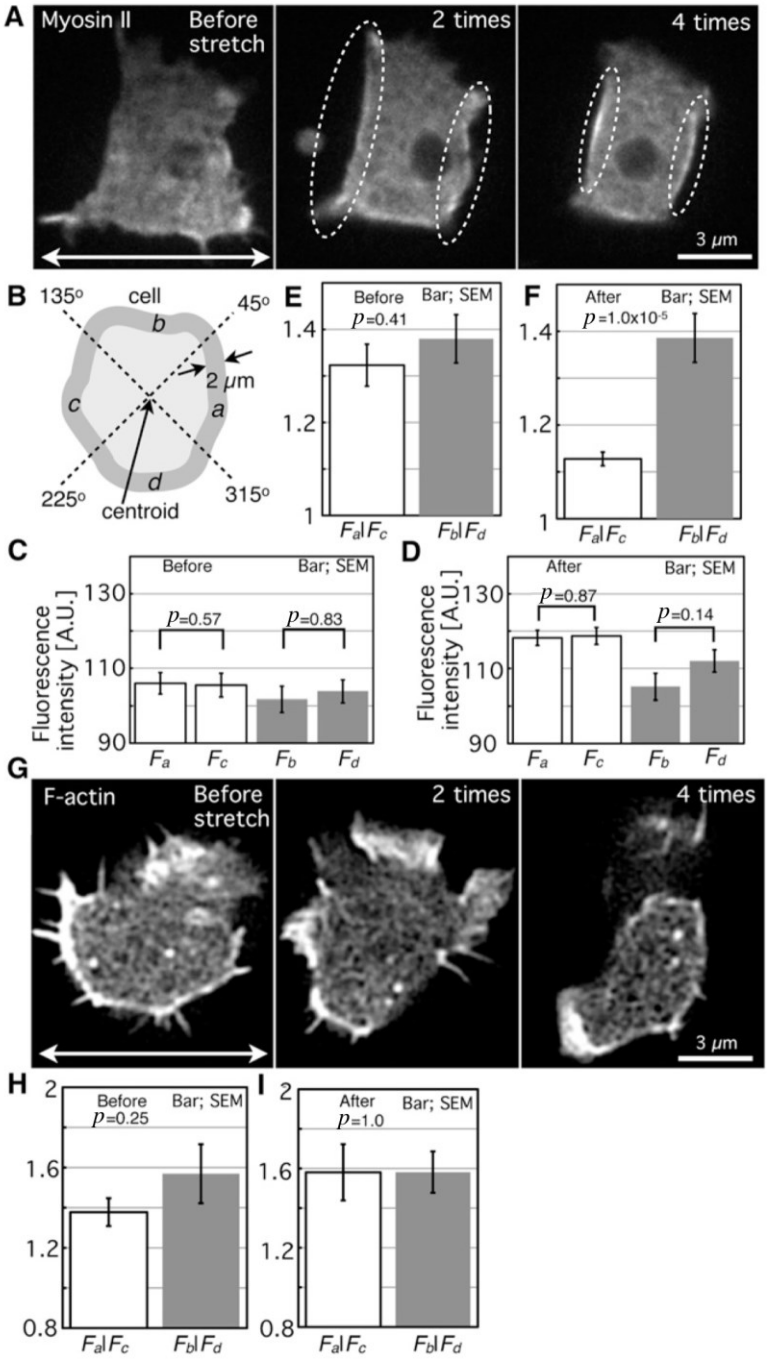
A
Myosin II
Before stretch
2 times
4 times
3 μm
B
135°
cell
45°
b
2 μm
c
a
d
225°
centroid
315°
E
Before
Bar; SEM
p=0.41
1.4
1.2
1
Fa|Fc
Fb|Fd
F
After
Bar; SEM
p=1.0x10-5
1.4
1.2
1
Fa|Fc
Fb|Fd
C
Before
Bar; SEM
Fluorescence intensity [A.U.]
130
110
90
p=0.57
p=0.83
Fa
Fc
Fb
Fd
D
After
Bar; SEM
Fluorescence intensity [A.U.]
130
110
90
p=0.87
p=0.14
Fa
Fc
Fb
Fd
G
F-actin
Before stretch
2 times
4 times
3 μm
H
Before
Bar; SEM
p=0.25
2
1.6
1.2
0.8
Fa|Fc
Fb|Fd
I
After
Bar; SEM
p=1.0
2
1.6
1.2
0.8
Fa|Fc
Fb|Fd

Figure 3-5. Molecular accumulations by cyclic substrate stretching. (A) GFP-myosin II. Left; before stretching, center; after two stretches, right; after four stretches. Double-headed arrow; stretch-direction. Dotted ovals; GFP-myosin II accumulations. (B – F) Quantitative evaluation of GFP-myosin II accumulation. (B) Definition of the four areas *a, b, c* and *d*. (C) F_i values before stretching. $F_a - F_d$ are the maximum fluorescence values of GFP-myosin II in *a*-*d* in B (n = 62). (D) F_i values after four stretches (n = 53). (E) $F_a|F_c$ and $F_b|F_d$ before stretching. $F_i|F_j$ is expressed as the larger of F_i and F_j divided by the smaller. (F) $F_a|F_c$ and $F_b|F_d$ after four stretches. (G) GFP-ABD120k. (H and I) Quantitative evaluation of GFP-ABD120k accumulation before stretching (H; n = 29) and after four stretches (I; n = 21). The *p*-values were calculated using Student's t-test.

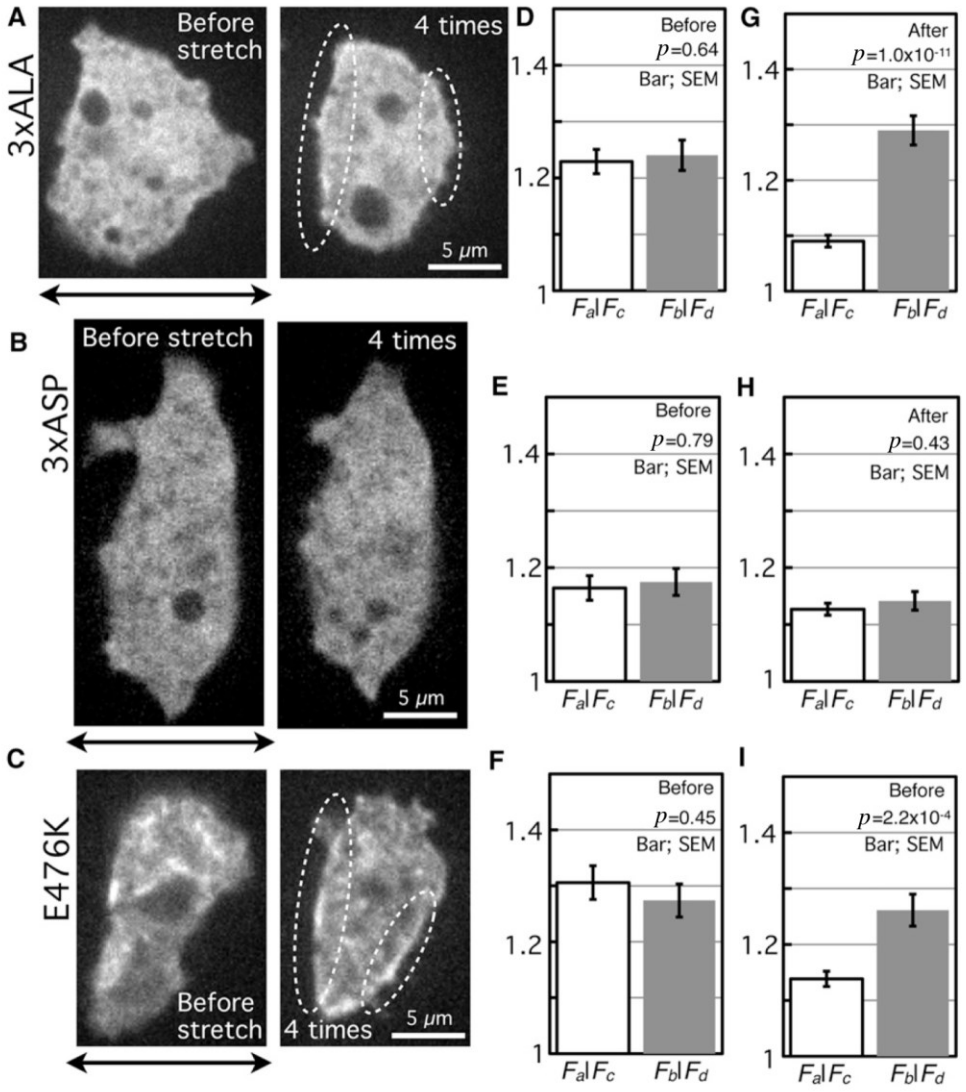

Figure 3-6. Accumulations of myosin II variants by cyclic substrate stretching. (A – C) GFP-3×ALA, GFP-3×ASP, and GFP-E476K myosin II. Left; before stretching, right; after four stretches. Double-headed arrows; stretch-direction. Dotted ovals; accumulations of myosin II variants. (D – I) Quantitative evaluations. The definition of $F_i|F_j$ is the same as those in Figure 3-5. From top to bottom, GFP-3×ALA, GFP-3×ASP, and GFP-E476K myosin II are shown. (D – F) Before stretching (GFP-3×ALA; n = 61, GFP-3×ASP; n = 66, GFP-E476K; n = 54). (G – I) After four stretches (GFP-3×ALA; n = 57, GFP-3×ASP; n = 63, GFP-E476K; n = 53). The *p*-values were calculated using Student's t-test.

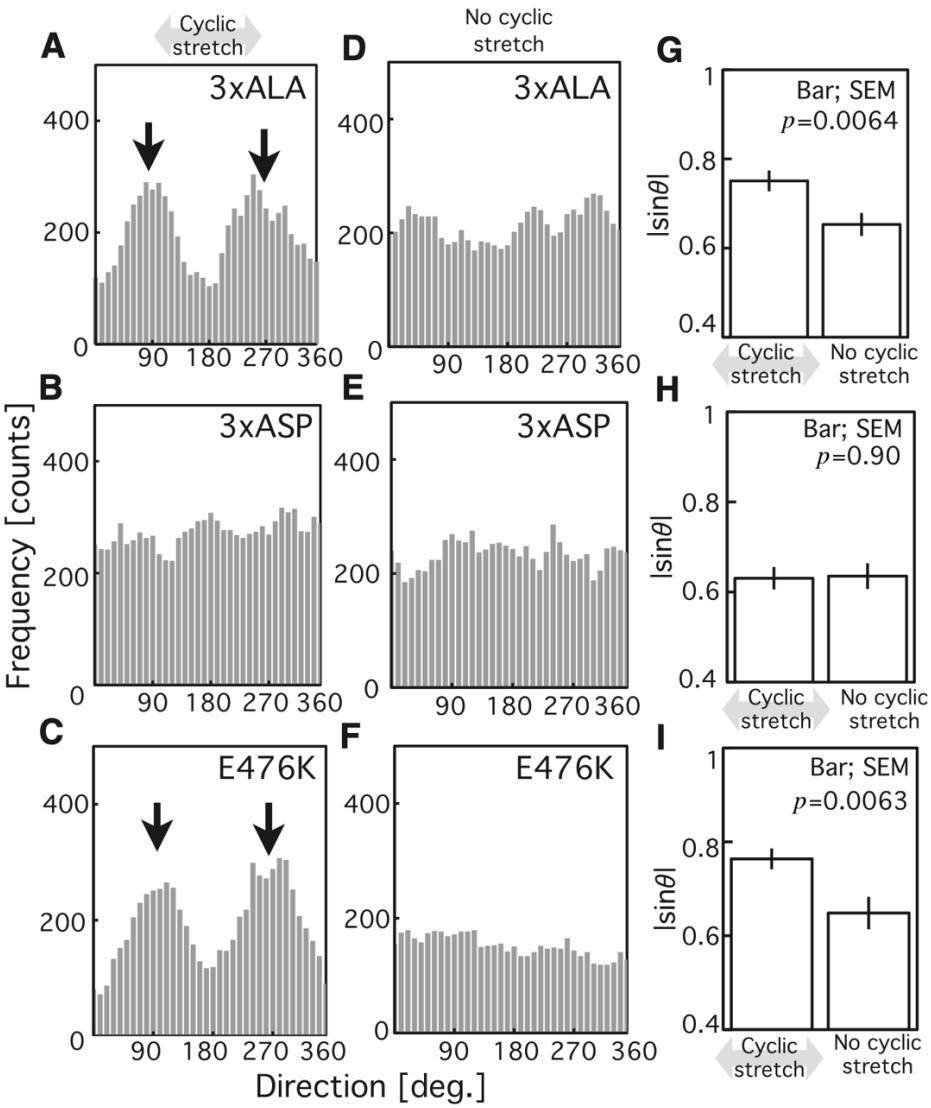

Figure 3-7. Movements of *mhcA*$^{-}$ cells expressing GFP-myosin II variants. (A – C) Frequencies of the migration-direction (θ) of 3×ALA, 3×ASP and E476K cells under cyclic substrate stretching. The data in A – C are compilation of 109 cells from 6 experiments, 149 cells from 8 experiments and 106 cells from 6 experiments, respectively. Peaks at 90 and 270˚ are indicated by arrows in A and C. (D – F) Frequencies of the migration-direction of 3×ALA, 3×ASP and E476K cells under no cyclic substrate stretching. The data in D – F are compilation of 119 cells from 8 experiments, 128 cells from 8 experiments and 83 cells from 5 experiments, respectively. (G – I) Average $|\sin\theta|$ values. The *p*-values were calculated using Student's t-test.

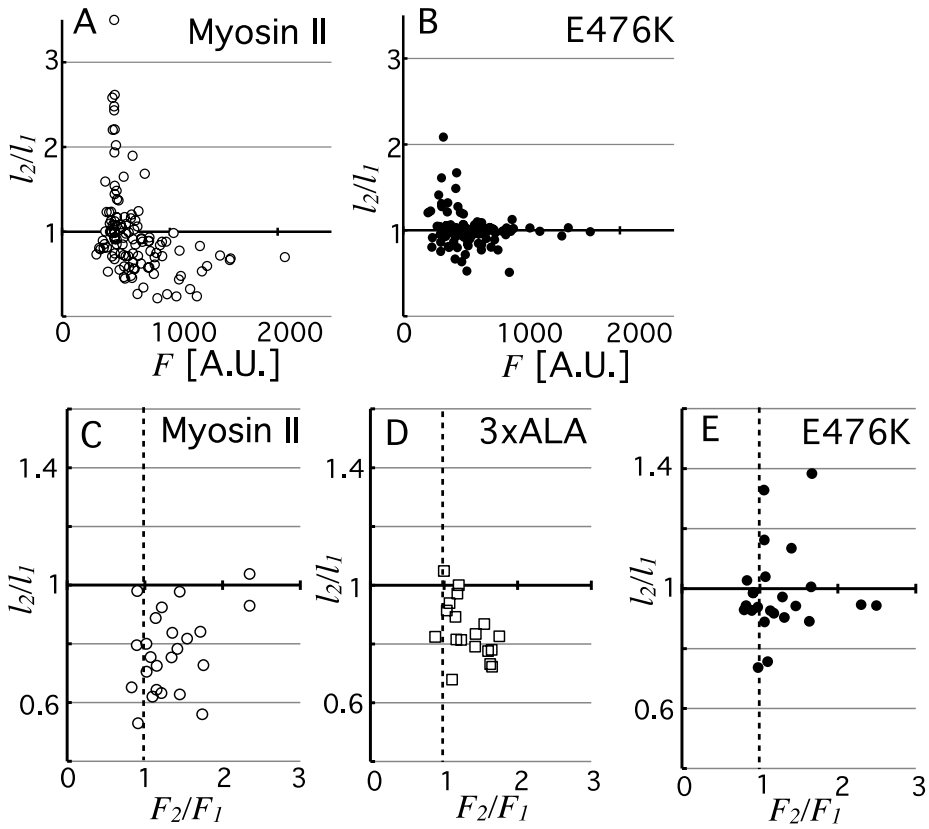

Figure 3-8. Accumulation of myosin II variants and pseudopod dynamics. (A and B) *mhcA*$^-$ cells expressing GFP-myosin II (A) or E476K (B) on a coverslip. The values l_1, l_2 and F were defined in Figure 3-1A - C. (C – E) *mhcA*$^-$ cells expressing GFP-myosin II (C), 3×ALA (D) and E476K cells (E) under cyclic substrate stretching. The values l_1, l_2, F_1 and F_2 were defined in Figure 3-1D - F.

Chapter 4

Directional Preference of Migration in Fast-Crawling Cell Types to Avoid the Direction of Cyclic Substrate Stretching

4-1 Abstract

In response to cyclic substrate stretching, *Dictyostelium discoideum* cells move in a direction perpendicular to the stretches. As the possible candidate mechanism for the origin of the directional preference in crawling migration, higher migration speed in the direction perpendicular to the stretches or the higher probability of a directional change to the perpendicular direction are considered. To determine which of the two mechanisms works, in this chapter, cyclic substrate stretching stimuli were applied to not only *Dictyostelium* cells but also neutrophil-like differentiated HL-60 cells. HL-60 cells accumulated myosin II along the both cell sides that were perpendicular to the stretch, and moved perpendicular to the stretches, which was similar to *Dictyostelium* cells. Analysis of the trajectories of and *Dictyostelium* cells and HL-60 cells showed that the higher probability of directional change to the direction perpendicular to the stretches was the origin of the directional preference in both cell-types. This directional preference of migration seems to be a property common to fast-crawling cell types.

4-2 Introduction

Crawling cells receive mechanical information from the substrate, because they cannot move without adhering to the substrate. As mentioned in Chapter 3, one of the most useful techniques to investigate the relationship between a mechanical signal from substrates and related cell functions is cyclic substrate stretching (Crosby et al., 2011; Desai et al., 2010; Naruse et al., 1998b). In the case of slow-crawling cell types, stress fibers rearrange themselves to the direction perpendicular to the stretches and the shape of the cells extends in the perpendicular direction (Birukov et al., 2003; Kaunas et al., 2005; Lee et al., 2010; Morioka et al., 2011; Sato et al., 2005; Tondon et al., 2012; Zhao et al., 2011). In contrast, in the case of fast-crawling cell types, it was found recently that *Dictyostelium* cells preferentially migrate perpendicular to the direction of cyclic substrate stretching as (Iwadate and Yumura, 2009a). In Chapter 3, it was revealed that the directional preference of migration in *Dictyostelium* cells is induced by a myosin II-dependent process.

These findings in *Dictyostelium* cells raise two new questions: (1) Is this directional preference of migration under cyclic substrate stretching limited to *Dictyostelium* cells, or is it common in other fast-migrating cell types? and (2) How do the cells realize directional preference of migration perpendicular to the stretching direction? As an answer to the second question, there are two possible origins of the directional preference of migration. One is that the migration speed in the direction perpendicular to the stretches is higher than that in parallel directions. The other is that the probability of a directional change from parallel to perpendicular to the stretches is higher than that of a change from perpendicular to parallel.

In this chapter, to answer these two questions (1) and (2), crawling migration of neutrophil-like differentiated HL-60 cells under cyclic substrate stretching was observed. Hl-60 cells also preferred to migrate perpendicular to the stretches. Then, detailed analysis of the trajectories of both cell types was carried out to clarify the origin of the directional preference of migration. The results in this chapter suggested that at least two fast-crawling cell types, namely HL-60 and *Dictyostelium* cells, share a common directional preference of migration perpendicular to the stretches, the main cause of which is the high probability of a directional change of migration to perpendicular to the stretch direction.

4-3 Materials and Methods

HL-60 Cell line

Preparation of HL-60 cells was described in Chapter 2.

Cyclic substrate stretching

Elastic substrates were made according to the methods described in Chapter 3. The surface of the substrates was coated with 50 μg/ml fibronectin in PBS (354008, BD Japan) to optimize for HL-60 cells. Cyclic substrate stretching was performed according to the methods described in Chapter 3. In changing the cycle times of cyclic substrate stretching, the velocities of stretching and relaxation were kept constant, and the duty ratio of stretch and shrinkage was also kept at 1:1.

Statistical analysis of cell migration

The analysis was performed according to the methods described in Chapter 3 (inset in Figure 3-3A). Migration speeds in the perpendicular and parallel directions to the stretches, and the probabilities of a directional change from perpendicular to parallel and vice versa, were estimated according to methods described in Chapter 2 (Figure 2-6A) with a minor modification. Briefly, as shown in Figure 4-1, “rigid” and “soft” directions in Figure 2-6A should be changed to the directions “parallel” and “perpendicular” to the stretches, respectively.

Trajectory data for *Dictyostelium* cells

Some trajectory data of RI9 *Dictyostelium* cells (Insall et al., 1994) under cyclic substrate stretching of a 10-s cycle time and different stretch ratios (zero, 10, 20 and 30%), and a 5-s cycle time and 20% stretching ratio ware obtained in a previous study (Iwadate and Yumura, 2009a). Trajectory data of RI9 cells, cAMP receptors-knockout *Dictyostelium* cell line, under 20% stretching ratio and 20-s cycle time were obtained by new experiments in this chapter.

Staining of filamentous actin and myosin IIA in HL-60 cells

Differentiated HL-60 cells mainly express the IIA isoform of myosin II (Shin et al., 2010). The staining of filamentous actin and myosin IIA was performed according to the methods described previously (Miyoshi and Adachi, 2012; Okeyo et al., 2009) with minor modifications. Briefly, cells were fixed with 4% paraformaldehyde in PBS for 15 min, permeabilized with 0.1% Triton X-100 in PBS for 10 min, and blocked with 0.2% gelatin in PBS for 30 min. The cells were then incubated with Alexa Fluor 488 phalloidin (0.33 U/ml, A12379; Life Technologies) and/or primary antibody: rabbit polyclonal anti-myosin IIA (1:200 dilution, M8064; Sigma-Aldrich, St Louis, MO) for 60 min. After several washes with 0.2% gelatin in PBS, the cells were incubated with secondary antibody: Alexa Fluor 546 Anti-rabbit IgG (1:2000 dilution, A-11071, Life Technologies) for 60 min. Fixation and staining were all carried out at room temperature.

Evaluation of myosin IIA distribution in fixed HL-60 cells

The analysis was performed according to the methods described in Chapter 3 (Figure 3-5B).

4-4 Results

Crawling migration of HL-60 cells perpendicular to the direction of cyclic substrate stretching

First, HL-60 cells were dispersed on an elastic substrate with cyclic stretching of a fixed stretch ratio (15%) and different cycle times (7.5, 15 and 30 s). Figure 4-2A – D show the trajectories of crawling cell migration under each cycle time and that under no cyclic substrate stretching stimulus. Figure 4-3A – D show the frequencies of each migration-direction (θ; inset in Figure 3-3A) calculated from the data in Figure 4-2A – D. The cells tended to migrate in a direction perpendicular to the stretches (90˚ or 270˚) when subjected to cyclic substrate stretching (Figures 4-2B – D, 4-3B – D), whereas they migrated equally frequently in all directions under no cyclic stretching (Figures 4-2A, 4-3A).

Figure 4-4A shows the $|\sin\theta|$ values calculated from the data in Figure 4-3A – D. The shorter cycle time, the higher the $|\sin\theta|$ value. These results indicate that HL-60 cells sense cyclic substrate stretching stimuli and migrate perpendicular to the stretching direction.

Next, we examined the effect of stretch ratio on the directionality of crawling migration of HL-60 cells. Crawling migration was analyzed under the cyclic substrate stretching of a fixed cycle time (15 s) and different stretch ratios (zero, 7.5, 15 and 30%). Figures 4-3A, C, E and F, and 4-4B show migration-directions under each stretch ratio, and the $|\sin\theta|$ values calculated from the data in Figure 4-2A, C, E and F. As shown in Figure 4-4B, the higher the stretch ratio, the higher the $|\sin\theta|$ value, indicating the directional preference of migration is positively correlated with the stretch ratio, as was the cycle time dependency (Figure 4-4A).

Migration velocities parallel or perpendicular to the direction of cyclic substrate stretching

To test whether cyclic substrate stretching affects the migration velocity for each direction, the velocity in each direction was calculated under various stretch conditions of HL-60 cells (Figure 4-5). Slight but statistically significant differences in migration velocity between the parallel direction (//) and the perpendicular direction ($\perp$) were obtained only in the case of the shortest cycle time (Figure 4-5D) and the highest stretch ratio (Figure 4-5F).

Next, to test whether this situation is common in *Dictyostelium* cells, we calculated the migration velocities of RI9 *Dictyostelium* cells under cyclic substrate stretching with various stretch conditions (Figure 4-6). RI9 cells are totally insensitive to cAMP. Thus, it is presumed that the direction of migration is determined only by the force from the substrate, not chemotaxis. In the case of *Dictyostelium* cells too, only with highest stretch ratio of 30%, the velocity in the perpendicular direction ($\perp$) was statistically significantly higher than that in the parallel direction (//), with only a small difference seen (Figure 4-6F).

These results indicate that cyclic substrate stretching induces little difference in the migration velocity of fast-crawling cell types between the perpendicular and the parallel directions.

Directional change of migration, the main cause of directional preference of crawling migration

First, the trajectories of HL-60 cells under cyclic substrate stretching were analyzed. Probabilities of

directional change from perpendicular to parallel (Figure 4-7A) and that from parallel to perpendicular (Figure 4-7B) were calculated under a range of stretch conditions (Figure 4-7C and D). When the stretch ratio was fixed at 15%, the probability from perpendicular to parallel did not change at a 15-s cycle time or longer (red columns in Figure 4-7C). Only at a cycle time of 7.5 s, the probability decreased (* in Figure 4-7C). The probability of from parallel to perpendicular increased with shortening the cycle time (blue columns in Figure 4-7C). In contrast, when the cycle time was fixed at 15 s, the probability from perpendicular to parallel did not change at stretch ratios of 15% or smaller (red columns in Figure 4-7D). Only at a 30% stretch ratio, the probability decreased (* in Figure 4-7D). The probability from parallel to perpendicular increased with increasing the stretch ratio (blue columns in Figure 4-7D).

The probability of directional change of crawling migration was also calculated from the trajectories of RI9 *Dictyostelium* cells. The resultant graphs (Figure 4-7 E and F) show the same characteristics as those of HL-60 cells. At a 20% stretch ratio, the probability from perpendicular to parallel did not change at a 10-s cycle time or longer (red columns in Figure 4-7E). Only at a cycle time of 5 s, the probability decreased (* in Figure 4-7E). As with HL-60 cells, the probability from parallel to perpendicular increased with shortening cycle time (blue columns in Figure 4-7E). On the other hand, at a 10-s cycle time, the probability from perpendicular to parallel did not change at stretch ratios of 20% or smaller (red columns in Figure 4-7F). Only at a 30% stretch ratio, the probability decreased (* in Figure 4-7F). The probability from parallel to perpendicular increased with increasing stretch ratio (blue columns in Figure 4-7F).

Myosin IIA localization in HL-60 cells caused by cyclic substrate stretching

To change the migration direction from parallel to perpendicular, cyclic substrate stretching stimuli should affect where in the migrating HL-60 cells actin polymerization or actomyosin contraction takes place. To examine which of them is affected by the cyclic stretching stimuli, we fixed the cells after 30 min of cyclic stretching stimuli at a 15% stretch ratio and 15-s time cycles and simultaneously stained myosin IIA with antibody and F-actin with Alexa phalloidin. Typical localizations of myosin IIA and F-actin are shown in Figure 4-8A – D. In response to the cyclic substrate stretching in left-right direction, myosin IIA appeared to localize equally along both edges of the left and the right sides in the cell (I and III in Figure 4-8).

The localization of myosin IIA was estimated quantitatively (Figure 4-8E and F). The ratio of the greater to the smaller fluorescence intensity of myosin IIA in the left-right pair ($F_I|F_{III}$ in Figure 4-8E) was significantly less than that in the top-bottom pair ($F_{II}|F_{IV}$ in Figure 4-8E) and those ($F_I|F_{III}$ and $F_{II}|F_{IV}$ in Figure 4-8F) without cyclic substrate stretching, indicating that left-right symmetrical forces induce the localization of myosin IIA at a similar level.

In contrast, actin filaments appeared to localize randomly, irrespective of cyclic substrate stretching (Figure 4-8C and D). The localizations of actin filaments (Figure 4-8G and H) were estimated in the same way as for myosin IIA. There was no significant difference in the ratios of the greater to the smaller fluorescence intensity of F-actin between the left-right pair ($F_I|F_{III}$ in Figure 4-8G) and the top-bottom

pair ($F_{II}|F_{IV}$ in Figure 4-8G). Without cyclic stretching too, there was no significant difference in the two pairs (Figure 4-8H). These results strongly suggest that the almost equal localization of myosin IIA along left and right sides is the cause of preferential migration perpendicular to the direction of stretching, as is the case with *Dictyostelium* cells described in Chapter 3.

4-5 Discussion

HL-60 cells showed preferential migration in a direction perpendicular to the stretch, in response to cyclic substrate stretching (Figure 4-2). As described in Chapter 3, this reaction is the same as that seen in the other fast-crawling cell type, *Dictyostelium*, suggesting that the reaction is not limited to a particular cell type but may be common in fast-crawling cells, including HL-60 cells and *Dictyostelium* cells. This directional preference of migration appears to be a strategy adopted by fast-crawling cell types in which they do not enhance actin polymerization to go faster where they want to go, but localize myosin II to avoid a direction they do not want to go. A possible merit that the fast-crawling cells generate directional preference of migration via mechanosensing will be described later in Chapter 7.

In both HL-60 cells and *Dictyostelium* cells, the probability of a directional change to perpendicular direction raised on increasing the stretch ratio or on decreasing the cycle time (blue columns in Figure 4-7C-F). In contrast, the velocity in the perpendicular direction also became significantly higher than that in the parallel direction only when subjected to strong cyclic stretching stimuli (Figures 4-5D, F and 4-6F). Such strong stimuli may cause the stretching sides of the cells to peel off from the substrate, decreasing the velocity in the parallel direction, and reducing the probability of a directional change to parallel migration (*s in Figure 4-7). Thus, the main cause for preferential crawling migration perpendicular to the stretches should be a rise in the probability of a directional change to perpendicular. This agrees closely with the results showing that myosin IIA is localized equally along both stretching sides (Figure 4-8A and E, and Figure 3-5A in Chapter 3) because the portion where myosin II localizes is the rear in freely-crawling cells (Shin et al., 2010).

The aim of this study was to clarify the common behavior in fast-crawling cell types related to the forces from the substrates by means of trajectory analysis. We did not study here the signaling cascade in detail. Thus, the mechano-sensor molecules which respond to the forces from the substrate and the subsequent signal transduction pathway are unknown, although myosin II was found to be present in the pathway. Structural change of actin filaments such as extension of helical pitch of them is a possible candidate for increasing myosin II affinity, since an actin meshwork is required for myosin II localization (Bosgraaf and van, 2006; Uyeda et al., 2011).

In this chapter, we revealed that the direction of two fast-crawling cell types, namely HL-60 cells and *Dictyostelium* cells, can be artificially controlled by applying force via the substrate. Although the cells do not receive such mechanical stimulation under actual physiological conditions, they receive the forces from the substrate caused by their own traction forces. Thus, the artificial mechanical stimulation to the cell are useful to know the relationship between the cell migration and mechanical signal from the substrate. The reaction forces are likely to depend on the rigidity of the substrate. As shown in Figure 2-2A in Chapter 2, we revealed that *Dictyostelium* cells exert larger traction forces on the rigid substrate than on the soft one. This situation is the same with neutrophils (Shin et al., 2010). Sensing such reaction forces has been proposed as “active touch” (Kobayashi and Sokabe, 2010). Durotaxis in the slow-crawling cell types (Jiang et al., 2006; Lazopoulos and Stamenović, 2008; Lo et al., 2000) and preferential migration of fast-crawling cell types in the soft direction as demonstrated in Chapter 2 should be examples of active touch. For a detailed mechanism of how myosin II localizes in response to the force from the substrate, our hypothesis will be discussed in Chapter 7.

Figures

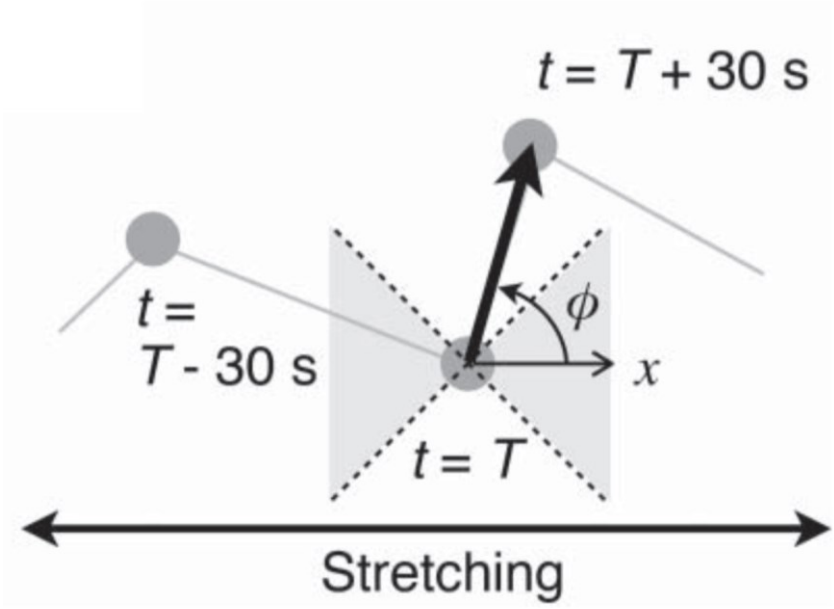

Figure 4-1. Definition of migration direction. A vector from a center of a cell at $t = T$ to that at $t = T + 30$ s was defined (thick arrow). The angle between the x-axis (x) and the vector was defined as the migration direction (φ) at $t = T$. When φ was between 315 and 45˚ or between 135 and 225˚ (gray regions), the migration direction was defined as "parallel" to the stretching direction, and when it was between 45 and 135˚ or between 225 and 315˚ (white regions), it was defined as "perpendicular."

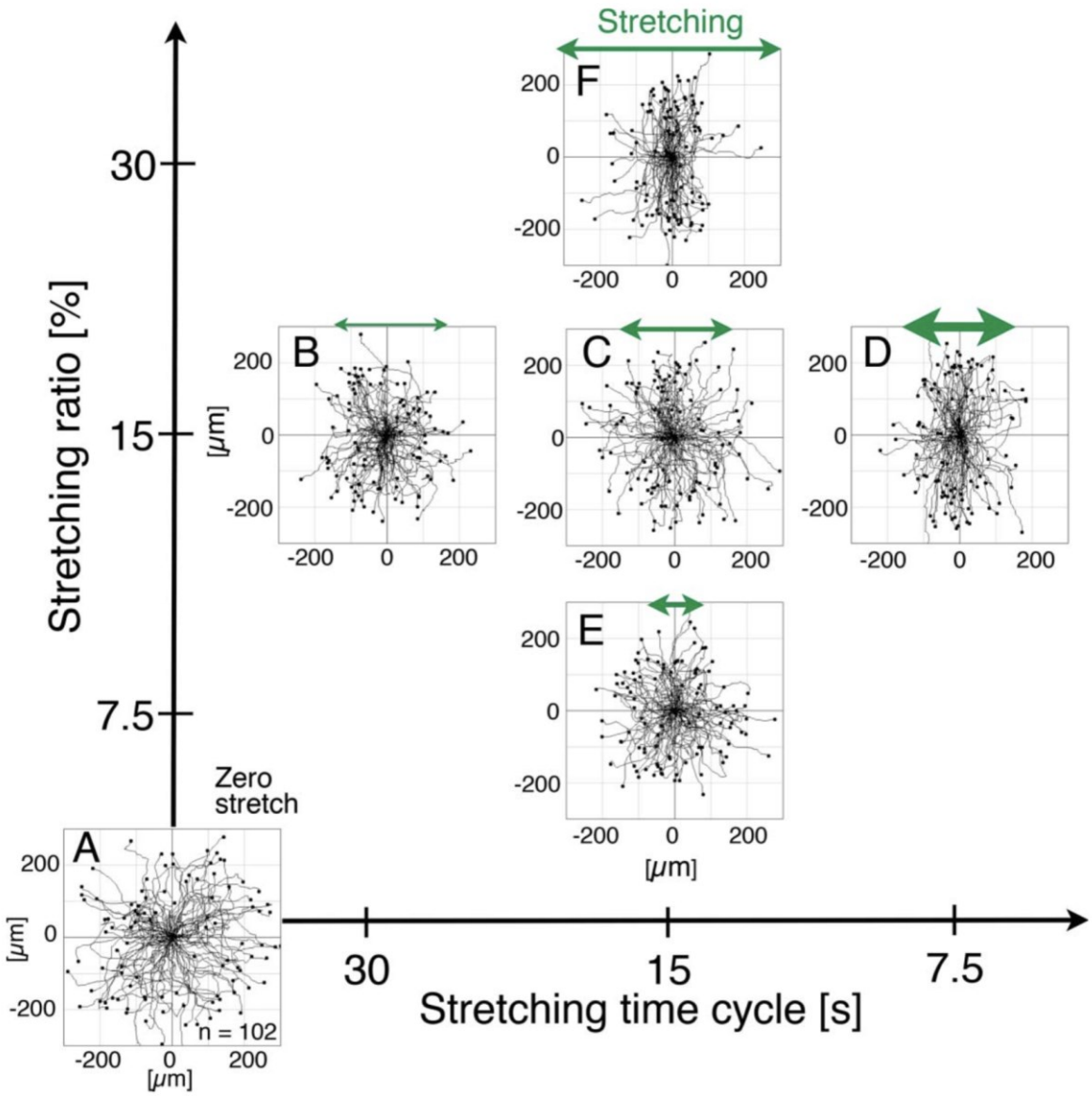

Figure 4-2. Migration trajectories of HL-60 cells for 30 min. Stretch ratio and cycle time in each graph (A - E) are shown in x- and y-axis of the large coordinate. (A) Without cyclic stretching (n = 102 from 4 trials). (B) Cyclic stretching at 15% stretch ratio and 30-s cycle time (n = 101 from 4 trials). (C) 15% and 15 s (n = 103 from 4 trials). (D) 15% and 7.5 s (n = 101 from 4 trials). (E) 7.5% and 15 s (n = 101 from 5 trials). (F) 30% and 15 s (n = 101 from 4 trials). Stretch conditions are shown as green double-headed arrows. Thickness and length of the arrows mean frequency and stretching ratio, respectively.

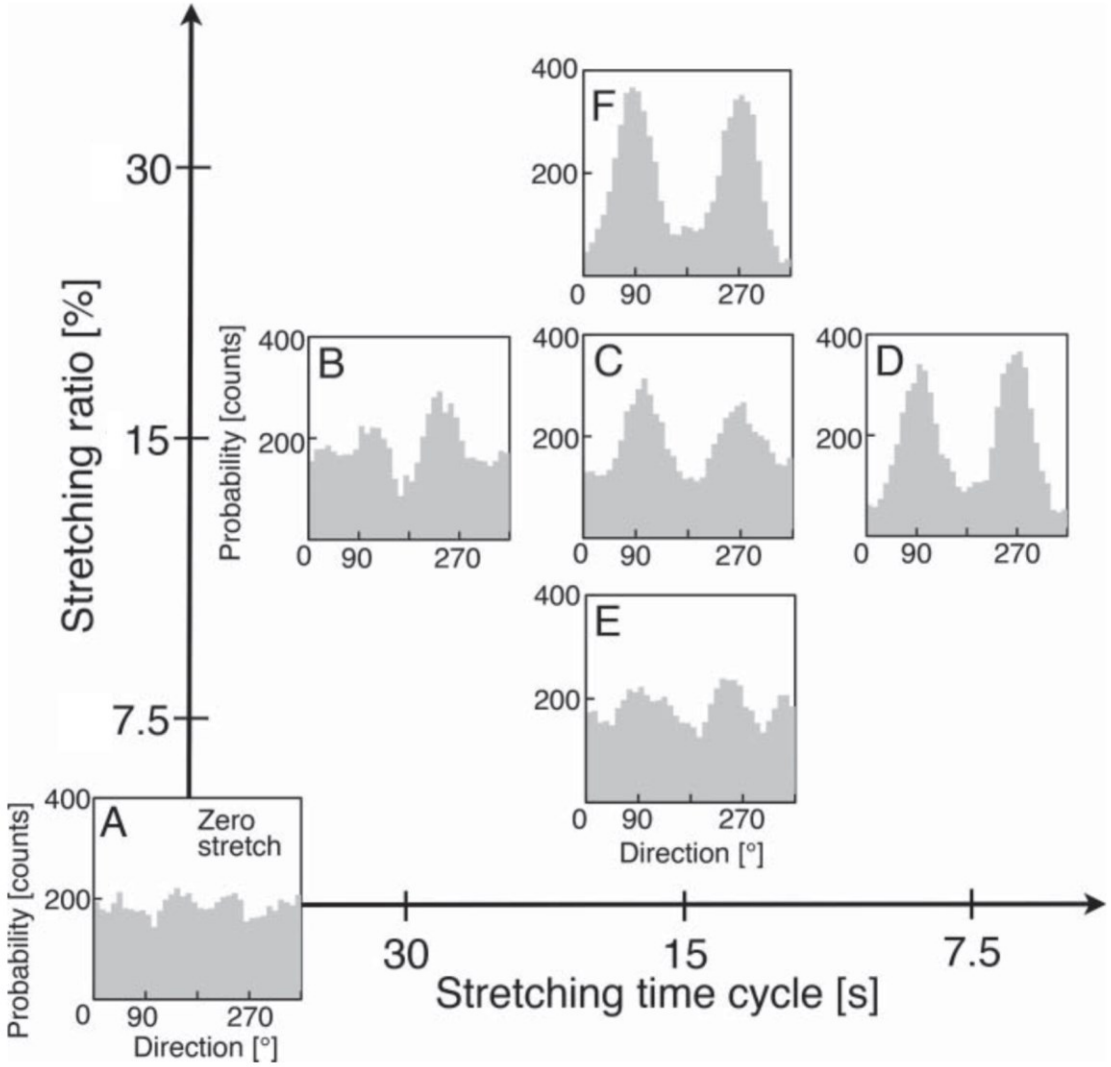

Figure 4-3. Frequencies of migration direction (θ) of HL-60 cells. (A – F) Calculated from the corresponding trajectories in Figure 4-2.

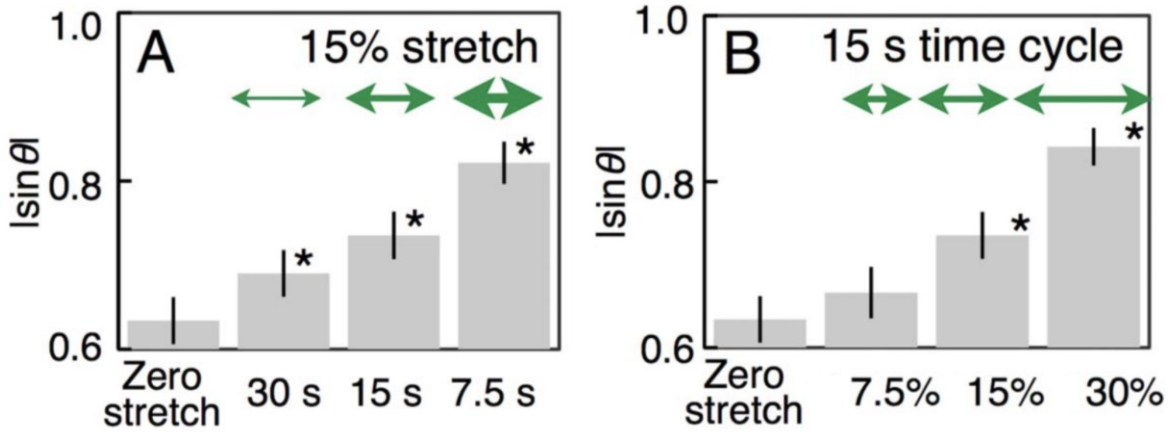

Figure 4-4. |sinθ| values of HL-60 cells. (A) Cyclic stretching with a 15% stretch ratio and zero, 30, 15 and 7.5-s cycle times (n = 102, 101, 103 and 101 from the left). (B) Cyclic stretching with a 15-s cycle time and zero, 7.5, 15 and 30% stretch ratios (n = 102, 101, 103 and 101 from the left), Mean ± SEM are shown. *$p < 0.05$, compared with 'Zero stretch' using the Tukey-Kramer test.

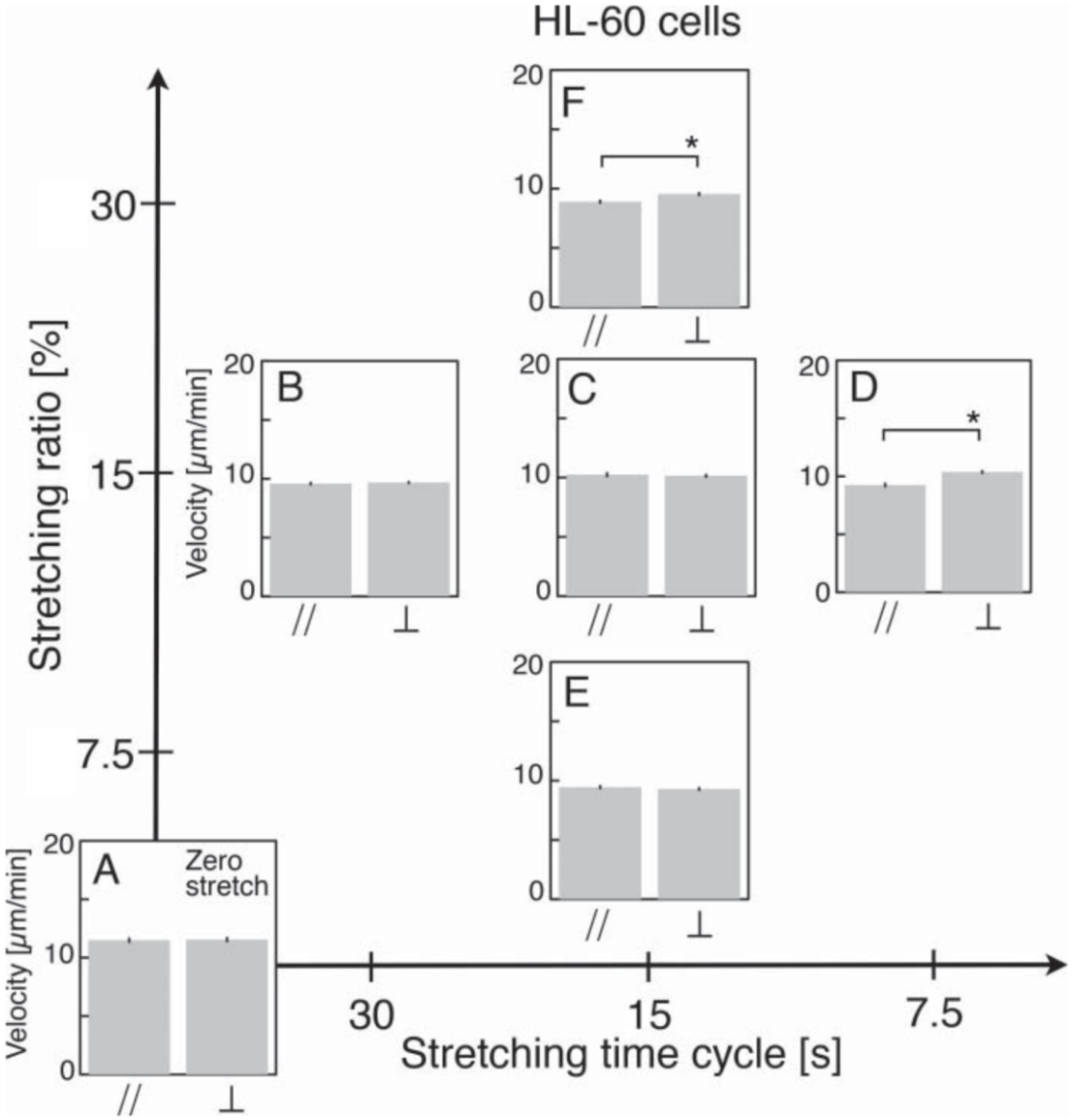

Figure 4-5. Velocity of HL-60 cells. (A – F) Calculated from the corresponding trajectories in Figure 4-2. The symbols "//" and "⊥" mean the parallel and the perpendicular to the stretching direction, respectively. Mean ± SEM are shown. *$p < 0.05$ using Welch's *t*-test.

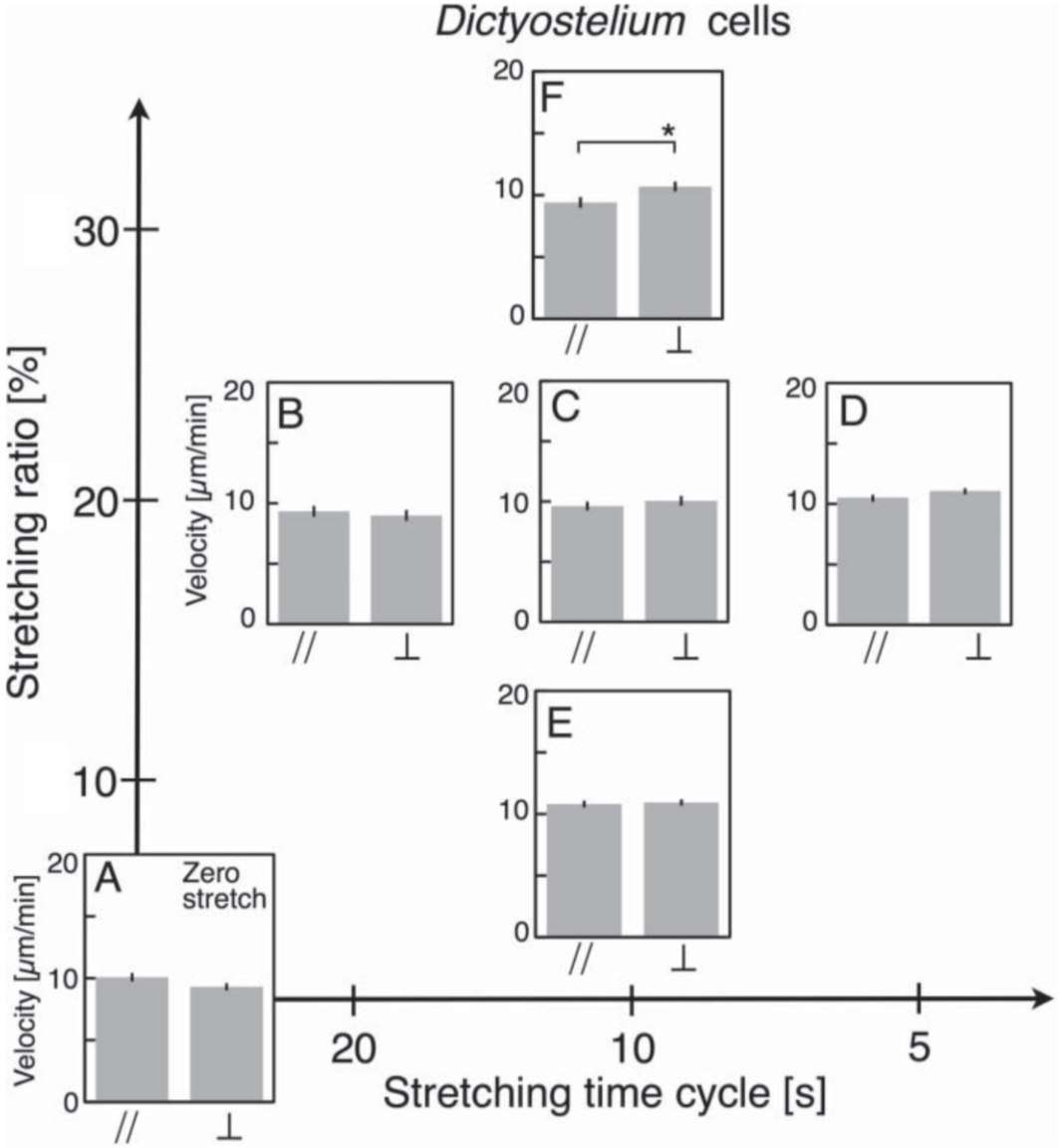

Figure 4-6. Velocity of RI9 *Dictyostelium* cells. (A, C – F) Calculated from the trajectory data, Figures 2F, 3C, G, A and E in the previous study (Iwadate and Yumura, 2009b), respectively. (B) Calculated from the data newly obtained in this study. n = 55, 54, 61, 85, 89 and 50 cells from A to F. Mean ± SEM are shown. *$p < 0.05$ using Welch's *t*-test.

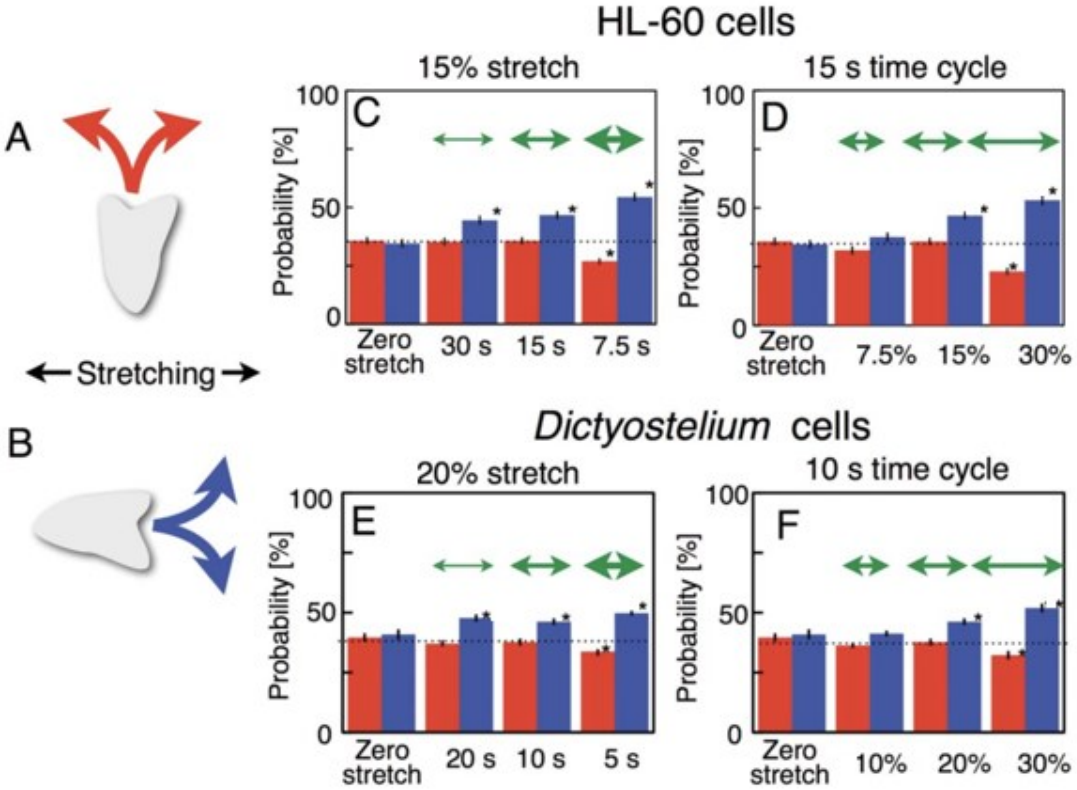

Figure 4-7. Probability of a directional change in HL-60 cells and RI9 *Dictyostelium* cells. (A and B) Schematic illustration of a directional change from perpendicular to parallel to the stretch direction (A) and vice versa (B). (C) HL-60 cells with a fixed 15% stretch ratio. (D) HL-60 cells with a fixed 15-s cycle time. (E) *Dictyostelium* cells with a fixed 20% stretch ratio. (F) *Dictyostelium* cells with a fixed 10-s cycle time. Color of each column in C - F corresponds to the A and B. Dotted lines in C – F mean the average of red and blue columns at zero stretch. Data represents mean ± SEM (C: n = 102, 101, 103 and 101 cells, D: n = 102, 101, 103 and 101 cells, E: n = 55, 54, 61 and 85 cells, F: n = 55, 89, 61 and 50 cells from the left). * $p < 0.05$, compared with zero stretch using the Tukey-Kramer test.

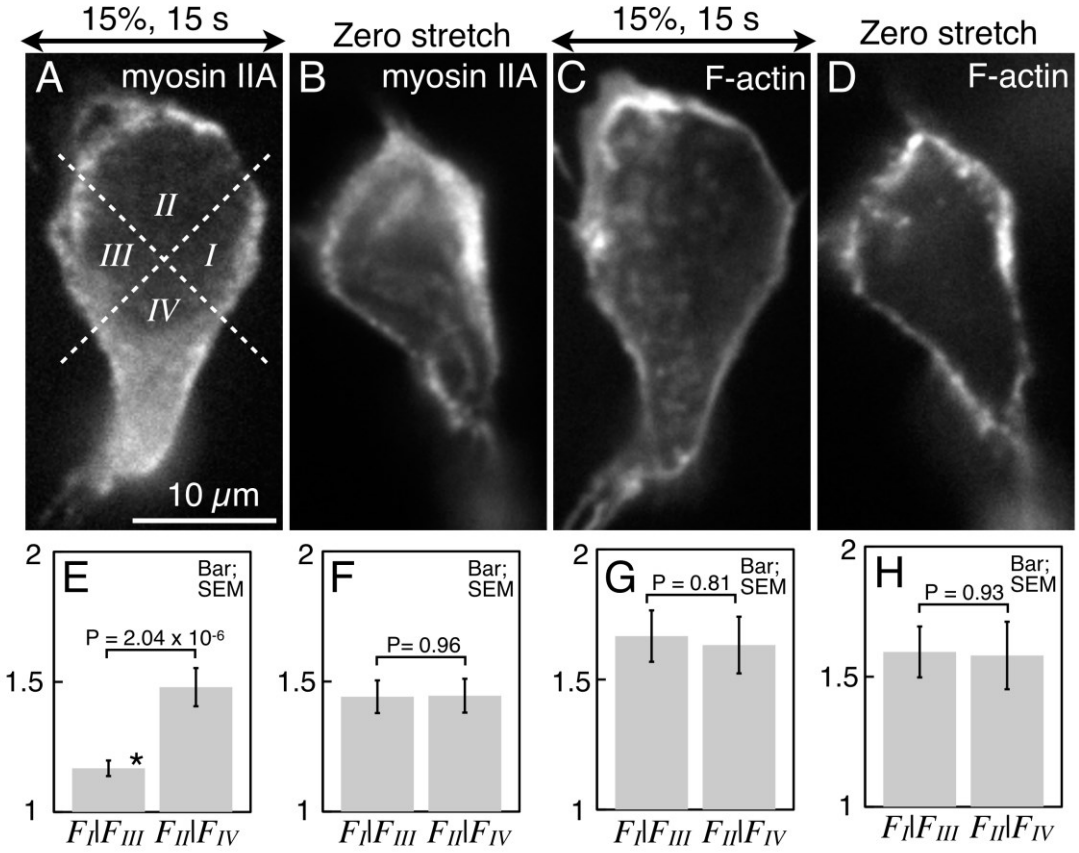

Figure 4-8. Localization of myosin IIA and actin filaments in HL-60 cells caused by cyclic substrate stretching in the left-right direction. (A) Localizations of myosin IIA after 30 min of cyclic substrate stretching at a 15% stretch ratio and 15-s time cycle (typical from 33 cells). (B) Those with zero cyclic stretching (typical from 32 cells). (C and D) Typical localizations of actin filaments in the same cells of A and B, respectively. (E) $F_I|F_{III}$ and $F_{II}|F_{IV}$ for myosin IIA after cyclic stretching. (F) $F_I|F_{III}$ and $F_{II}|F_{IV}$ for myosin IIA with zero cyclic stretching. (G) $F_I|F_{III}$ and $F_{II}|F_{IV}$ for actin filaments after cyclic stretching. (H) $F_I|F_{III}$ and $F_{II}|F_{IV}$ for actin filaments with zero cyclic stretching. Data represent mean ± SEM (E and G; n = 33 cells. F and H; n = 32 cells. *$p < 0.05$, Welch's t-test).

Chapter 5

Bidirectional Migration of Fish Keratocytes in Response to Cyclic Substrate Stretching

5-1 Abstract

Crawling cells can decide their migration direction in response to forces from the substrate. Such reaction varies according to cell type, fast- and slow-crawling cell types. Under cyclic substrate stretching in the left-right direction, the intracellular stress fibers in slow-crawling cell types, such as fibroblasts, rearrange themselves to the top-bottom direction, and the shape of the cells extends in the same top-bottom direction, In contrast, fast-crawling cell types, such as neutrophil-like differentiated HL-60 cells and *Dictyostelium* cells, which have no stress fibers, show crawling migration in the top-bottom direction. Fish epidermal keratocytes are also known as fast-crawling cell types. However, they have stress fibers, which are typical slow-crawling cell types structures. Under cyclic substrate stretching in the left-right direction, intact keratocytes rearrange their stress fibers to the top-bottom direction in the same way as fibroblasts and migrate in the left-right direction. However, blebbistatin-treated stress fiber-less keratocytes migrate in the top-bottom direction, in the same way as seen in HL-60 cells and *Dictyostelium* cells. Our results show that keratocytes have a hybrid mechanosensing system of both fast- and slow-crawling cell types, to generate the polarity needed for migration.

5-2 Introduction

We have revealed some of how cyclic substrate stretching controls the migration of fast-crawling cell types and described them in Chapter 3 and 4. In contrast, the effect of cyclic substrate stretching to the slow-crawling cell types has been widely investigated (Birukov et al., 2003; Kaunas et al., 2005; Lee et al., 2010; Morioka et al., 2011; Sato et al., 2005; Tondon et al., 2012; Zhao et al., 2011), as mentioned in the previous chapters. Those findings can be summarized as follows. Under cyclic substrate stretching, slow-crawling cell types such as fibroblasts rearrange the intracellular stress fibers to the direction perpendicular to the stretch direction, and their cell shape extends in that direction. Binding of cofilin to the actin filaments when the stretched stress fibers are relaxed is considered as the primary cause of parallel stress fiber disassembly (Hayakawa et al., 2011; Hayakawa et al., 2014). In contrast, typical fast-crawling cell types such as neutrophil and *Dictyostelium* cells have no stress fibers. Under cyclic substrate stretching, HL-60 cells and *Dictyostelium* cells migrated perpendicular to the stretches direction by increasing the frequency of directional change from parallel to perpendicular direction. This may be due to symmetrical myosin II accumulation along the edges of left and right sides.

Fish keratocytes are epidermal wound-healing cells in fish skin (Goodrich, 1924; Morita et al., 2011; Ream et al., 2003). Their migration speed is almost the same as those of neutrophils and *Dictyostelium* cells (Euteneuer and Schliwa, 1984). Each cell consists of a spindle-shaped cell body and broad crescent-shaped lamellipodium in front of it. During their crawling migration, they keep not only the whole cell shape but also the shape of the lamellipodia and the cell body almost constant (Barnhart et al., 2011; Keren et al., 2008; Lee et al., 1993; Verkhovsky et al., 1999). However, unlike neutrophils and *Dictyostelium* cells, they have stress fibers in their cell body (Nakashima et al., 2015; Nakata et al., 2016; Sonoda et al., 2016; Svitkina et al., 1997). The orientation of the stress fibers in the keratocyte cell body is always perpendicular to the direction of crawling migration.

The question in this chapter is which direction keratocytes migrate under cyclic substrate stretching. There are two possibilities. One is that they move perpendicular to the stretch-direction like HL-60 cells and *Dictyostelium* cells, and the other is that the stress fibers are rearranged to the direction perpendicular to the stretch direction, as do slow-crawling cell types. In the latter case, the cells migrate parallel to the stretch, because the orientation of the stress fibers in keratocyte is always perpendicular to the migration direction.

To answer this question, we observed crawling migration of keratocytes under cyclic substrate stretching and analyzed their trajectories. A unique characteristic of keratocytes was revealed by the observation and the analysis, i.e., stress fibers in intact keratocytes rearrange themselves to the direction perpendicular to the stretch direction, like slow-crawling cells, and migrate parallel to the stretch direction. In contrast, stress fiber-less keratocytes migrated perpendicular to the stretches, like fast-crawling cells. These results suggest that keratocytes have two distinct mechanosensing mechanisms to decide the migration direction, one that depends on stress fibers and the other that does not.

5-3 Materials and Methods

Cell culture

A goldfish, *Carassius auratus*, was anesthetized in a solution containing Tricaine. A single scale was removed with tweezers without sacrificing the fish, and washed 3 times in culture medium, DMEM (08457-55, Nacalai Tesque) supplemented with 10% fetal calf serum (Nichirei) and antibiotic/antimycotic solution (Sigma-Aldrich). Then, the scale was placed external side up on the floor of a square chamber, whose bottom was made of a coverslip (No. 1, Matsunami). A small piece of the other coverslip was put on the scale as a weight. The chamber was kept in 5% CO_2 at 37 ˚C until the scale adhered to the surface of the glass floor for 30 - 60 min. Then, after the upper small glass piece was carefully removed, culture medium was poured into the chamber and the chamber kept at 5% CO_2 and 37 ˚C again overnight to allow the keratocytes to spread from the scale. Then, the keratocytes were washed briefly with Dulbecco's phosphate-buffered saline without Ca^{2+} and Mg^{2+} (PBS– –), and treated with 0.1% trypsin and 1 mM EDTA in PBS for 30 - 60 s. The trypsin was quenched with a ten-fold excess of culture medium.

Cyclic substrate stretching

Elastic substrates were made according to the methods described in Chapter 3. The surface of the substrate was coated with collagen (Cellmatrix I-C, Nitta Gelatin, Osaka, Japan) to optimize for keratocytes. Cyclic substrate stretching was performed according to the methods described in Chapter 3. In all the experiments, cycle time and duty ratio of stretching and relaxation were adjusted to 5 s and 1:1, respectively.

Pharmacological treatments

The agents, (±)-blebbistatin (13186, Cayman, MI, USA) or jasplakinolide (11705, Cayman) were applied to the cells on the elastic sheets. About 15 - 30 minutes after the application, cyclic substrate stretching was started. All experiments were performed in the presence of the reagents without removal. Final concentrations of blebbistatin and jasplakinolide in the medium were 25 μM and 30 nM, respectively.

Statistical analysis of cell migration

The analysis was performed according to the methods described in Chapter 3 (inset in Figure 3-3A) with a minor modification. Briefly, in preparing histograms of $|\sin\theta|$ (θ; inset in Figure 5-1D), the probability of migration direction was obtained by dividing the number in each direction by the total count number. Migration speeds in the perpendicular and parallel directions to the stretch direction, and the probabilities of a directional change from perpendicular to parallel and vice versa, were estimated according to methods described in Chapter 4 (Figure 4-1) with a minor modification. Briefly, the "$t = T$ + 30 s" in Figure 4-1 was changed to "$t = T$ + 120 s".

Staining of actin filaments

Actin filaments were stained according to the methods described in Chapter 4, except that Alexa Fluor 546 phalloidin (0.33 U/ml, A22283; Life Technologies) was used instead of Alexa Fluor 488 phalloidin.

Microscopy

Fluorescence images of fixed cells were captured in the same way as described in Chapter 3.

5-4 Results

Crawling migration of intact keratocytes parallel to the direction of cyclic substrate stretching

First, crawling migration of intact keratocytes was observed when cyclic substrate stretching of different stretch ratios (zero, 20 and 30%) was applied in the left-right direction. Trajectories of crawling cells in each stretch ratio are shown (Figure 5-1A – C). Probabilities of migration directions (θ; inset in Figure 5-1D) were calculated from the trajectories (Figure 5-1D – F). The cells tended to migrate parallel to the stretch direction when subjected to cyclic stretching with a 30% stretch ratio (Figure 5-1C, F), whereas they migrated equally frequently in all directions in its absence (Figure 5-1A and D). When subjected to cyclic stretching with a 20% stretch ratio, migration parallel to the stretch direction was not detected clearly (Figure 5-1B and E).

The $|\sin\theta|$ was calculated from the data in Figure 5-1A – C to provide an index of directional preference of migration (Figure 5-1G). The value with a 30% stretch ratio (right in Figure 5-1G) is significantly lower than that with zero stretching stimulus (left in Figure 5-1G), although there was no significant difference in the value between 20% stretch ratio (middle in Figure 5-1G) and zero stretching stimulus (left in Figure 5-1G), indicating that keratocytes can sense cyclic stretching stimuli with a ≥30% stretch ratio and migrate parallelly to the stretch direction. These results suggest that keratocytes prefer a direction parallel to the stretching. This reaction differs from other fast-crawling cell types such as HL-60 cells and *Dictyostelium* cells.

To reveal how keratocytes realize directional preference of migration parallel to the stretch direction, first, we examined whether the migration velocity parallel to the stretch is higher than that perpendicular to it. We calculated two velocities given zero stretching stimulus and under cyclic stretching stimuli with a 30% stretch ratio. With zero stretching stimulus (the two left-hand columns in Figure 5-1H), there was no significant difference in the velocity between the x-axis direction (left $\perp$ in Figure 5-1H) and the y-axis (left // in Figure 5-1H). In contrast, with a 30% stretch ratio (the two right-hand columns in Figure 5-1H), the velocity perpendicular to the stretch direction was significantly decreased (compare the $\perp$ columns in Figure 5-1H). Thus, the velocity parallel to the stretch direction (right // column in Figure 5-1H) became significantly greater than that perpendicular to the stretch direction (right $\perp$ column in Figure 5-1H).

Next, the probability of directional change from perpendicular to parallel was compared with that from parallel to perpendicular were compared. With zero stretching stimulus, there was no significant difference between from perpendicular to parallel (left red column in Figure 5-1I), and vice versa (left blue column in Figure 5-1I). However, with a 30% stretch ratio, the probability from perpendicular to parallel significantly increased (compare the red columns in Figure 5-1I), while that from parallel to perpendicular decreased (compare the blue columns in Figure 5-1I). Thus, under cyclic stretching with a 30% stretch ratio, the probability from perpendicular to parallel (right-hand red column in Figure 5-1I) was significantly greater than that the other way around (right-hand blue column in Figure 5-1I).

These results suggest that the causes of preferential migration parallel to the stretching direction are three-fold: (1) a decrease in the velocity in the perpendicular direction, (2) an increase in the probability of a directional change from perpendicular to parallel, and (3) a decrease in that from parallel to perpendicular.

Cyclic substrate stretching with a ≤20% stretch ratio did not affect the migration-direction of keratocytes. Thus, in all the following experiments, we applied those with a 30% stretch ratio.

Jasplakinolide-treated keratocytes migrate equally in all directions under cyclic substrate stretching

Judging by moving speed alone, keratocytes should be a type of fast-crawling cell. However, they moved parallel to the stretch direction whereas neutrophil-like differentiated HL-60 cells and *Dictyostelium* cells migrate perpendicular to the stretch direction, as shown in Chapter 3 and 4 (Iwadate and Yumura, 2009a; Iwadate et al., 2013; Okimura et al., 2016). The most conspicuous difference in the cytoskeleton between keratocytes and the other fast-crawling cell types is the presence or absence of stress fibers. Stress fibers may play an indispensable role in the directional preference of migration parallel to the stretches.

To test whether the depolymerization of stress fibers in response to the cyclic substrate stretching is required for the directional preference of migration of keratocytes, as is the case of slow-crawling cell types (Birukov et al., 2003; Kaunas et al., 2005; Lee et al., 2010; Morioka et al., 2011; Sato et al., 2005; Tondon et al., 2012; Zhao et al., 2011), we applied cyclic substrate stretching to jasplakinolide-treated keratocytes. Jasplakinolide inhibits the depolymerization of stress fibers composed of actin filaments. Even though keratocytes migrate in the medium containing 50 nM jasplakinolide, the rate of actin retrograde flow rate in lamellipodium decreased (Fuhs et al., 2014). In our preliminary experiments, 30 nM jasplakinolide did not decrease the rate of actin retrograde flow in lamellipodium of keratocytes. Thus, we applied 30 nM jasplakinolide to migrating keratocytes.

The trajectories of cell migration in the presence of jasplakinolide without and with cyclic substrate stretching are shown in Figure 5-2A and B, respectively. Figure 5-2C and D show the probability of migration direction (θ). The cells tended to move equally frequently in all directions, irrespective of the presence or absence of cyclic substrate stretching. There was no significant difference in the $|\sin\theta|$ values of the cells given zero stretching stimulus and under cyclic substrate stretching (Figure 5-2E).

We then compared the migration velocity of cells in the presence of jasplakinolide (Figure 5-2F). With zero stretching stimulus, there was no significant difference between the perpendicular direction (left $\perp$ in Figure 5-2F) and the parallel direction (left // in Figure 5-2F). In contrast, under cyclic substrate stretching (two right-hand columns in Figure 5-2F), the velocity parallel to the stretching direction showed a statistically significant decrease (compare the // columns in Figure 5-2F). However, the decrease was very small, and there was no significant difference between the perpendicular direction and the parallel direction (compare the two right-hand columns in Figure 5-1H).

The probability of directional changes in the presence of jasplakinolide was also analyzed (Figure 5-2G). With zero stretching stimulus, there was no significant difference between perpendicular to parallel (left red column in Figure 5-2G) and parallel to perpendicular (left blue column in Figure 5-2G). Application of cyclic substrate stretching changed neither the probability from perpendicular to parallel (compare the red columns in Figure 5-2G) nor that vice versa (compare the blue columns in Figure 5-2G). As a result, under cyclic substrate stretching as well, there was no significant difference in the probability of a directional change from perpendicular to parallel or vice versa in the presence of jasplakinolide (compare the two right-hand columns in Figure 5-2G).

Stress fibers in jasplakinolide-treated keratocytes under cyclic substrate stretching

To test whether the depolymerization of stress fibers was inhibited by jasplakinolide throughout the application of cyclic substrate stretching, jasplakinolide-treated cells were fixed after cyclic substrate stretching for 30 minutes and stained with Alexa Fluor 546 phalloidin. Then, relationship between the anterior-posterior polarity of the fixed cells and the presence or absence of the stress fibers in the cell body was analyzed (Figure 5-3). In this analysis, the anterior-posterior polarity of the fixed cell (thick arrow in Figure 5-3A) was determined as the direction perpendicular to the long axis of the cell (dotted line in Figure 5-3A). When the angle (ψ) between the *x*-axis (*x* in Figure 5-3A) and the thick arrow was between 315 and 45˚ or between 135 and 225˚, the migration direction was defined as "parallel" to the direction of stretching, and when it was 45 - 135˚ or 225 - 315˚, it was defined as "perpendicular".

Typical cells migrating parallel and perpendicular to the stretch are shown in Figure 5-3B and C, respectively. Figure 5-3D and E show fluorescence intensity of Alexa phalloidin along the green lines in Figure 5-3B and C, respectively. The red and blue arrowheads in Figure 5-3D and E indicate the accumulated actin filaments at the rear end of the cell (red arrowheads in Figure 5-3B and C) and those at the boundary of lamellipodium and cell body (blue arrowheads in Figure 5-3B and C), respectively. When the peaks (green arrowheads in Figure 5-3D and E) whose intensity is higher than 150% of the minimum intensity (dotted lines in Figure 5-3D and E) were detected between the two peaks indicated by rad and blue arrowheads, the cells were judged to retain stress fibers in the cell body (green arrowheads in Figure 5-3B and C). Under cyclic substrate stretching, 75 of 81 cells whose migration direction was parallel to the stretch retained stress fibers (top graph in Figure 5-3F). Similarly, 54 of 65 cells whose migration direction was perpendicular to the stretch direction also retained stress fibers (bottom graph in Figure 5-3F).

The presence or absence of stress fibers was also measured in the intact keratocytes after cyclic substrate stretching for 30 minutes. Figure 5-4A shows an enlarged view of a single typical trajectory in Figure 5-1C. As shown in Figure 5-4A, the cells under cyclic substrate stretching condition did not always keep their migration direction parallel to the stretch direction but sometimes made turns. Typical cells migrating parallel and perpendicular to the stretch are shown in Figure 5-4B and C, respectively. Figure 5-4D and E show fluorescence intensity of Alexa phalloidin along the green lines in Figure 5-4B and C, respectively. Under cyclic substrate stretching, 82 of 94 cells moving parallel to the stretches

retained their stress fibers (top in Figure 5-4F). However, only 21 of 93 cells moving perpendicular to the stretch direction retained the stress fibers (bottom in Figure 5-4F).

The results presented here suggest in keratocytes that cyclic substrate stretching triggers depolymerization of the stress fibers aligned parallel to the stretch, a phenomenon seen in slow-crawling cell types (Hayakawa et al., 2011; Hayakawa et al., 2014).

Preferential Crawling migration of stress fiber-less keratocytes perpendicular to the stretch

Treatment with low concentrations of blebbistatin, which is a myosin II ATPase inhibitor, disassembles stress fibers in keratocytes. We applied cyclic substrate stretching stimuli to keratocytes in a medium containing 25 μM (±)-blebbistatin. Figure 5-5A and B are typical cells before and after the treatment with blebbistatin. Only before the treatment, the stress fibers can be seen (green arrow in Figure 5-5A). The trajectories of cell migration without and with cyclic substrate stretching are shown in Figure 5-5C and D, respectively. Although the length of the trajectories was shortened by the inhibition of myosin II ATPase (compare Figures 5-5C and D to Figures 5-1A and 5-2A), the cells did in fact migrate. Figure 5-5E and F show the probability of migration direction (θ). Different from the intact cells, under cyclic substrate stretching the cells migrated perpendicular to the stretches (Figure 5-5D and F), whereas they migrated equally frequently in all directions under no cyclic stretching (Figure 5-5C and E). The $|\sin\theta|$ values for cells under cyclic substrate stretching (right in Figure 5-5G) were significantly larger than those under no cyclic stretching (left in Figure 5-5G).

This directional preference to the direction perpendicular to the stretches is identical to those of other fast-crawling cell types such as HL-60 cells and *Dictyostelium* cells, as demonstrated in Chapter 3 and 4 (Iwadate and Yumura, 2009a; Iwadate et al., 2013; Okimura et al., 2016). Thus, how stress fiber-less keratocytes migrate in a direction perpendicular to the stretch was also investigated. First, we compared the migration velocity perpendicular to the stretch and that parallel to them. Under no substrate stretching, there was no significant difference in the velocity between the perpendicular and the parallel directions (compare the two left-hand columns in Figure 5-5H). When cyclic substrate stretching was applied (the two right-hand columns in Figure 5-5H), the velocities changed in neither the perpendicular (compare the $\perp$ columns in Figure 5-5H) nor the parallel (compare the // columns in Figure 5-5H) direction. Thus, there was no significant difference in the velocity between the perpendicular direction and in the parallel directions (compare the two right-hand columns in Figure 5-5H) even under cyclic substrate stretching.

Next, we calculated the probability of directional changes. Under no substrate stretching condition, there was no significant difference in the probability of a directional change from perpendicular to parallel and parallel to perpendicular (compare the two left-hand columns in Figure 5-5I). When cyclic substrate stretching was applied, the probability of a directional change from perpendicular to parallel did not change (compare the red columns in Figure 5-5I), but that from parallel to perpendicular significantly increased (compare the blue columns in Figure 5-5I).

As a result, when subjected to cyclic stretching, the probability of a directional change from parallel to perpendicular was significantly higher than that in the other way around (compare the two right-hand columns in Figure 5-5I). This suggests a preferential directional change of migration direction from parallel to perpendicular to the stretch direction is the main cause of directional preference. This situation is just the same as the cases of the other fast-crawling cells such as intact HL-60 cells and *Dictyostelium* cells as shown in Chapter 4.

The presence or absence of stress fibers was also measured in the blebbistatin-treated keratocytes after cyclic substrate stretching. Figure 5-6A and B are typical cells moving parallel and perpendicular to the stretch direction, respectively. Figure 5-6C and D show fluorescence intensity of Alexa phalloidin along the green lines in Figure 5-6A and B, respectively. Even when subjected to cyclic substrate stretching, cells never had stress fibers regardless of the migration direction (Figure 5-6E)

5-5 Discussion

The aims of this study were to elucidate the directional preference of migration of keratocytes, that move fast like fast-crawling cell types but have stress fibers like slow-crawling cell types, under the cyclic substrate stretching condition. The results in this chapter showed that keratocytes have a unique bidirectional migration property, in which intact keratocytes migrate parallel to the stretch direction, whereas blebbistatin-treated stress fiber-less keratocytes migrate perpendicular to the stretch direction.

Parallel migration of intact keratocytes seems be realized by the following three factors: (I) decrease in velocity in the direction perpendicular to the stretches (compare the $\perp$ columns in Figure 5-1H), (II) increase in probability of directional change perpendicular to parallel (compare the red columns in Figure 5-1I), and (III) decrease in probability of direction change from parallel to perpendicular (compare the blue columns in Figure 5-1I). Although the mechanism of factor (III) cannot be explained from the results in this chapter, (I) and (II) may be induced by the depolymerization of stress fibers which had been aligned parallel to the stretching direction (Figure 5-4C). This is because, stress fibers contribute to the stability of crawling migration in keratocytes (Nakata et al., 2016).

In contrast, perpendicular migration of blebbistatin-treated stress fiber-less keratocytes appears to be realized by an increased directional change from parallel to the perpendicular direction to the stretches (the blue columns in Figure 5-5I). This situation is just the same as those of HL-60 cells and *Dictyostelium* as discussed in detail in Chapter 4.

Directional preference of migration perpendicular to the stretching direction appears only after treatment of the cells with blebbistatin in this study. Without any treatment, cells preferred to migrate parallel to the direction of stretching. Why is migration parallel to the stretching direction dominant over migration perpendicular to the stretching direction? Keratocytes sometimes take on a non-polarized round shape, with the cell body at the center, surrounded by a ring-shaped lamellipodium (Barnhart et al., 2015; Verkhovsky et al., 1999; Yam et al., 2007). Transformation from the non-polarized round shape to the motile polarized shape begins with the local retraction of a part of the ring-shaped lamellipodium (Barnhart et al., 2015; Yam et al., 2007). During this contraction, stress fibers are formed by the local concentration of actomyosin at the site of retraction (Verkhovsky et al., 1999). The polarized cell then begins to migrate, with the stress fibers at the rear. This fact suggests that the configuration of stress fibers dominates other dynamics of the cytoskeleton to generate polarity needed for migration. Migration parallel to the stretching direction appears to be dependent on the dynamics of stress fibers. Thus, migration that is parallel to the stretching direction may be dominant over the perpendicular version.

To summarize, results in this chapter demonstrated that stress fibers play an important role in the crawling migration in keratocytes. In the process of further study, we found a unique behavior of stress fibers in keratocytes, which will be presented in the next chapter,

Figures

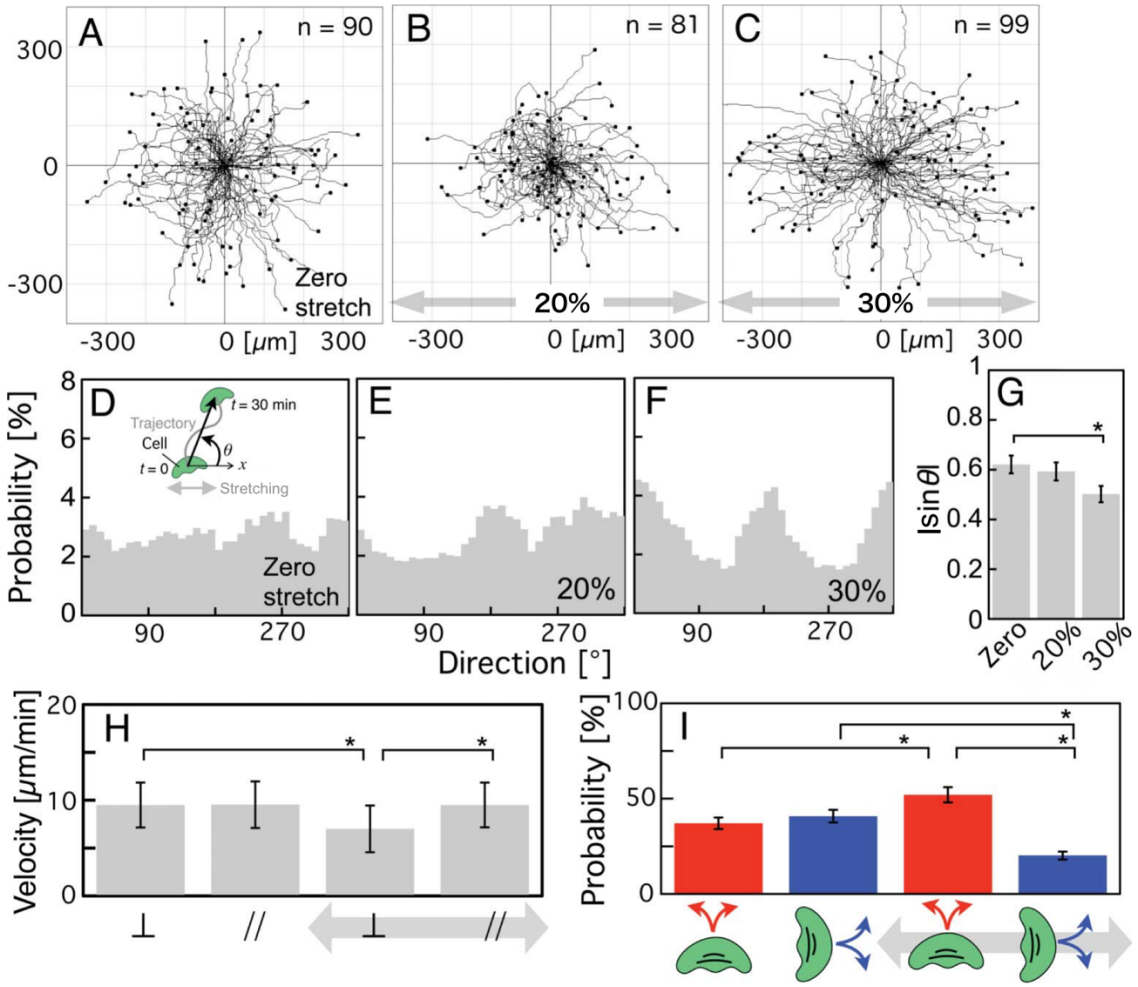

Figure 5-1. Migrations of intact keratocytes under cyclic substrate stretching with various stretch ratios. (A – C) Migration trajectories of zero stretching stimulus (A, from 10 experiments), a 20% stretch ratio (B, from 6 experiments), and a 30% stretch ratio (C, from 8 experiments). Gray arrows; direction of stretches. (D – F) Probability of migration direction (θ; inset in D). (G) The $|\sin\theta|$ values. (H) Migration velocities. The two left-hand and two right-hand columns were respectively calculated from the data in A and C. The velocities perpendicular and parallel to the stretches are indicated as ⊥ and //, respectively. (I) Probability of a directional change calculated from the data in A (two left-hand columns) and C (two right-hand columns). The red and blue columns respectively represent the probability of a switch from perpendicular to parallel and vice versa. The bars in G and I, and H indicate SEM and SD, respectively. The *p*-values were calculated using Student's t-test. $*p < 0.05$.

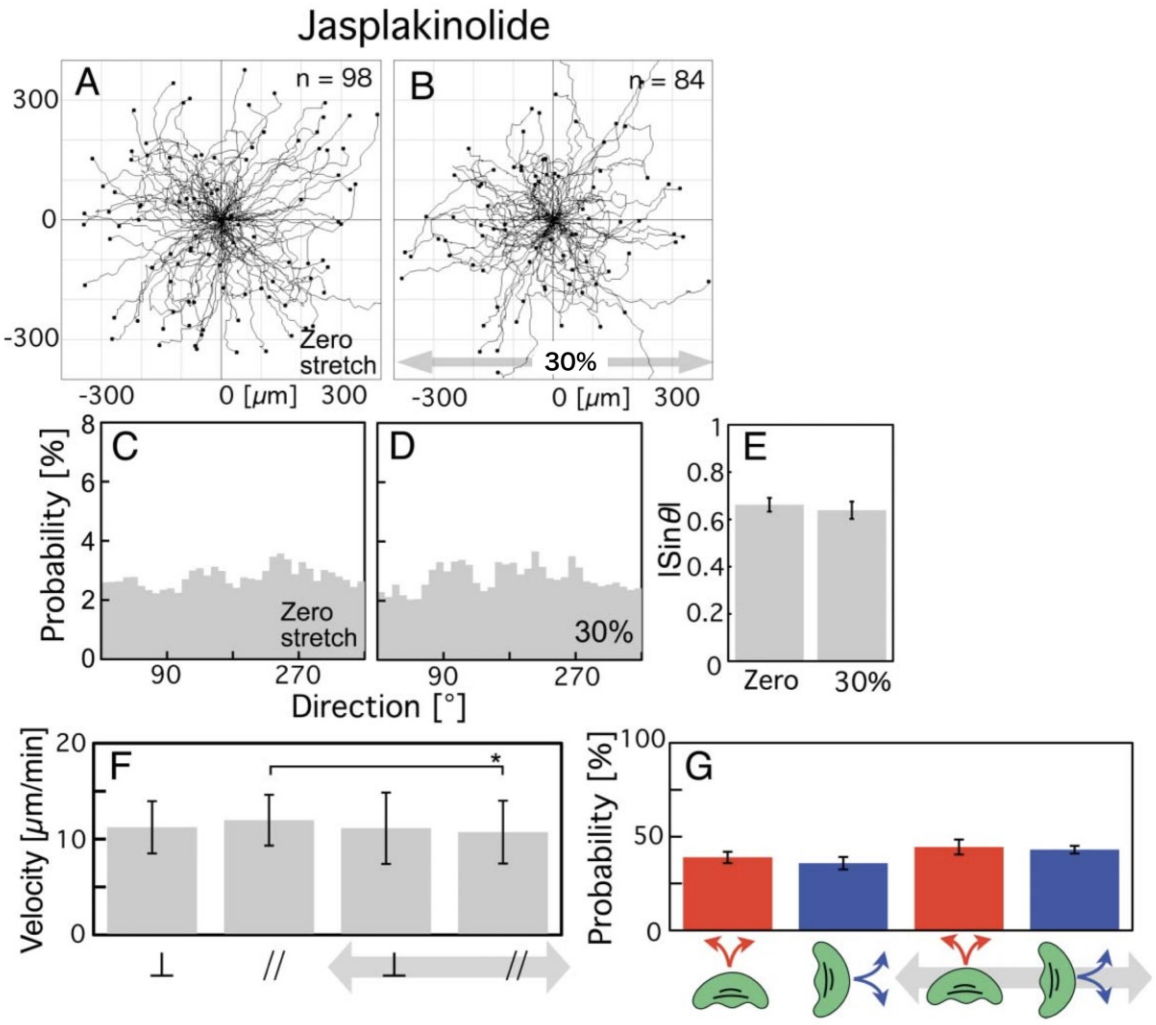

Figure 5-2. Migrations of jasplakinolide-treated keratocytes. (A and B) Migration trajectories of cells given zero stretching stimulus (A, from 8 experiments), and a 30% stretch ratio (B, from 7 experiments). (C and D) Probability of migration direction (θ). (E) The $|\sin\theta|$ values. (F) Migration velocities. The two left-hand and two right-hand columns were respectively calculated from the data in A and B. (G) Probability of a directional change calculated from the data in A (two left-hand columns) and B (two right-hand columns). The bars in E and G, and F indicate SEM and SD, respectively. The *p*-values were calculated using Student's t-test. $*p < 0.05$.

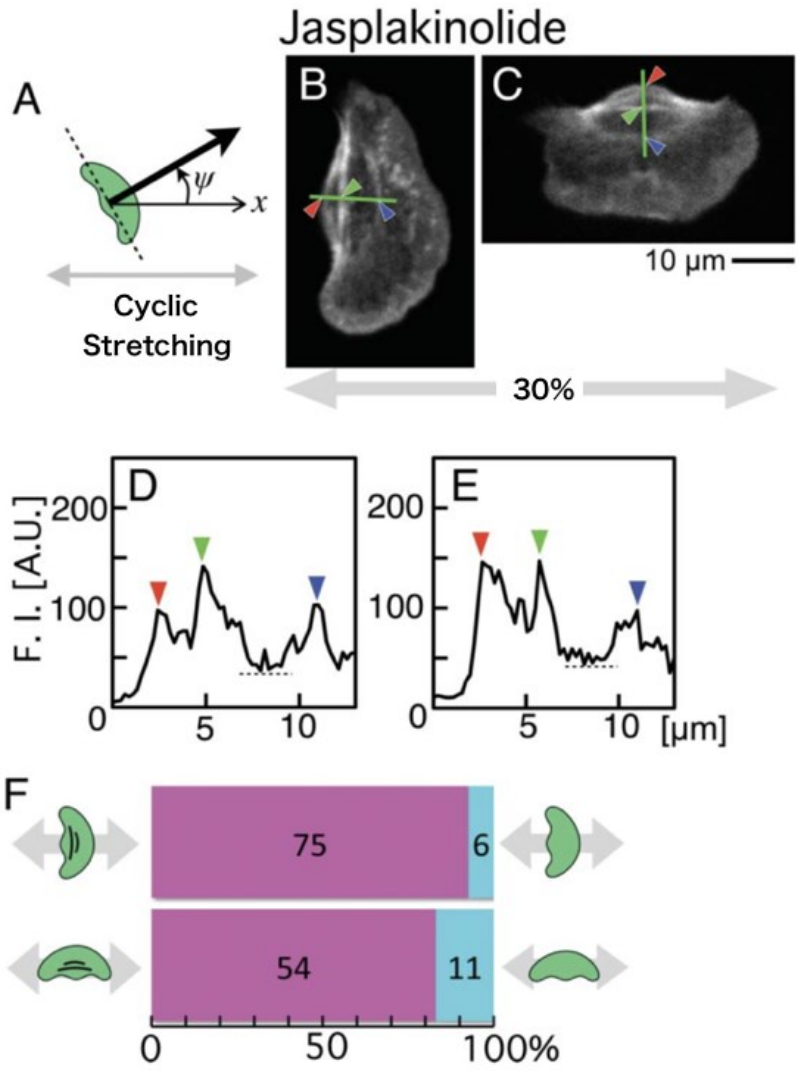

Figure 5-3. Stress fibers in jasplakinolide-treated keratocytes subjected to cyclic substrate stretching. (A) Definition of migration direction (ψ). (B and C) Fluorescence images of Alexa phalloidin in cells migrating parallel (B, typical of 81 cells) and perpendicular (C, typical of 65 cells) to the stretches. (D and E) Fluorescence intensity of Alexa phalloidin along the green lines in B (D) and C (E), respectively. Red, green and blue arrowheads correspond to the arrowheads of the same color in B and C. When the intensity of the middle peak was higher than 150% of the minimum intensity (dotted lines in D and E), the cell was judged to retain stress fibers. (F) Numbers of cells with stress fibers (magenta) and without (cyan). Top and bottom: cells moving parallel and perpendicular to the stretches.

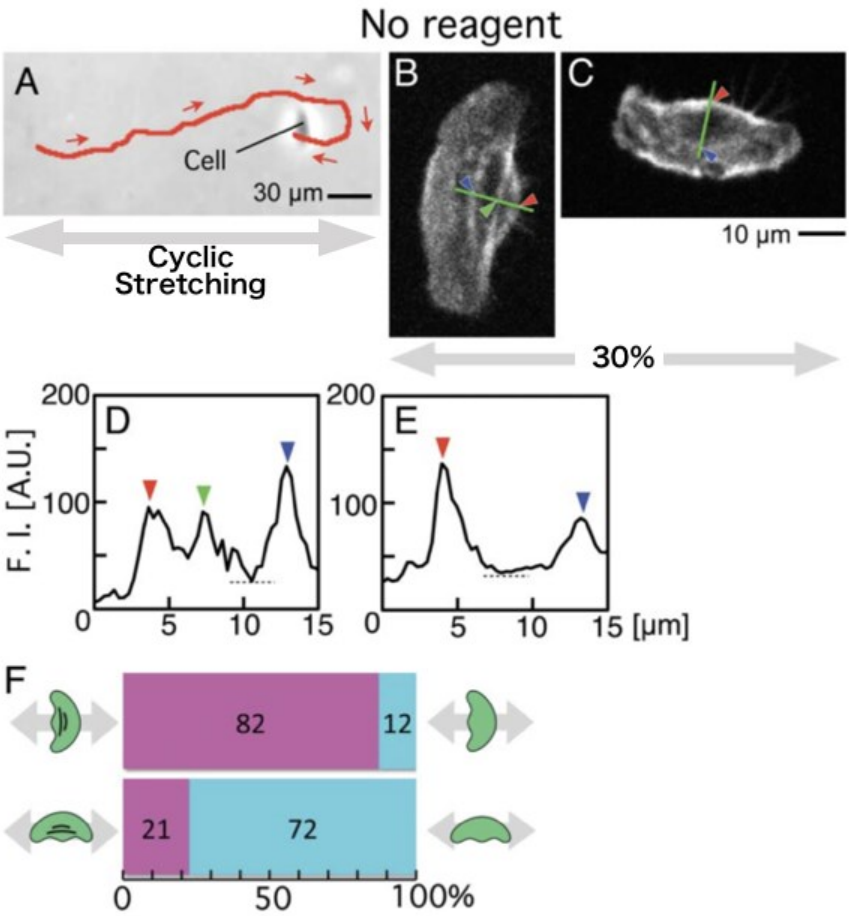

Figure 5-4. Stress fibers in intact keratocytes subjected to cyclic substrate stretching. (A) A typical migration trajectory (red line) of an intact keratocyte subjected to cyclic substrate stretching for 30 min, extracted from Figure 5-1C. Red arrows indicate the migration direction. (B and C) Fluorescence images of Alexa-phalloidin in cells migrating parallel (B typical of 94 cells) and perpendicular (C typical of 93 cells) to the stretches. (D and E) Fluorescence intensity of Alexa phalloidin along the green lines in B (D) and C (E), respectively. Presence or absence of stress fibers were defined in the same manner as in Figure 5-3D and E. (F) Numbers of cells with stress fibers (magenta) and without (cyan). Top and bottom: cells moving parallel and perpendicular to the stretches.

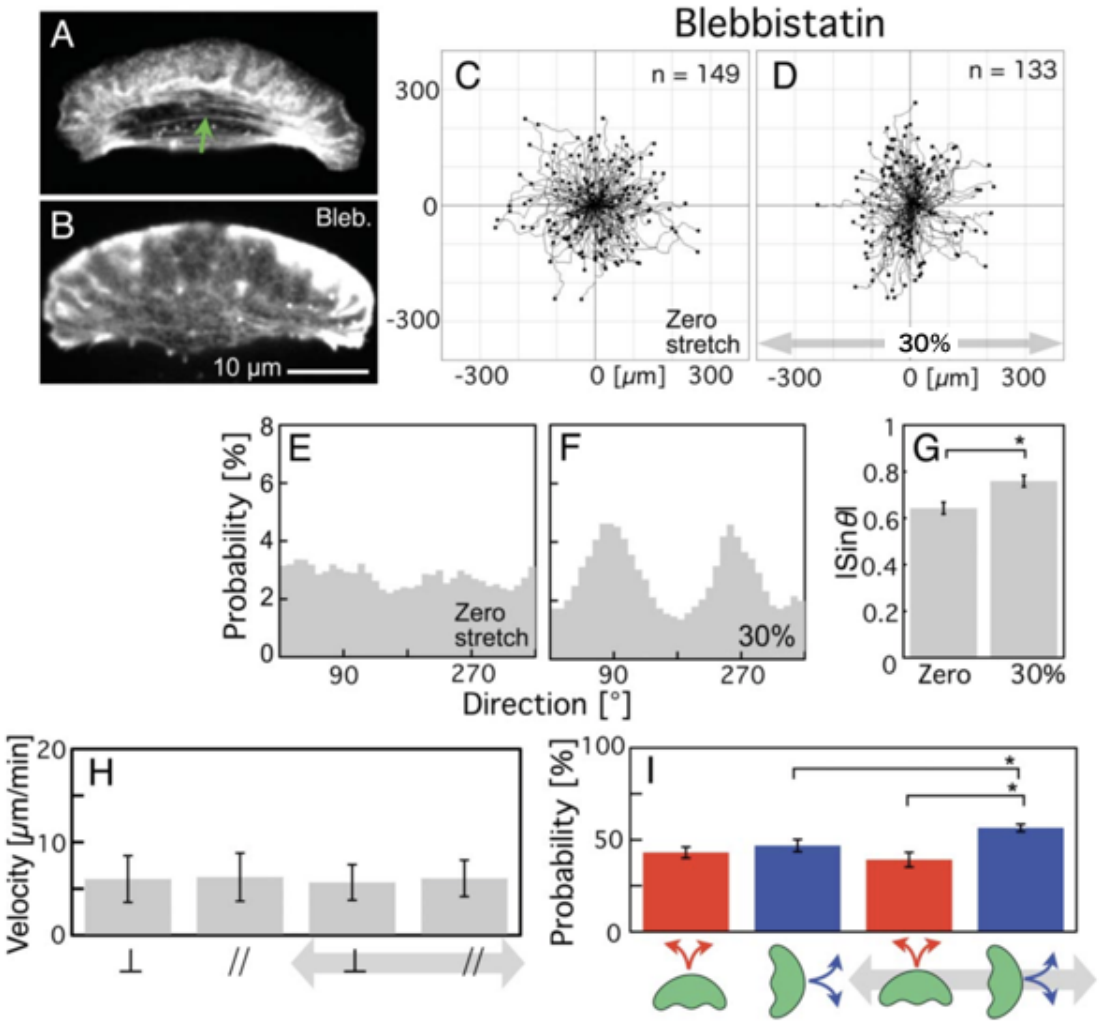

Figure 5-5. Migration of blebbistatin-treated keratocytes. (A and B) Fluorescence images of Alexa phalloidin in cells before (A) and after (B) treatment with blebbistatin. The green arrow; a stress fiber. To confirm the presence or absence of stress fibers, brightness of both images has been enhanced. (C and D) Migration trajectories of cells given zero stretching stimulus (C, from 9 experiments) and a 30% stretch ratio (D, from 6 experiments). (E and F) Probability of migration direction (θ). (G) The $|\sin\theta|$ values. (H) Migration velocities. The two left-hand and two right-hand columns were respectively calculated from the data in C and D. (I) Probability of a directional change calculated from the data in C (two left-hand columns) and D (two right-hand columns). The bars in G and I, and H indicate SEM and SD, respectively. The *p*-values were calculated using Student's t-test. *$p < 0.05$.

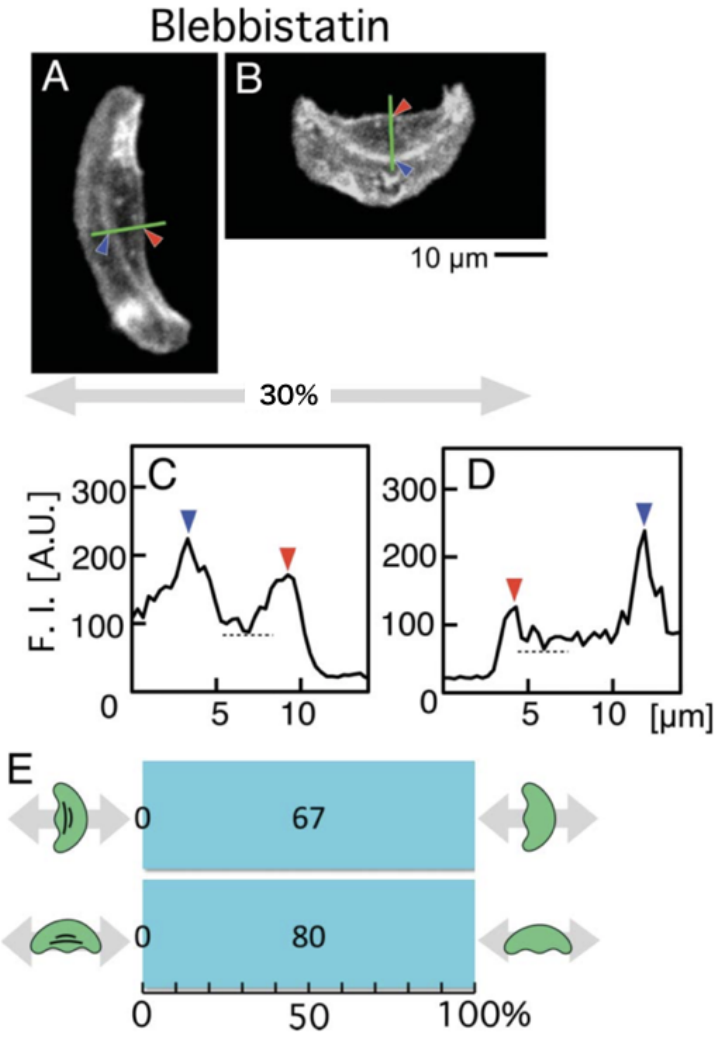

Figure 5-6. Stress fibers in blebbistatin-treated keratocytes subjected to cyclic stretching. The migration direction was determined as in Figure 5-3A. (A and B) Fluorescence images of Alexa phalloidin in cells migrating parallel (A, typical of 67 cells) and perpendicular (B, typical of 80 cells) to the stretches. (C and D) Fluorescence intensity of Alexa phalloidin along the green lines in A (C) and B (D), respectively. Presence or absence of stress fibers were judged in the same manner as in Figure 5-3D and E. (E) Numbers of cells with stress fibers (magenta) and without (cyan). Top and bottom: cells moving parallel and perpendicular to the stretches.

Chapter 6

Stress Fiber Rotation in Crawling Keratocytes

6-1 Abstract

Keratocytes have a frontal crescent-shaped lamellipodium and a rear spindle-shaped cell body, and maintain their overall shape during crawling migration. During crawling, leading edge expansion and rear retraction are respectively induced by actin polymerization and contraction of stress fibers, in a manner similar to slow-crawling cell types. Stress fibers align almost perpendicular to the migration direction in the spindle-shaped cell body. In the previous chapter, we found that stress fibers in keratocytes play an important role in directional preference of migration. In the process of further studying of the role of stress fibers in keratocytes, we found a unique behavior of them. In this chapter, first, we show that the stress fibers are configured to surround the cytoplasm including a nucleus in their cell body. Their arrangement was just like seam of a rugby ball, from which some air had leaked out and the bottom got flattened. Then, we directly show, in sequential 3-dimensional recordings of crawling migration of a single keratocyte, their rolling motion during crawling migration. Surgical excision of the lamellipodial leading edge from a migrating keratocyte did not stop the rolling. Destruction of the stress fibers decreased the migration speed. The rotation of these stress fibers seems to play the role of an autonomous wheel in crawling migration of keratocytes.

6-2 Introduction

It is widely accepted that most of crawling cell migration is driven by either of the following two mechanisms, depending on the cell types. One is a combination of the frontal expansion by actin polymerization (Mogilner and Oster, 1996; Parsons et al., 2010; Pollard and Borisy, 2003; Theriot and Mitchison, 1991) and the rear retraction of by actomyosin contraction (Jay et al., 1995), typically shown in fibroblasts (Chen, 1981; Galbraith and Sheetz, 1997; Wang, 1985), neutrophils (Hind et al., 2016; Lam and Huttenlocher, 2013; Parent, 2004; Shin et al., 2010; Torres and Coates, 1999) and *Dictyostelium* cells (Iwadate and Yumura, 2008b; Iwadate et al., 2013; Parent, 2004). The other is bleb-driven migration in which extension of the front cortex is induced not by local actin polymerization but by strong hydrostatic pressure generated by actomyosin contraction at the rear, typically shown in the crawling protist *Amoeba proteus* (Pomorski et al., 2007; Stockem et al., 1982).

When a part of skin is broken, in order to repair the wound, epidermal cells begin to migrate from the sides of the wound into the wound site (Martin, 1997; Reid et al., 2005; Zhao et al., 2006). In fish, keratocytes play this role in the wound-healing process (Goodrich, 1924). Each keratocyte cell consists of a spindle-shaped cell body containing a nucleus and a single large, crescent-shaped lamellipodium in front of the cell body (Keren et al., 2008; Lee et al., 1993). In order to move while maintaining their shape, actin polymerization pushes the leading edge of the lamellipodium (Nakata et al., 2016; Okeyo et al., 2009; Svitkina et al., 1997; Wilson et al., 2010) with graded extension rate that is fast in the center and slow on both sides (Lee et al., 1993; Mizuno and Sekiguchi, 2011; Nakata et al., 2016). In contrast, along the rear end of the cell body, it is regarded that contraction of stress fibers drives its retracts the rear (Barnhart et al., 2011; Doyle and Lee, 2005; Fournier et al., 2010; Svitkina et al., 1997), in the same way as other cell types containing stress fibers (Chen, 1981; Galbraith and Sheetz, 1997; Wang, 1985).

Left and right ends of the cell body adhere to the substrate via focal adhesions (Lee et al., 1993; Nakashima et al., 2015; Nakata et al., 2016; Sonoda et al., 2016). Stress fibers in keratocytes are positioned to connect the left and right focal adhesions in the cell body (Barnhart et al., 2011; Doyle and Lee, 2005; Lee and Jacobson, 1997; Okimura and Iwadate, 2016; Sonoda et al., 2016). The direction of the contractile forces exerted by the stress fibers, detected as traction forces applied to the substrate, are almost perpendicular to the migration-direction (Burton et al., 1999; Doyle and Lee, 2005; Doyle et al., 2004; Fournier et al., 2010; Fuhs et al., 2014; Jurado et al., 2005; Nakashima et al., 2015; Nakata et al., 2016). In a simplified view, it seems that in order to efficiently retract the rear of the cell, the stress fibers should be aligned parallel to the migration-direction in order to exert their traction force in the direction parallel to the migration-direction. From the unique alignment of stress fibers in keratocytes, we speculated that they may play a role for migration other than the retraction of the rear.

Several investigators, having observed movements of endocytosed beads, suggested that the cell body rolls during migration (Anderson et al., 1996; Svitkina et al., 1997). However, it has not been clarified which cytoskeleton drives the rotation. In this chapter, using sequential three-dimensional (3D) recordings, first, we reveal that the stress fibers are configured to surround the cytoplasm, including the nucleus, in their cell body. Their arrangement was just like seams of a rugby ball from which some air

had leaked out and the bottom got flattened. Then, we directly show the rolling of the rugby ball. The rolling did not stop by the cutting off the leading edge, where actin polymerization takes place, from a migrating keratocyte, indicating that the rotation is not a result of frontal actin polymerization. Destruction of a part of the stress fibers during cell migration slowed the migration speed and induced the collapse of the left-right balance of the crawling migration. These results suggest that the rotation of stress fibers should not be merely a result of progress of keratocytes but contributes to it as one of the driving forces and the steering. Keratocytes seem to move forward by combination of the rotation of the stress fiber and actin polymerization.

6-3 Materials and Methods

Culture of keratocytes

Keratocytes from the scales of Central American cichlids (*Hypsophrys nicaraguensis*) were cultured as described in Chapter 5 with a minor modification. The main changes were the use of culture medium (L-15, L5520: Sigma-Aldrich) instead of DMEM and the keeping scales not at 5% CO_2 and 37 ˚C but at 23 °C.

Staining of fixed keratocytes

Fixed cell staining was performed according to the methods described previously (Miyoshi and Adachi, 2012; Nakata et al., 2016) and as described in Chapter 4 with a minor modification. The main changes were the use of Alexa Fluor 546 phalloidin (0.33 units/ml, A22283; Life Technologies) instead of Alexa Fluor 488 phalloidin, Alexa Fluor 488 anti-rabbit IgG (1:2,000 dilution, A-11034, Life Technologies) instead of Alexa Fluor 546 anti-rabbit IgG as secondary antibody, and the change in the concentration of Triton X-100 from 0.1% to 0.02%.

Live cell electroporation

Using a small-volume electroporator (Tsugiyama et al., 2013), Alexa Fluor 546 phalloidin (A22283: Life Technologies) or Alexa Fluor 488 phalloidin (A12379: Life Technologies) was loaded into live keratocytes adhering to the substrate.

Treatment with blebbistatin

The agent (±)-blebbistatin (13186; Cayman) was dissolved at 100 mM in DMSO and then diluted 2,000 times with the culture medium. Thus, the final concentrations of blebbistatin in the medium were 50 μM.

Confocal microscopy

Fluorescence images of live and fixed cells were captured in the same way as described in Chapter 3 with a minor modification. As the main changes, high speed z-axis scanner (NZ100CE, Prior, Cambridge, UK) was used for fast live cell recording to construct a 3D cell image. To construct a single 3D cell image of a certain position, about 40 slices of the optical sections were recorded at 0.5-μm intervals. The time interval for recording each optical section was 56-ms. Thus, it takes about 2 seconds to record a 3D image at a certain position.

Cutting off the leading edge from a migrating keratocyte was performed by manipulating a glass microneedle using a micromanipulator (MO-202: Narishige, Tokyo, Japan) under confocal microscopy.

Light sheet microscopy

Light sheet microscope used in this study had been previously built by S. Nonaka (Takao et al., 2012). Fluorescence images of live cells were recorded through a 40× objective lens (CFI Fluor 40×W: Nikon).

Optical sections were recorded at 1.2-μm intervals. One hundred slices of the optical sections were recorded at 25-ms intervals to construct a 3D image of a cell.

Local destruction of stress fibers

Local destruction of stress fibers in a single migrating keratocyte was performed by the application of a beam at a wavelength of 355 nm for several seconds from a laser (FTSS 355-50, CryLaS, Berlin, Germany) through a 100× objective lens (CFI Plan Fluor 100×/1.30 Oil: Nikon) as described previously (Nakata et al., 2016).

3D image reconstruction

3D images were reconstructed using a software (FluoRender, SCI, Univ. of Utah, UT, USA).

6-4 Results

Three-dimensional architecture of stress fibers in keratocyte cell body

Keratocytes maintain their characteristic overall half-moon shape, consisting of anterior crescent-shaped lamellipodium and posterior spindle-shaped cell body, during crawling migration (Figure 6-1A). The shape of the cell body and the lamellipodium, and the ratio of the sizes of the two parts also do not change during the migration. A dense meshwork of thin actin filaments occupies most of the area in the lamellipodium. In contrast, several stress fibers are present in the cell body, instead of the thin actin filaments (Barnhart et al., 2011; Doyle and Lee, 2005; Lee and Jacobson, 1997; Okimura and Iwadate, 2016; Sonoda et al., 2016). To capture a 3D view of the stress fibers accurately, we simultaneously stained filamentous actin and myosin IIA in fixed keratocytes, and optical sections of the *x*-*y* horizontal plane were captured (Figure 6-1B – E).

As shown in Figure 6-1B, optical sections from the bottom to top were obtained at 0.3-μm intervals. In Figure 6-1C, colocalization of filamentous actin and myosin IIA is shown as white color. Stress fibers, composed of actomyosin, were detected in the bottom optical sections (yellow arrows in Figure 6-1C) and also in the upper sections (cyan arrows in Figure 6-1C). The both ends of the upper stress fibers seems to be extended into the lower optical sections (cyan arrowheads in Figure 6-1C).

Next, optical sections parallel to the *x*-*z* plane were made at 1.3-μm intervals (Figure 6-1D, E) from the reconstructed 3D images. Cyan arrows in Figure 6-1E indicate an identical stress fiber. The position of the arrows is high in the middle part and low in both the right and left parts of the cell, indicating that the upper stress fiber is extended with curvature along the contour of the cell body. In contrast, the position of the yellow arrows, which indicate a lower stress fiber, is the same in each panel in Figure 6-1E, indicating that the lower stress fiber extends straight and parallel to the substrate. These observations show that the stress fibers are arranged to surround the cytoplasm in the keratocyte's cell body. Their arrangement was just like seams of a rugby ball from which some air had leaked out and the bottom got flattened.

The large green area in Figure 6-1E represented the nucleus. In the case of keratocytes, the cell nucleus was stained with myosin IIA antibody, which is consistent with previous observations (Okeyo et al., 2009; Svitkina et al., 1997).

Rolling of stress fibers in a crawling keratocyte

Next, we stained stress fibers in live keratocytes and observed the crawling migration of keratocytes under high speed 3D microscopy. As shown in Figure 6-2A, the sequential 3D images clearly show the rotating of stress fibers.

Figure 6-2B shows the time series of optical sections parallel to the *x*-*z* plane made from the sequential 3D images. The bright spots in the "Left", "Center" and "Right" cross sections in Figure 6-2B represent an identical stress fiber, which clearly rotated. The angular velocities of the stress fibers at each cross section of the left, center and right in Figure 6-2B were calculated (Figure 6-2C). As shown in Figure 6-2D, there was no significant difference in the angular velocity among the cross sections at the left, center and right.

Next, the migration velocity of stress fibers was estimated by the calculation of (the radius of the cell body) × (the angular velocity of it) (rω in Figure 6-2E). The estimated velocity was about 5 μm/min. As shown in Figure 6-2E, it was half of the real migration velocity calculated from the trajectory of migrating keratocytes. This result agrees with the previous studies in which the velocities were calculated from observations of endocytosed bead movements (Anderson et al., 1996; Svitkina et al., 1997). These results indicate that stress fiber-rotation may not be the source of crawling migration and that may play a role in steering for the migration. We speculated that the combination of the stress fiber-rotation and other power sources such as actin polymerization at the leading edge (Small et al., 1995; Theriot and Mitchison, 1991; Wilson et al., 2010) should realize the crawling migration (Anderson et al., 1996; Verkhovsky et al., 1999). We tested this hypothesis in the following experiments.

Stress fibers are not passively rotated by the propulsion of keratocytes

The result that rω was half of the migration velocity suggests that the stress fibers may be slipped passively. Here, to investigate whether the stress fibers are slipping in all migrating cells, we observed the crawling cell migration with various speeds, and compared the propulsion speeds between the stress fibers and the cell body on the ventral surface of migrating cells (Figure 6-3A – E).

Figure 6-3A and B are the images of the actin cytoskeleton in a typical crawling keratocytes of fast and slow speeds, respectively. Figure 6-3C and D are kymographs made from Figure 6-3A and B, respectively. Cropped areas are indicated as white squares in Figure 6-3A and B. In the fast cell, not only the cell rear (cyan arrow in Figure 6-3C), but also the ventral stress fibers (yellow arrow in Figure 6-3C) clearly moved forward. In contrast, in the slow cell, the speed of stress fibers (yellow arrow in Figure 6-3D) was almost zero, although the cell rear moved forward (cyan arrow in Figure 6-3D).

Figure 6-3E shows the relationship between speed of ventral stress fiber and that of cell body among the population of cells. The slope of the regression line, shown as dotted line in Figure 6-3E, obtained by the Least Squares method was 1.02. From the regression line, the speed of the cell body when the propulsion speed of stress fiber is zero was estimated to be 5.29 μm/min. This value is almost the same as the value estimated from the rotation of the stress fibers (rω in Figure 6-2E). The match between these two values suggests the intriguing possibility that the rotation of stress fibers may not be a passive result of keratocyte propulsion but actively rotating, at least when frontal actin polymerization is weak and the cell propulsion speed is slow. However, the possibility in which stress fibers are rotated passively by the actin polymerization or function as a brake cannot be excluded completely.

To test whether stress fibers are rotated passively by the actin polymerization, we cut the leading edge from a migrating keratocyte by a glass microneedle while recoding 3D stress fiber images, and observed whether the rotation of stress fibers stopped or not just after the cutting. As shown in Figure 6-3F, the stress fibers continued to rotate even after the cutting.

Crawling migration of stress fiber-less keratocytes

If the of the stress fiber-rotation contributes to the propulsion of keratocytes, removal of them should

have a serious damage on the motility. As mentioned in Chapter 5, treatment with blebbistatin induces disassembly of stress fibers. We simultaneously stained filamentous actin and myosin IIA in fixed blebbistatin-treated keratocytes, and found that stress fibers were disassembled in the cell body by the treatment with blebbistatin. We detected no cell-body rotation from 17 blebbistatin-treated cells (Figure 6-4B). As shown in Figure 6-4C, migration velocity of the blebbistatin-treated cells was significantly lower than that of untreated cells.

Blebbistatin inhibits myosin II ATPase, suggesting that some effect other than disassembly of stress fibers may affect the migration. Thus, next, a portion of stress fibers was directly ablated by laser beam (yellow arrow in Figure 6-5A). Figure 6-5B and C are contours of the cell body traced from differential interference contrast (DIC) images (Figure 6-5A) and their centers every 4 s before and after the ablation. The velocity of the centers after ablation obtained from 7 cells was slower than that before ablation as shown in Figure 6-5D (t-test; $p = 0.07$). When the laser beam was applied to the area near but not covering the stress fibers, the migration manner of the cell never changed (Figure 6-5G).

Next, we compared the migration directionality between intact cells and blebbistatin-treated cells. Directionality is defined as the linear distance between the start and end points of migration for 30 min divided by the pathlength of the trajectory. As shown in Figure 6-4D, the directionality significantly decreased by the blebbistatin treatment. Also, in the experiment of laser ablation of stress fibers, the migration directions were compared between just after the ablation (Figure 6-5E) and those without ablation (Figure 6-5F). Clearly, the migration direction became unstable by the ablation of the stress fibers.

6-5 Discussion

In this chapter, we showed a unique arrangement of stress fibers in keratocyte, that was just like seams of a rugby ball from which some air had leaked out and the bottom got flattened. Furthermore, the rugby ball was rotating. It seems that the stress fiber-rotation should not be merely a result of progress of keratocytes but contributes to it. The results in this chapter suggest that the rotation of stress fibers should play a role in steering and may actively contribute to propulsion as one of the driving forces when frontal actin polymerization is weak and the cell propulsion speed is slow.

Roy et al. observed that the left-right balance of the crawling migration of keratocytes was collapsed by the activation of thymosin ß4, an inhibitor of actin polymerization, at the local area in the cell body (Roy et al., 2001). They concluded that the local disruption of stress fibers by thymosin β4 was the cause of the collapse of the left-right balance of the cell. Their results support our hypothesis that stress fibers are required to maintain the left-right balance of the crawling migration of keratocytes.

It is widely accepted that there are three types of stress fibers in slow-crawling cell types such as fibroblasts. They are (1) dorsal stress fibers and (2) ventral stress fibers that are linked to adhesion sites and (3) transverse actin arcs that slide along dorsal stress fibers away from the front of the cell to the rear (Burnette et al., 2011; Hotulainen and Lappalainen, 2006; Pellegrin and Mellor, 2007; Titus, 2017). The arrangement and the movement of the stress fibers in the cell body of keratocytes shown in this chapter are clearly different from that of slow-crawling cell types.

Not only migrating half-moon shaped keratocyte but also stationary circular keratocytes can be sometimes observed in the cultivation chamber. In contrast to migrating keratocytes, arrangement of stress fibers in the circular keratocytes are radially symmetric (Yam et al., 2007). Tee et al. observed self-organization of the actin cytoskeleton in fibroblasts (Tee et al., 2015). The radially symmetric alignment of stress fibers in the circular keratocytes is similar to the actin-network in the early stage of self-organization in fibroblasts plated on a circular fibronectin area. Tee et al. showed that myosin IIA-enriched transverse fibers moved centripetally in permeabilized fibroblasts. Just like the stress fibers in keratocytes as shown in Figure 6-4, the transverse fibers disassembled by the treatment with blebbistatin. In our observation, at the bottom of the migrating keratocyte, the stress fibers moved to the rear in the cell frame of reference. It may move with the same mechanism as the centripetal movement of transverse fibers in fibroblasts.

The driving force of the stress fiber rotation remains a mystery. Both of the left and right ends of bottom stress fibers are connected to the substrate via focal adhesions (Lee and Jacobson, 1997). The contractile forces of stress fibers are detected as traction forces in the substrate under the focal adhesions (Fournier et al., 2010; Fuhs et al., 2014; Nakata et al., 2016). At the rear end of a migrating keratocyte, detachment of both ends of a stress fiber from the substrate is driven by the contraction of itself. This detachment movement of the rear stress fiber retracts the rear (Barnhart et al., 2011; Doyle and Lee, 2005; Fournier et al., 2010; Svitkina et al., 1997). To clarify the driving force of stress fiber rotation is an interesting future issue.

Figures

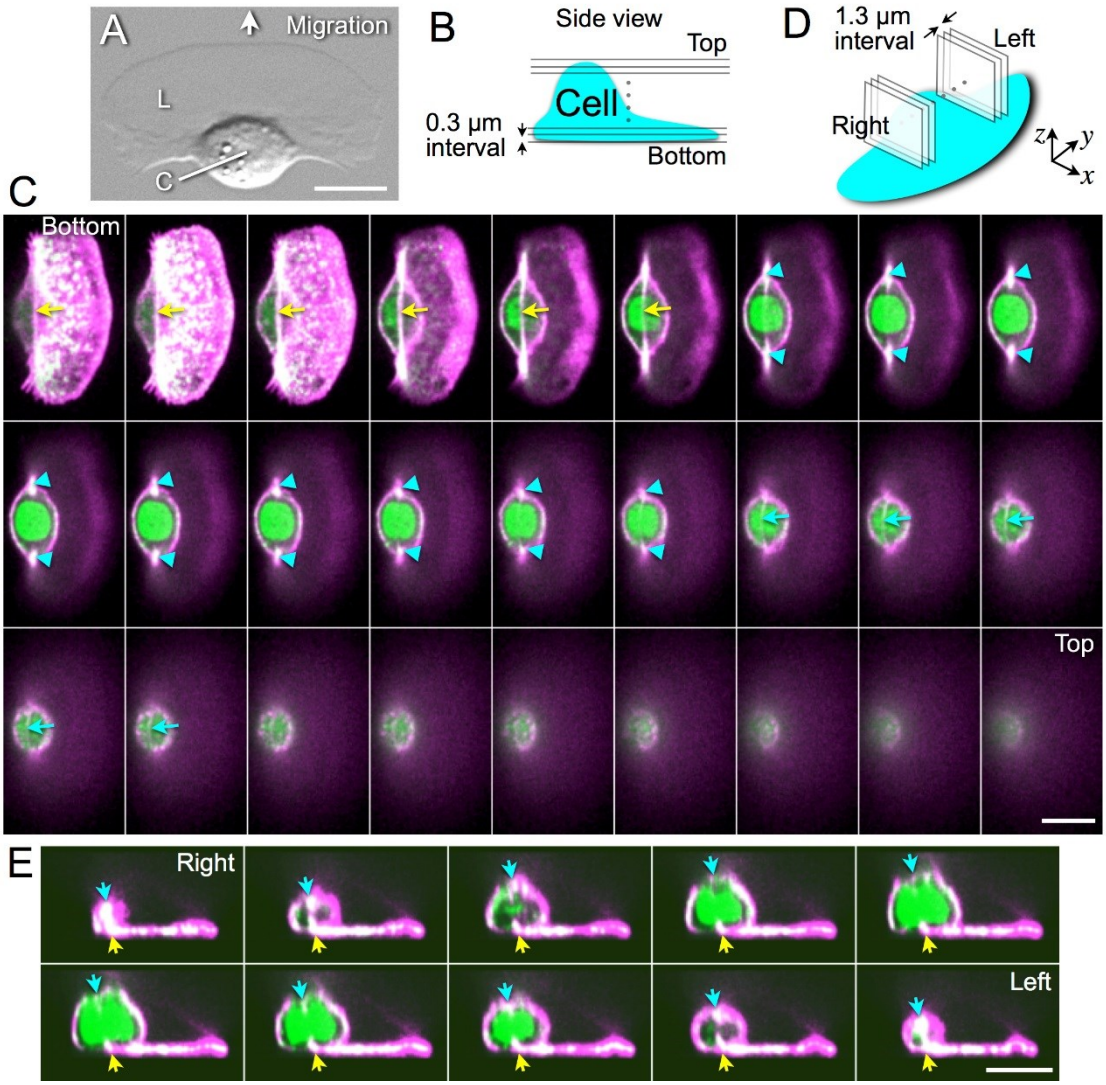

Figure 6-1. 3D arrangement of stress fibers in a keratocyte. (A) A DIC image. L: lamellipodium, C: cell body. (B) Positions of the *x*-*y* optical sections. (C) Sequential *x*-*y* optical sections. Filamentous actin (magenta) and myosin IIA (green). Colocalization of them appears white. Yellow and cyan arrows: a bottom and a top stress fiber (white). Cyan arrowheads: ends of the top stress fiber. (D) Positions of the *x*-*z* optical sections. (E) Sequential *x*-*z* optical sections. Yellow and cyan arrows: stress fibers correspond to those indicated by the same-color arrows in C. Scale bars = 10 μm. Images in C and E are typical of 43 cells.

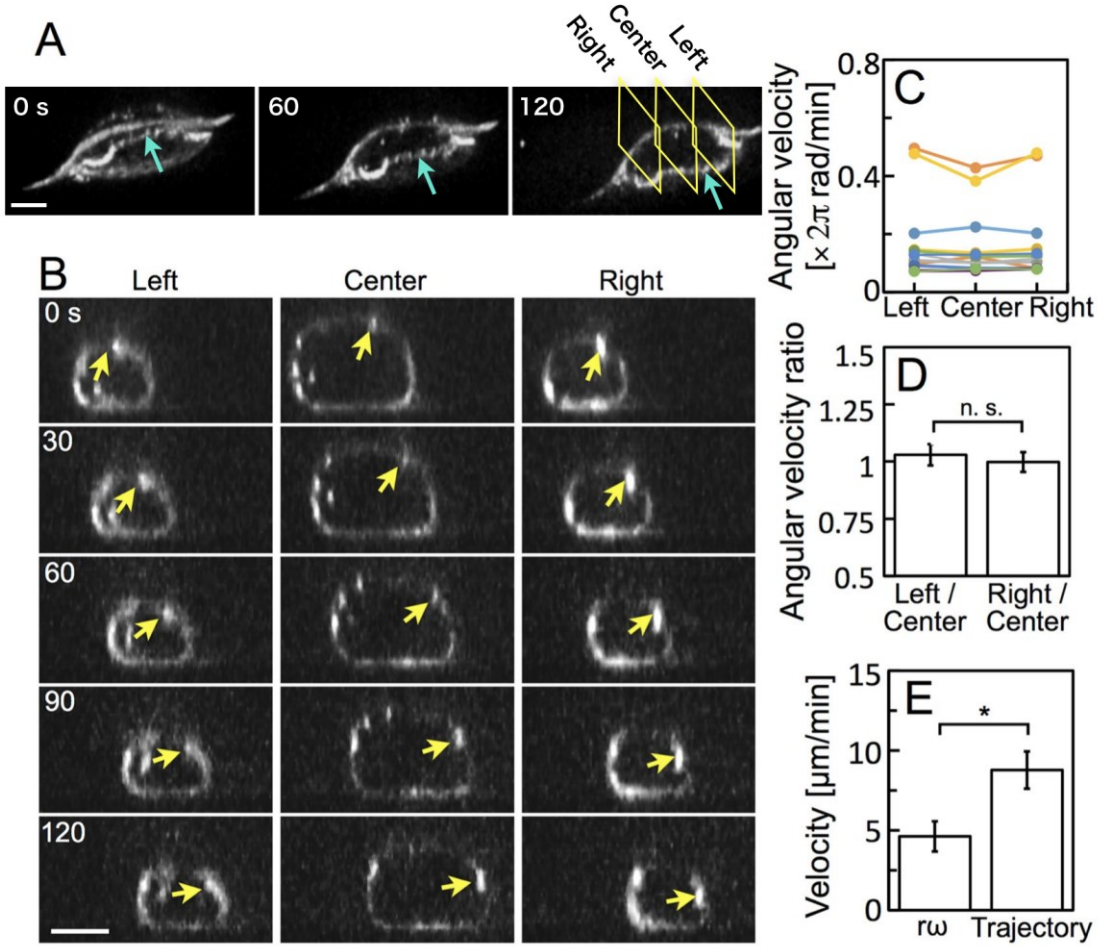

Figure 6-2. Stress fiber rotation in a migrating keratocyte. (A) Sequential 3D images. Cyan arrows: a stress fiber. Yellow squares show positions of three optical sections, Left, Center and Right in B. The Left and Right planes were positioned such that the distance between the two planes corresponds to 80% of the width of the cell body. Center plane is located at the middle of the Left and Right planes. (B) Three *x*-*z* optical sections made from A. Yellow arrows indicate an identical single fiber. (C) Angular velocity of the stress fibers. 12 different cells are represented in different colors. (D) Angular velocity ratios calculated from the data in C. (E) Migration velocity of the cells. rω: estimated as (radius) × (angular velocity) at Center. Trajectory: calculated from the migration trajectory of the cell. Bars in D and E: SEM. The *p*-values were calculated using Student's *t*-test. $*p < 0.05$. Scale bar = 5 μm.

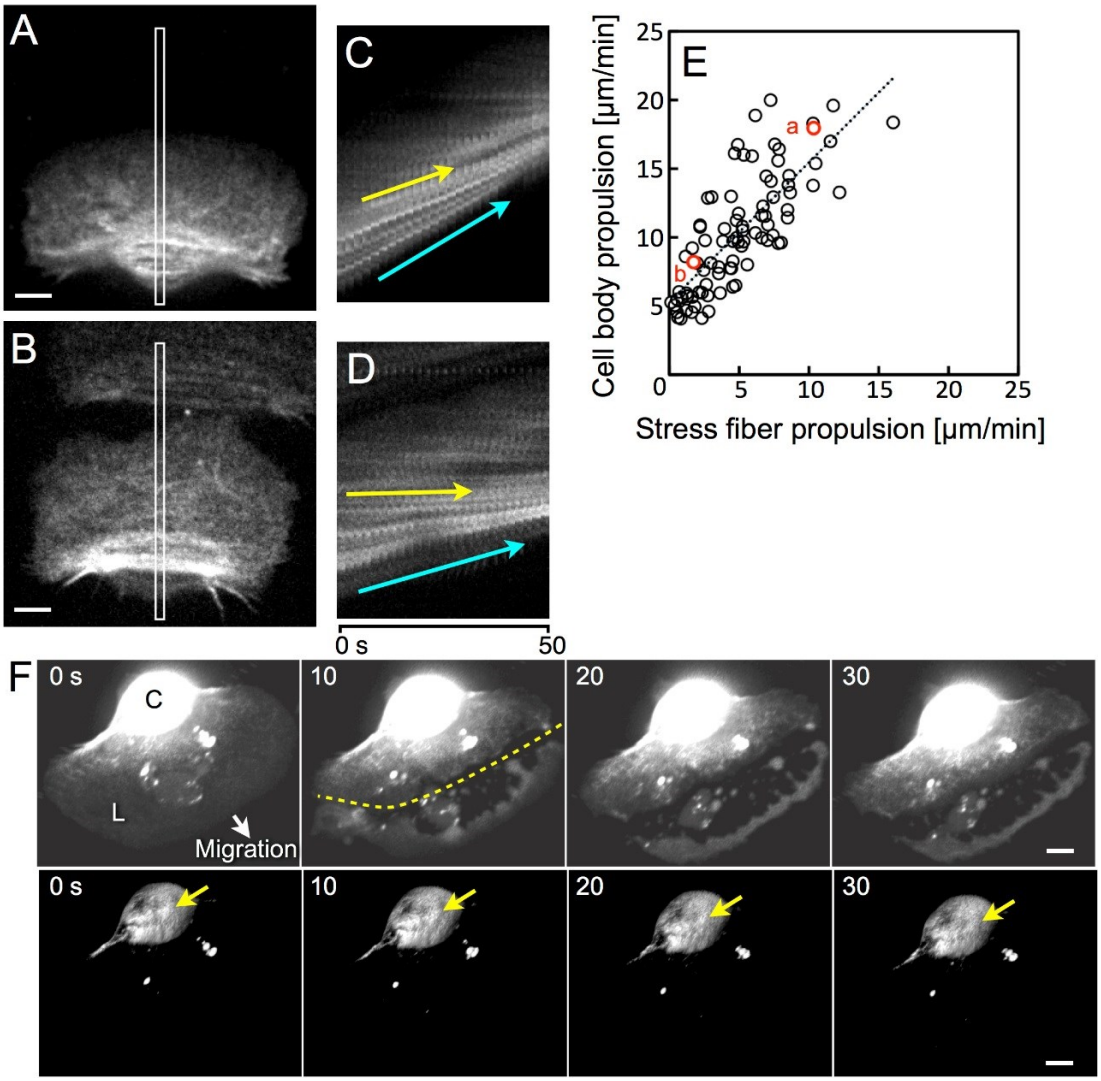

Figure 6-3. Detailed movement of stress fibers. (A and B) Filamentous actin images on the ventral surface of a fast (A) and a slowly migrating keratocytes (B). (C and D) Kymographs from sequential images at 2-s intervals. Cropped areas are shown as white squares in A and B. Yellow and cyan arrows mean movements of the stress fibers and cell edge, respectively. (E) Relationship of the propulsion speeds between the stress fiber and the cell body in the laboratory frame of reference. n = 87 cells from 14 experiments. Red circles represent the data from A and B. Correlation coefficient (γ) was 0.78. Straight dotted line is a regression line, $y = 1.02x + 5.29$, obtained by the Least Squares method. (F) Sequential 3D images. Upper and lower images are the same the photos, except that the brightness in the upper row has been increased to see lamellipodium. From 0 to 10 s, leading edge was cut off along the yellow dotted line in 10 s. L: lamellipodium, C: cell body, Yellow arrows: an identical stress fiber. Images in F are typical of 11 experiments. Scale bars = 5 μm.

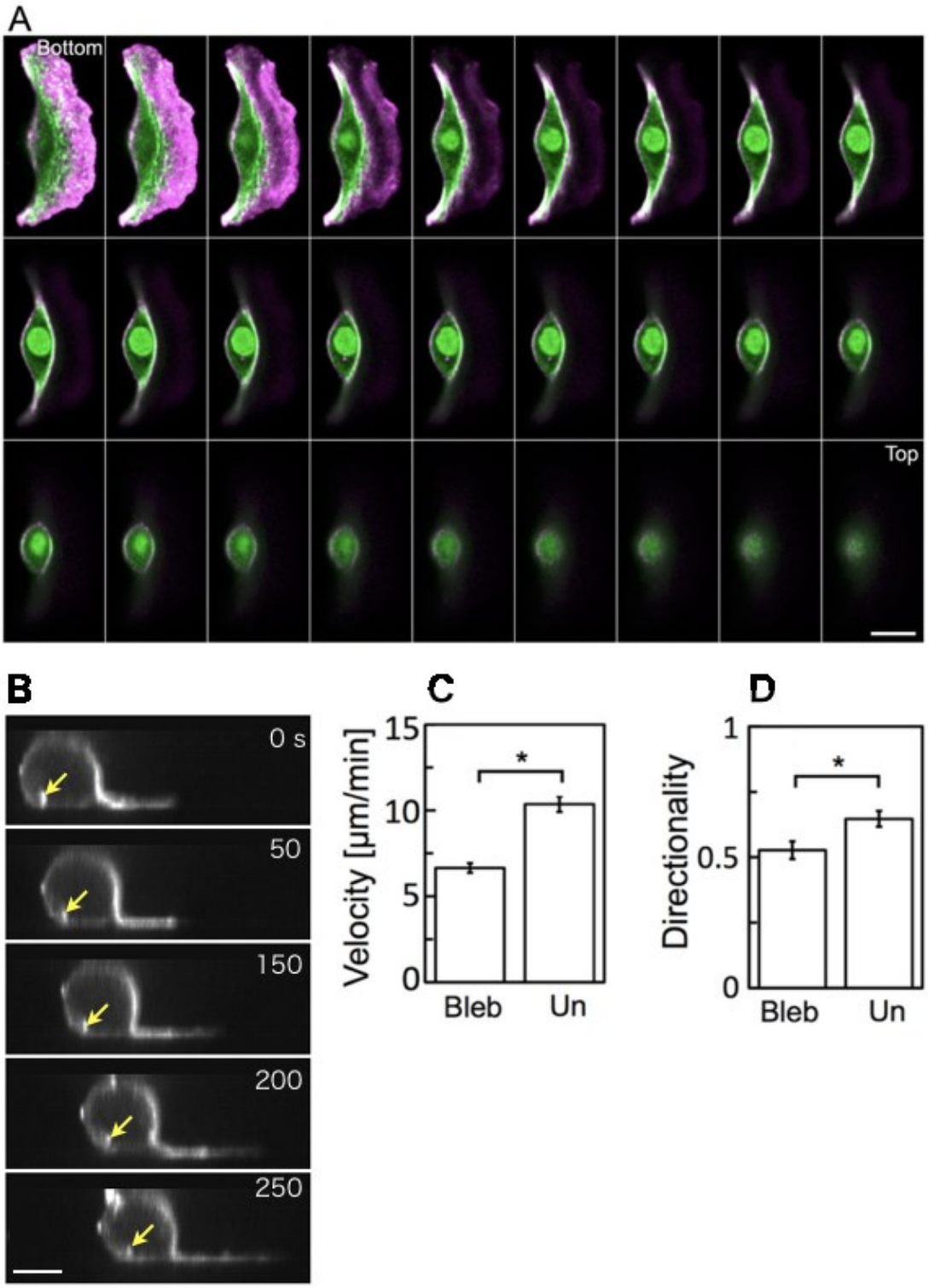
A
Bottom
Top
B
0 s
50
150
200
250
C
Velocity [μm/min]
15
10
5
0
*
Bleb
Un
D
Directionality
1
0.5
0
*
Bleb
Un

Figure 6-4. Removal of stress fibers from keratocytes and the resultant unstable migration. (A) Sequential *x*-*y* optical sections. Colocalization of filamentous actin (magenta) and myosin IIA (green) appears white. Height of each optical section is shown in Figure 6-1B. Scale bars = 10 μm. Images are typical of 21 cells. (B) Time series of a *x*-*z* optical section. Yellow arrows indicate an identical single bright grain. Scale bars = 5 μm. Images are typical of 17 cells. (C) Migration velocity. Bleb: blebbistatin-treated keratocytes (typical of 43 cells from 3 experiments). Un: intact keratocytes calculated from the data in Figure 6-3E. (D) Directionality. Bleb: blebbistatin-treated keratocytes (typical of 41 cells from 3 experiments). Un: intact keratocytes (n = 44 cells from 3 experiments). Error bars in B and C: SEM. The *p*-values were calculated using Student's *t*-test. $*p < 0.05$.

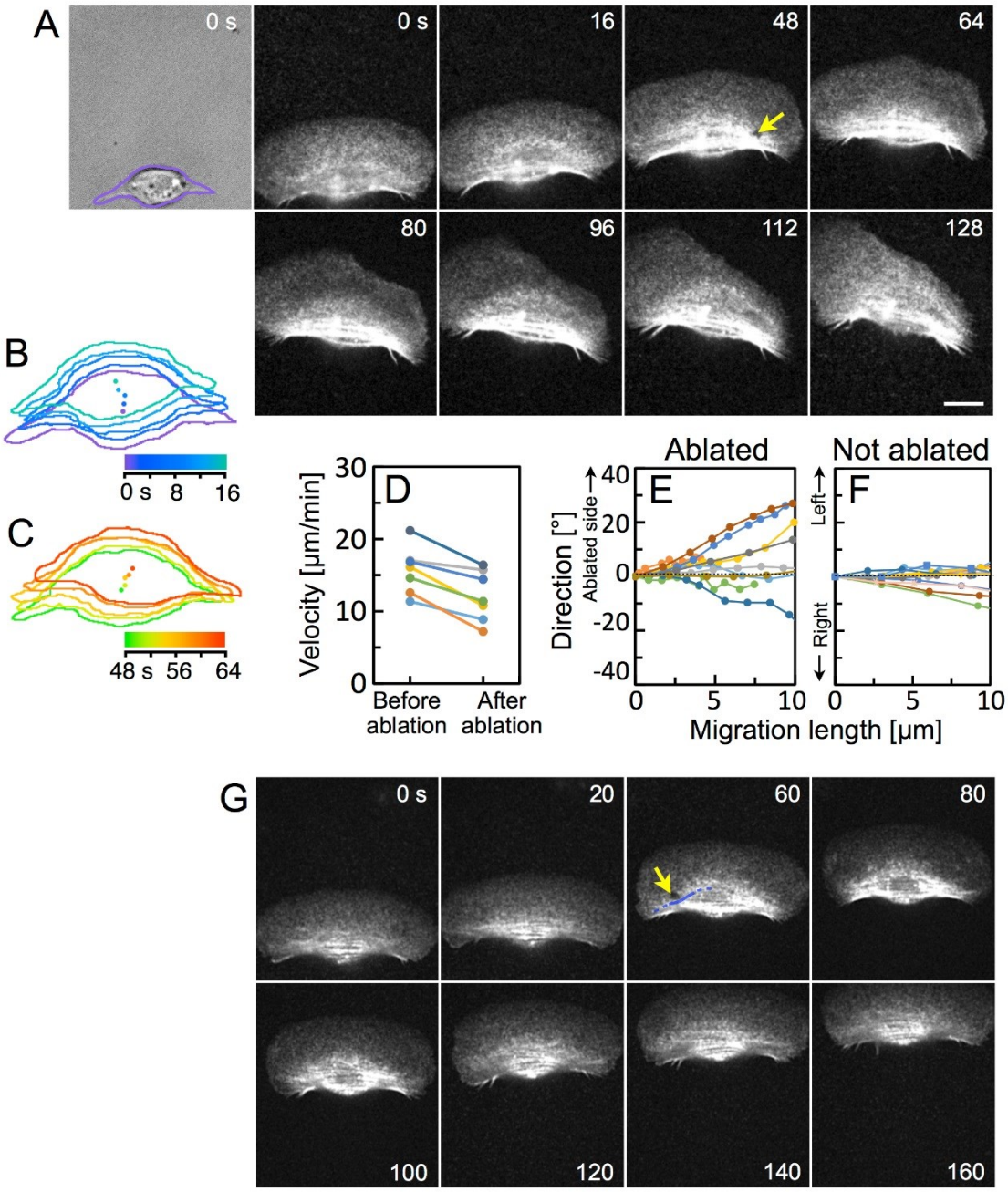
A
0 s
0 s
16
48
64
80
96
112
128
B
0 s 8 16
C
48 s 56 64
D
Velocity [μm/min]
30
20
10
0
Before ablation
After ablation
Ablated
Not ablated
E
F
Direction [°]
Ablated side
40
20
0
-20
-40
Left
Right
0 5 10
0 5 10
Migration length [μm]
G
0 s
20
60
80
100
120
140
160

Figure 6-5. Ablation of stress fibers. (A) A DIC image of a migrating keratocyte and time series of filamentous actin in the same cell. Before the 48-s frame, a part of the stress fibers was ablated (yellow arrow in 48 s). Contour of the cell body in the DIC image is traced with a purple line. Images in A are typical of 7 experiments. (B and C) Contours of the cell body and its centers of every 4 s before and after the ablation, respectively. (D) Comparison of the speeds of the centers of the cell bodies before and after the ablation (n = 7 cells). (E) Migration directions just after the ablation of stress fibers (n = 10 cells). (F) Migration directions of freely migrating cells (n = 13 cells). (G) Ablation of filamentous actin outside, but vicinity, of the stress fibers. Before the 40-s frame, actin filaments outside, but vicinity, of stress fibers were ablated (yellow arrow in 60 s). The stress fiber near the irradiation area is traced with a blue line. Images in G are typical of 5 experiments. Scale bars = 10 μm.

Chapter 7
General Discussion

Many kinds of unicellular organisms and the cells in tissues show crawling migration. Crawling cells can be classified, according to their migration velocity, into slow-crawling and fast-crawling cell types. Rigidity sensing by slow-crawling cell types has been studied by numerous investigators since the discovery of durotaxis (Lo et al., 2000). However, the mechanism by which fast-crawling cell types detect rigidity has hitherto been unknown. In this study, first in Chapter 2, we demonstrate a novel rigidity sensing function in fast-crawling cell types. They choose to migrate in the "soft" direction on an anisotropic substrate. Interestingly, rigidity sensing for migration in the soft direction appears to have an entirely different mechanism from that of slow-crawling cell types.

From the results in Figure 2-2, it is logical to infer that *Dictyostelium* cells on an anisotropic substrate exert greater traction forces in the rigid direction. If this is the case, the cells would be subjected to greater reaction forces in the same rigid direction from the substrate and would, we assume, migrate in that direction. Surprisingly, though, the cells prefer to migrate perpendicular to the rigid direction (Figures 2-4 and 2-5). This situation is identical to migration under cyclic substrate stretching. Under cyclic substrate stretching, *Dictyostelium* cells and HL-60 cells are repeatedly subjected to stretching forces from the substrate, and migrate in a direction perpendicular to these forces as shown in Chapter 5. The requirement to accumulate myosin II, an ATPase-deficient mutant myosin II suffices, for novel rigidity sensing is also the same as for the directional preference of migration under the cyclic substrate stretching. From these observations, we propose the following novel mechanism for rigidity sensing as illustrated in Figure 7-1. 1) Cells on a substrate of uneven stiffness extend pseudopods to random direction. 2) Pseudopods on a rigid substrate would receive larger reaction force, and this recruits myosin II. Accumulated myosin II suppresses the further extension of the pseudopod. 3) Cells migrate in the direction of a pseudopods on softer substrate, in which myosin II is not accumulated.

In this study, we did not identify the mechanism by which myosin II accumulates along the edge of the cell in the rigid direction of the substrate. Many investigators have reported the ability of myosin II to bind actin filaments in a force-dependent manner (Chanet et al., 2017; Finer et al., 1994; Kee et al., 2012; Luo et al., 2012; Merkel et al., 2000; Schiffhauer et al., 2016; Schiffhauer et al., 2019). Myosin II accumulates in the stretched portion of *Dictyostelium* cells, suggesting that the binding affinity of myosin II for actin filaments increases when the actin filaments are stretched (Uyeda et al., 2011). Based on this observation, we propose a hypothesis on how myosin II accumulates along the edge of the cell in the rigid direction of the substrate, as illustrated in Figure 7-2. When cells migrate on an anisotropic substrate, in both pseudopods in the soft (Figure 7-2A – C), and rigid (Figure 7-2D – F) direction of the substrate, actin polymerization (the black arrows in Figure 7-2A and D) pushes the front of the cell forward and the substrate pushes the cell backward with the same force through focal adhesions (green

ellipse in Figure 7-2A – F). In the soft direction of the substrate (Figure 7-2A – C), the displacement of the edge of the pseudopod (right-headed arrows in Figure 7-2B and C) is smaller than that of the substrate (left-headed arrows in Figure 7-2B and C), because the substrate is more elastic than the cell cortex. In this case, the cortical actin filaments do not deform much. On the other hand, in the rigid direction (Figure 7-2D – F), the displacement of the tip of the pseudopod (right-headed arrows in Figure 7-2E) is larger than that of the substrate (left-headed arrow in Figure 7-2E), because the substrate is less elastic than the cell cortex. Cortical actin filaments are then extended and the affinity of myosin II for those actin filaments increases. This induces the myosin II to accumulate there. Accumulated myosin II suppresses further actin polymerization as speculated from the result of Figure 3-8. As a result of this series of processes, the pseudopod continues to extend only in the soft direction. However, the role of myosin II is not only the suppression of actin polymerization but also the contraction of pseudopod as actomyosin. As myosin II accumulates, the contractile force of actomyosin increases. When the contractile force exceeds the structural strength of the actin filaments (a central actin filament shown in Figure 7-2E), the actin filaments will be collapsed by contraction of the pseudopod (Figure 7-2F). Thus, the contractile force of actomyosin may enhance the directional migration in soft direction, although it is not necessarily required. Experimental examination of this possibility is an interesting future issue.

In our preliminary experiments, we observed myosin II dynamics in the migrating *Dictyostelium* cells in a narrow tunnel. Interestingly, the cells migrated forward, repeating the elongation and retraction of pseudopods with myosin II accumulating at the leading edge of the expanded pseudopods, similar to climbing a ladder (Figure 7-3). This observation supports the above hypothesis.

Dictyostelium cells exerted greater traction forces on a more rigid substrate (Figure 2-2). Very active actin polymerization may take place strongly in the pseudopods in the rigid direction of the anisotropic substrate. If this is true, then a great deal of myosin II will also accumulate.

To verify our hypotheses (Figures 7-1 and 7-2), it will be necessary to simultaneously measure the distribution of the cell cortex-tension and structural changes in the actin filaments *in vivo*. The recent development of super-resolution microscopy should enable structural changes in actin filaments to be measured *in vivo*. The difference in cell cortex-tension between the front and the rear of a migrating keratocyte has been measured directly using optical tweezers (Lieber et al., 2013; Lieber et al., 2015). However, it is difficult to clarify the distribution of cortex tension throughout a migrating cell. The expression of tension-sensitive protein (Cost et al., 2015; Gates et al., 2019; Iwai and Uyeda, 2008; Iwai and Uyeda, 2010; Jurchenko and Salaita, 2015; Li et al., 2018; Liu et al., 2017; Ma and Salaita, 2019; Mohammed et al., 2019a; Popescu et al., 2006) may also enable the details of the distribution of cell-cortex tension to be detected. Combining this method with super-resolution microscopy may, in the near future, enable simultaneous measurement of the distribution of cell cortex-tension and structural changes in cortical actin filaments.

The physiological significance of rigidity sensing by fast-crawling cell types remains a mystery. Migration in the soft direction may be simply due to mechanical properties of the cells and might not be physiologically significant. There is, however, an interesting alternative hypothesis. It is reported that

freely-crawling cells, such as *Dictyostelium* (Li et al., 2008) and microglia (Yang et al., 2011), continue to turn in a direction symmetrical to the previous turn when they travel long distances. This behavior may increase their chances to find a target over that of performing a random walk (Li et al., 2008). It has not been clarified how the cells realize this zigzag crawling migration. *Dictyostelium* cells exert traction forces on the substrate at their extending pseudopods (Iwadate and Yumura, 2008a). At the same time, the cells receive a reaction force from the substrate. The reaction force has the same amplitude as the traction, but the direction is opposite. As mentioned above, it is presumed that *Dictyostelium* cells exert greater traction forces in the rigid direction and receive greater reaction forces from the substrate. This study also shows that *Dictyostelium* and HL-60 cells migrate to avoid the directions in which they receive larger forces from the substrate as shown in Chapter 3 and 4. The above facts and the results of this study suggest that the rigidity sensing of fast-crawling cell types may be what induces their zigzag crawling movement. Because, the cells may migrate forward, repeating the elongation and retraction of pseudopods with myosin II accumulating alternately left and right as shown in Figure 7-3.

In Chapter 5, we found that keratocytes have bimodal mechanosensing system for directional preference of migration. It is very interesting that the two different mechano-sensing systems in single cells play two different significant roles. The role of the crawling migration of intact keratocytes on fish skin is wound-healing (Morita et al., 2011). For this purpose, keratocytes migrate not as single cells but as a sheet composed of multiple cells during wound healing (McDonald et al., 2013; Rapanan et al., 2014). In this situation, the rear cells seem to be pulled by the leading cells, or leading cells seem to be pushed by the rear cells in the similar way as in the cyclic stretching of substrate (Mohammed et al., 2019b). Interestingly, keratocytes perform collective movement as a epidermal sheet, in which adjacent cells are connected by adherence junctions at both ends of stress fibers (Matsumoto and Sugimoto, 2007; Morita et al., 2011; Rapanan et al., 2014; Rapanan et al., 2015). The mechanism of directional preference of migration, which depends on stress fibers as revealed in Chapter 5, may contribute to the collective cell migration on fish skin as well.

We found that the stress fibers in crawling keratocytes rotate in a wheel-like fashion and play a unique role in migration as shown in Chapter 6. Migrating fibroblasts (Watanabe and Mitchison, 2002), keratinocytes (Frank and Carter, 2004) and a protist *Vannella* sp. (Smirnov et al., 2007; Smirnov et al., 2016) sometimes spontaneously adopt shapes that resemble keratocytes during their migration. Also, the rat Nara bladder tumor (NBT-II) cells treated with imatinib (Chen et al., 2013), an Abl family kinase inhibitor, and *amiB*$^{-}$ *Dictyostelium* cells (Asano et al., 2004) adopt the keratocyte-like shapes. Moreover, it is reported that the configuration of stress fibers in the *x*-*y* plane in the NBT-II cells is identical to that in keratocytes (Chen et al., 2013). Thus, the rotating movement of stress fibers may not be a special phenomenon seen only in fish keratocytes but a universal mechanism for crawling migration that does not depend on the cell type.

Concluding Remarks

1. We demonstrated a novel form of rigidity sensing, by which fast-crawling cell types choose to migrate in the “soft” direction on an anisotropic substrate in a myosin II-dependent manner [Chapter 2].

2. In response to the cyclic substrate stretching, fast-crawling cell types migrate in a direction that is perpendicular to the direction of stretching. We demonstrated that this mechanosensing reaction also requires myosin II [Chapter 3, 4].

3. In response to the cyclic substrate stretching, stress fibers in slow-crawling cell types rearrange themselves to the direction that is perpendicular to the direction of stretching. We demonstrated that keratocytes show two distinct mechanosensing reactions in response to the cyclic substrate stretching: one that depends on stress fibers like slow-crawling cell types, and the other that does not depend on them, as seen in fast-crawling cell types [Chapter 5].

4. We demonstrated that the wheel-like rotation of stress fibers contributes to the crawling migration of keratocytes, although it is not the only driving force [Chapter 6].

Figures

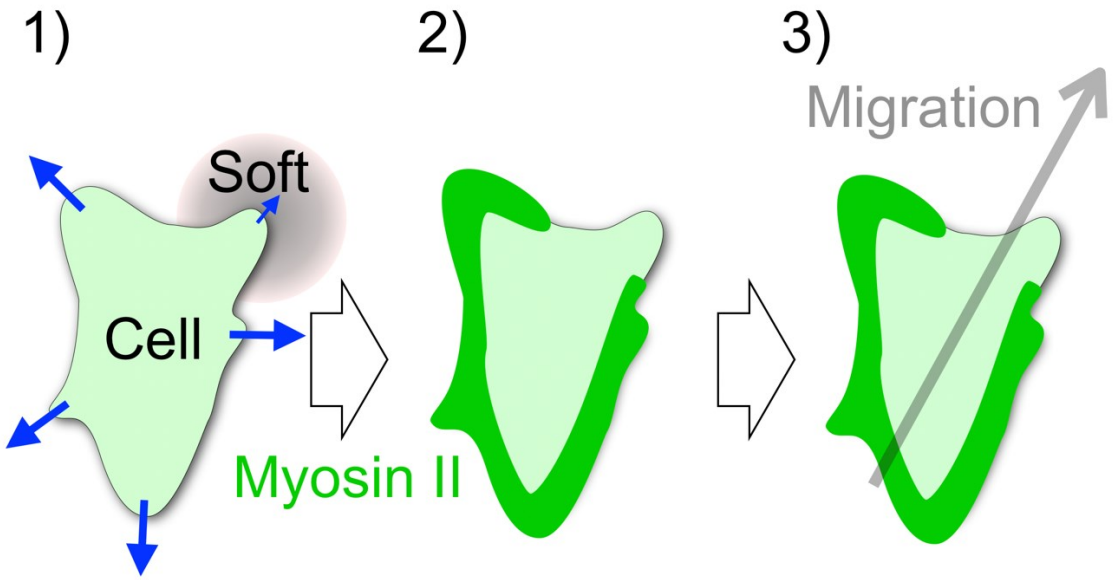

Figure 7-1. A hypothetical mechanism for novel rigidity sensing. 1) Cells on a substrate of uneven stiffness extend pseudopods to random directions (blue arrows). 2) Pseudopods on a rigid substrate would receive larger reaction force, and this recruits myosin II. Accumulated myosin II suppresses the further extension of the pseudopod. 3) Cells migrate in the direction of the pseudopod in which myosin II is not accumulated.

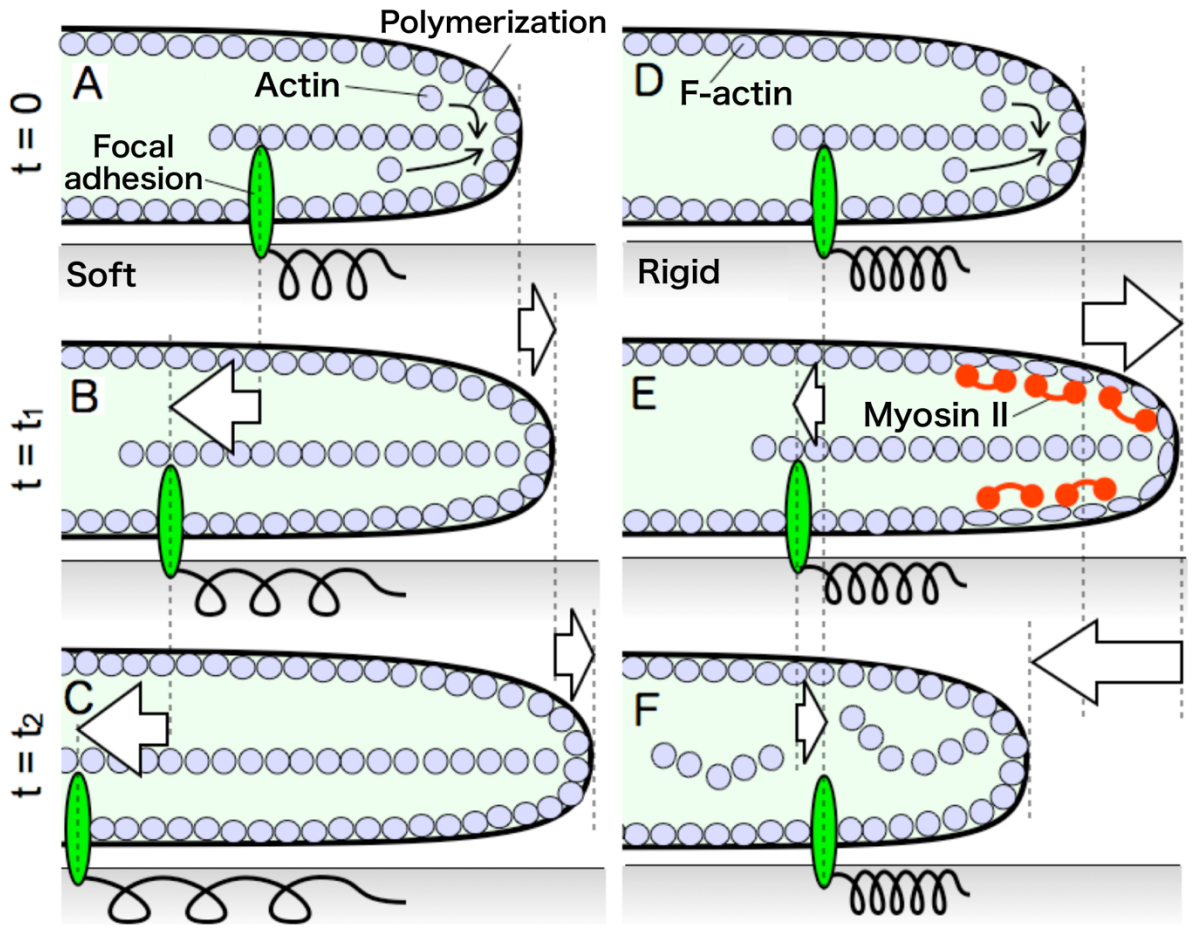

Figure 7-2. The hypothetical response of pseudopods in a crawling cell on anisotropic substrate. (A – C) A pseudopod extended in the soft direction. (D – F) A pseudopod extended in the rigid direction. See text for details.

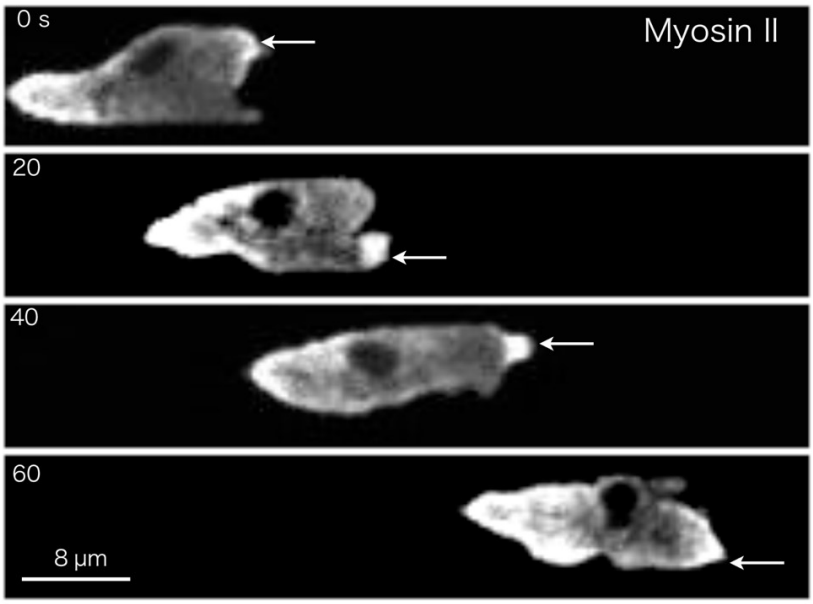

Figure 7-3. Myosin II dynamics in a migrating *Dictyostelium* cell. The cell migrates from left to right in a narrow tunnel (8 μm in width and 5 μm in height). Myosin II accumulates not at the rear edge but at the frontal tip of pseudopods (arrows).

Acknowledgements

The experiments in this study were performed in Biophysics Laboratory at Yamaguchi University. I would like to express my deep gratitude to my supervisor, Associate Professor Y. Iwadate (Yamaguchi University), for his valuable discussions, precious advice and continuous encouragement. I am deeply grateful to Professor T.Q.P. Uyeda (Waseda University) for critical reading of the manuscript and his invaluable detailed comments and discussions. I would like to thank Prof. M. Takano and Prof. K. Yasuda (Waseda University) for constructive comments and discussions throughout the writing of the manuscript.

I thank Associate Prof. Y. Sakumura, (NAIST) for his instructions in the analysis method in Chapters 2 and 4. I am grateful to Associate Prof. K. Shimabukuro (Ube College) for his help in obtaining the electron microscopic images in Chapter 2. I thank Lecturer K. Sato. (Tokushima University), Associate Prof. Y. Nakashima (Kumamoto University) and Prof. K. Minami (Yamaguchi University) for providing me the microstretching device used in Chapter 3. I am indebted to Lecturer M. Tsujioka (Tokyo Medical and Dental University) for providing me the Sib A-null *Dictyostelium* cells used in Chapter 3 and Mr. K. Ueda (Yamaguchi University) for recording and analyzing the trajectory of migrating HL60 cells in Chapter 4. I thank Associate Prof. S. Nonaka and Dr. A. Taniguchi (NIBB) for recording the migrating keratocytes under light sheet microscopy in Chapter 6.

Finally, I would like to express my gratitude to past and present members of the Biophysics Laboratory for their encouragement and help.

References

Anderson, K. I., Wang, Y. L. and Small, J. V. (1996). Coordination of protrusion and translocation of the keratocyte involves rolling of the cell body. *J. Cell Biol.* **134**, 1209–1218.

Arai, Y., Shibata, T., Matsuoka, S., Sato, M. J., Yanagida, T. and Ueda, M. (2010). Self-organization of the phosphatidylinositol lipids signaling system for random cell migration. *Proc. Natl. Acad. Sci.*

Asano, Y., Mizuno, T., Kon, T., Nagasaki, A., Sutoh, K. and Uyeda, T. Q. P. (2004). Keratocyte-like locomotion in amiB-null *Dictyostelium* cells. *Cell Motil. Cytoskeleton* **59**, 17–27.

Barnhart, E. L., Lee, K.-C., Keren, K., Mogilner, A. and Theriot, J. A. (2011). An Adhesion-dependent switch between mechanisms that determine motile cell shape. *PLoS Biol* **9**, e1001059.

Barnhart, E., Lee, K.-C., Allen, G. M., Theriot, J. A. and Mogilner, A. (2015). Balance between cell-substrate adhesion and myosin contraction determines the frequency of motility initiation in fish keratocytes. *Proc. Natl. Acad. Sci. U. S. A.* **112**, 5045–5050.

Birukov, K. G., Jacobson, J. R., Flores, A. A., Ye, S. Q., Birukova, A. A., Verin, A. D. and Garcia, J. G. N. (2003). Magnitude-dependent regulation of pulmonary endothelial cell barrier function by cyclic stretch. *Am. J. Physiol. - Lung Cell. Mol. Physiol.* **285**, L785–L797.

Bollmann, L., Koser, D. E., Shahapure, R., Gautier, H. O. B., Holzapfel, G. A., Scarcelli, G., Gather, M. C., Ulbricht, E. and Franze, K. (2015). Microglia mechanics: immune activation alters traction forces and durotaxis. *Front. Cell. Neurosci.* **9**, 363.

Bosgraaf, L. and van, H. (2006). The regulation of myosin II in *Dictyostelium*. *Eur. J. Cell Biol.* **85**, 969–979.

Bretschneider, T., Diez, S., Anderson, K., Heuser, J., Clarke, M., Müller-Taubenberger, A., Köhler, J. and Gerisch, G. (2004). Dynamic actin patterns and Arp2/3 assembly at the substrate-attached surface of motile cells. *Curr. Biol.* **14**, 1–10.

Burnette, D. T., Manley, S., Sengupta, P., Sougrat, R., Davidson, M. W., Kachar, B. and Lippincott-Schwartz, J. (2011). A role for actin arcs in the leading-edge advance of migrating cells. *Nat. Cell Biol.* **13**, 371–381.

Burridge, K. and Guilluy, C. (2016). Focal adhesions, stress fibers and mechanical tension. *Exp. Cell Res.* **343**, 14–20.

Burton, K., Park, J. H. and Taylor, D. L. (1999). Keratocytes generate traction forces in two phases. *Mol. Biol. Cell* **10**, 3745–3769.

Case, L. B. and Waterman, C. M. (2015). Integration of actin dynamics and cell adhesion by a three-dimensional, mechanosensitive molecular clutch. *Nat. Cell Biol.* **17**, 955–963.

Chanet, S., Miller, C. J., Vaishnav, E. D., Ermentrout, B., Davidson, L. A. and Martin, A. C. (2017). Actomyosin meshwork mechanosensing enables tissue shape to orient cell force. *Nat. Commun.* **8**, 15014.

Chen, W. T. (1981). Mechanism of retraction of the trailing edge during fibroblast movement. *J. Cell Biol.* **90**, 187–200.

Chen, L., Vicente-Manzanares, M., Potvin-Trottier, L., Wiseman, P. W. and Horwitz, A. R. (2012). The integrin-ligand interaction regulates adhesion and migration through a molecular clutch. *PloS One* **7**, e40202.

Chen, Z., Lessey, E., Berginski, M. E., Cao, L., Li, J., Trepat, X., Itano, M., Gomez, S. M., Kapustina, M., Huang, C., et al. (2013). Gleevec, an Abl family inhibitor, produces a profound change in cell shape and migration. *PLoS One* **8**, e52233.

Chi, Q., Yin, T., Gregersen, H., Deng, X., Fan, Y., Zhao, J., Liao, D. and Wang, G. (2014). Rear actomyosin contractility-driven directional cell migration in three-dimensional matrices: a mechano-chemical coupling mechanism. *J. R. Soc. Interface* **11**,.

Chung, C. Y., Potikyan, G. and Firtel, R. A. (2001). Control of cell polarity and chemotaxis by Akt/PKB and PI3 kinase through the regulation of PAKa. *Mol. Cell* **7**, 937–947.

Clow, P. A. and McNally, J. G. (1999). In vivo observations of myosin II dynamics support a role in rear retraction. *Mol. Biol. Cell* **10**, 1309–1323.

Comer, F. I. and Parent, C. A. (2002). PI 3-Kinases and PTEN: How opposites chemoattract. *Cell* **109**, 541–544.

Cornillon, S., Gebbie, L., Benghezal, M., Nair, P., Keller, S., Wehrle-Haller, B., Charette, S. J., Brückert, F., Letourneur, F. and Cosson, P. (2006). An adhesion molecule in free-living *Dictyostelium* amoebae with integrin β features. *EMBO Rep.* **7**, 617–621.

Cost, A.-L., Ringer, P., Chrostek-Grashoff, A. and Grashoff, C. (2015). How to Measure Molecular Forces in Cells: A guide to evaluating genetically-encoded FRET-based tension sensors. *Cell. Mol. Bioeng.* **8**, 96–105.

Cramer, L. P., Siebert, M. and Mitchison, T. J. (1997). Identification of novel graded polarity actin filament bundles in locomoting heart fibroblasts: implications for the generation of motile force. *J. Cell Biol.* **136**, 1287–1305.

Crosby, L. M., Luellen, C., Zhang, Z., Tague, L. L., Sinclair, S. E. and Waters, C. M. (2011). Balance of life and death in alveolar epithelial type II cells: Proliferation, apoptosis, and the effects of cyclic stretch on wound healing. *Am. J. Physiol. - Lung Cell. Mol. Physiol.* **301**, L536–L546.

Dembo, M., Oliver, T., Ishihara, A. and Jacobson, K. (1996). Imaging the traction stresses exerted by locomoting cells with the elastic substratum method. *Biophys. J.* **70**, 2008–2022.

Deng, J., Petersen, B. E., Steindler, D. A., Jorgensen, M. L. and Laywell, E. D. (2006). Mesenchymal stem cells spontaneously express neural proteins in culture and are neurogenic after transplantation. *Stem Cells Dayt. Ohio* **24**, 1054–1064.

Desai, L. P., White, S. R. and Waters, C. M. (2010). Cyclic mechanical stretch decreases cell migration by inhibiting phosphatidylinositol 3-kinase- and focal adhesion kinase-mediated JNK1 activation. *J. Biol. Chem.* **285**, 4511–4519.

Doyle, A. D. and Lee, J. (2005). Cyclic changes in keratocyte speed and traction stress arise from Ca2+-dependent regulation of cell adhesiveness. *J. Cell Sci.* **118**, 369–379.

Doyle, A., Marganski, W. and Lee, J. (2004). Calcium transients induce spatially coordinated increases in traction force during the movement of fish keratocytes. *J. Cell Sci.* **117**, 2203–2214.

Dulyaninova, N. G., House, R. P., Betapudi, V. and Bresnick, A. R. (2007). Myosin-IIA heavy-chain phosphorylation regulates the motility of MDA-MB-231 carcinoma cells. *Mol. Biol. Cell* **18**, 3144–3155.

Egelhoff, T. T., Lee, R. J. and Spudich, J. A. (1993). *Dictyostelium* myosin heavy chain phosphorylation sites regulate myosin filament assembly and localization in vivo. *Cell* **75**, 363–371.

Eliott, S., Joss, G. H., Spudich, A. and Williams, K. L. (1993). Patterns in *Dictyostelium* discoideum: The role of myosin II in the transition from the unicellular to the multicellular phase. *J. Cell Sci.* **104**, 457–466.

Elosegui-Artola, A., Oria, R., Chen, Y., Kosmalska, A., Pérez-González, C., Castro, N., Zhu, C., Trepat, X. and Roca-Cusachs, P. (2016). Mechanical regulation of a molecular clutch defines force transmission and transduction in response to matrix rigidity. *Nat. Cell Biol.* **18**, 540–548.

Engler, A. J., Sen, S., Sweeney, H. L. and Discher, D. E. (2006). Matrix elasticity directs stem cell lineage specification. *Cell* **126**, 677–689.

Euteneuer, U. and Schliwa, M. (1984). Persistent, directional motility of cells and cytoplasmic fragments in the absence of microtubules. *Nature* **310**, 58–61.

Fernandez-Gonzalez, R., Simoes, S. de M., Röper, J.-C., Eaton, S. and Zallen, J. A. (2009). Myosin II dynamics are regulated by tension in intercalating cells. *Dev. Cell* **17**, 736–743.

Finer, J. T., Simmons, R. M. and Spudich, J. A. (1994). Single myosin molecule mechanics: piconewton forces and nanometre steps. *Nature* **368**, 113–119.

Fournier, M. F., Sauser, R., Ambrosi, D., Meister, J.-J. and Verkhovsky, A. B. (2010). Force transmission in migrating cells. *J. Cell Biol.* **188**, 287–297.

Frank, D. E. and Carter, W. G. (2004). Laminin 5 deposition regulates keratinocyte polarization and persistent migration. *J. Cell Sci.* **117**, 1351–1363.

Fuhs, T., Goegler, M., Brunner, C. A., Wolgemuth, C. W. and Kaes, J. A. (2014). Causes of retrograde flow in fish keratocytes. *Cytoskeleton* **71**, 24–35.

Galbraith, C. G. and Sheetz, M. P. (1997). A micromachined device provides a new bend on fibroblast traction forces. *Proc. Natl. Acad. Sci.* **94**, 9114–9118.

Galkin, V. E., Orlova, A., Lukoyanova, N., Wriggersd, W. and Egelman, E. H. (2001). Actin depolymerizing factor stabilizes an existing state of F-actin and can change the tilt of F-actin subunits. *J. Cell Biol.* **153**, 75–86.

Gates, E. M., LaCroix, A. S., Rothenberg, K. E. and Hoffman, B. D. (2019). Improving quality, reproducibility, and usability of FRET-based tension sensors. *Cytometry A* **95**, 201–213.

Giannone, G. and Sheetz, M. P. (2006). Substrate rigidity and force define form through tyrosine phosphatase and kinase pathways. *Trends Cell Biol.* **16**, 213–223.

Goodrich, H. B. (1924). Cell behavior in tissue cultures. *Biol. Bull.* **46**, 252–262.

Gupta, M., Doss, B., Lim, C. T., Voituriez, R. and Ladoux, B. (2016). Single cell rigidity sensing: A complex relationship between focal adhesion dynamics and large-scale actin cytoskeleton remodeling. *Cell Adhes. Migr.* **10**, 554–567.

Hadden, W. J., Young, J. L., Holle, A. W., McFetridge, M. L., Kim, D. Y., Wijesinghe, P., Taylor-Weiner, H., Wen, J. H., Lee, A. R., Bieback, K., et al. (2017). Stem cell migration and mechanotransduction on linear stiffness gradient hydrogels. *Proc. Natl. Acad. Sci. U. S. A.* **114**, 5647–5652.

Hayakawa, K., Tatsumi, H. and Sokabe, M. (2011). Actin filaments function as a tension sensor by tension-dependent binding of cofilin to the filament. *J. Cell Biol.* **195**, 721–727.

Hayakawa, K., Sakakibara, S., Sokabe, M. and Tatsumi, H. (2014). Single-molecule imaging and kinetic analysis of cooperative cofilin–actin filament interactions. *Proc. Natl. Acad. Sci.* **111**, 9810–9815.

Hind, L. E., Vincent, W. J. B. and Huttenlocher, A. (2016). Leading from the back: The role of the uropod in neutrophil polarization and migration. *Dev. Cell* **38**, 161–169.

Hoeller, O. and Kay, R. R. (2007). Chemotaxis in the absence of PIP3 gradients. *Curr. Biol.* **17**, 813–817.

Hofstetter, C. P., Schwarz, E. J., Hess, D., Widenfalk, J., El Manira, A., Prockop, D. J. and Olson, L. (2002). Marrow stromal cells form guiding strands in the injured spinal cord and promote recovery. *Proc. Natl. Acad. Sci. U. S. A.* **99**, 2199–2204.

Hotulainen, P. and Lappalainen, P. (2006). Stress fibers are generated by two distinct actin assembly mechanisms in motile cells. *J. Cell Biol.* **173**, 383–394.

Iijima, M. and Devreotes, P. (2002). Tumor suppressor PTEN mediates sensing of chemoattractant gradients. *Cell* **109**, 599–610.

Insall, R. H., Soede, R. D., Schaap, P. and Devreotes, P. N. (1994). Two cAMP receptors activate common signaling pathways in *Dictyostelium*. *Mol. Biol. Cell* **5**, 703–711.

Isenberg, B. C., DiMilla, P. A., Walker, M., Kim, S. and Wong, J. Y. (2009). Vascular smooth muscle cell durotaxis depends on substrate stiffness gradient strength. *Biophys. J.* **97**, 1313–1322.

Iwadate, Y. and Yumura, S. (2008a). Actin-based propulsive forces and myosin-II-based contractile forces in migrating *Dictyostelium* cells. *J. Cell Sci.* **121**, 1314–1324.

Iwadate, Y. and Yumura, S. (2008b). Molecular dynamics and forces of a motile cell simultaneously visualized by TIRF and force microscopies. *BioTechniques* **44**, 739–750.

Iwadate, Y. and Yumura, S. (2009a). Cyclic stretch of the substratum using a shape-memory alloy induces directional migration in *Dictyostelium* cells. *BioTechniques* **47**, 757–767.

Iwadate, Y. and Yumura, S. (2009b). Cyclic stretch of the substratum using a shape-memory alloy induces directional migration in *Dictyostelium* cells. *BioTechniques* **47**, 757–767.

Iwadate, Y., Okimura, C., Sato, K., Nakashima, Y., Tsujioka, M. and Minami, K. (2013). Myosin-II-mediated directional migration of *Dictyostelium* cells in response to cyclic stretching of substratum. *Biophys. J.* **104**, 748–758.

Iwai, S. and Uyeda, T. Q. P. (2008). Visualizing myosin–actin interaction with a genetically-encoded fluorescent strain sensor. *Proc. Natl. Acad. Sci.* **105**, 16882–16887.

Iwai, S. and Uyeda, T. Q. P. (2010). Myosin-actin interaction in *Dictyostelium* cells revealed by GFP-based strain sensor and validated linear spectral unmixing. *Cytometry A* **77A**, 743–750.

Jay, P. Y., Pham, P. A., Wong, S. A. and Elson, E. L. (1995). A mechanical function of myosin II in cell motility. *J. Cell Sci.* **108**, 387–393.

Jiang, G., Huang, A. H., Cai, Y., Tanase, M. and Sheetz, M. P. (2006). Rigidity sensing at the leading edge through αvβ3 integrins and RPTPα. *Biophys. J.* **90**, 1804–1809.

Jurado, C., Haserick, J. R. and Lee, J. (2005). Slipping or gripping? Fluorescent speckle microscopy in fish keratocytes reveals two different mechanisms for generating a retrograde flow of actin. *Mol. Biol. Cell* **16**, 507–518.

Jurchenko, C. and Salaita, K. S. (2015). Lighting up the force: Investigating mechanisms of mechanotransduction using fluorescent tension probes. *Mol. Cell. Biol.* **35**, 2570–2582.

Kamakura, S., Nomura, M., Hayase, J., Iwakiri, Y., Nishikimi, A., Takayanagi, R., Fukui, Y. and Sumimoto, H. (2013). The cell polarity protein mInsc regulates neutrophil chemotaxis via a noncanonical G protein signaling pathway. *Dev. Cell* **26**, 292–302.

Kaunas, R., Nguyen, P., Usami, S. and Chien, S. (2005). Cooperative effects of Rho and mechanical stretch on stress fiber organization. *Proc. Natl. Acad. Sci. U. S. A.* **102**, 15895–15900.

Kawano, T. and Kidoaki, S. (2011). Elasticity boundary conditions required for cell mechanotaxis on microelastically-patterned gels. *Biomaterials* **32**, 2725–2733.

Kee, Y.-S., Ren, Y., Dorfman, D., Iijima, M., Firtel, R., Iglesias, P. A. and Robinson, D. N. (2012). A mechanosensory system governs myosin II accumulation in dividing cells. *Mol. Biol. Cell* **23**, 1510–1523.

Keren, K., Pincus, Z., Allen, G. M., Barnhart, E. L., Marriott, G., Mogilner, A. and Theriot, J. A. (2008). Mechanism of shape determination in motile cells. *Nature* **453**, 475–480.

Kobayashi, T. and Sokabe, M. (2010). Sensing substrate rigidity by mechanosensitive ion channels with stress fibers and focal adhesions. *Curr. Opin. Cell Biol.* **22**, 669–676.

Kolega, J. (2003). Asymmetric distribution of myosin IIB in migrating endothelial cells is regulated by a Rho-dependent kinase and contributes to tail retraction. *Mol. Biol. Cell* **14**, 4745–4757.

Kölsch, V., Charest, P. G. and Firtel, R. A. (2008). The regulation of cell motility and chemotaxis by phospholipid signaling. *J Cell Sci* **121**, 551–559.

Kondo, T., Johnson, S. A., Yoder, M. C., Romand, R. and Hashino, E. (2005). Sonic hedgehog and retinoic acid synergistically promote sensory fate specification from bone marrow-derived pluripotent stem cells. *Proc. Natl. Acad. Sci. U. S. A.* **102**, 4789–4794.

Kuo, J.-C. (2013). Mechanotransduction at focal adhesions: integrating cytoskeletal mechanics in migrating cells. *J. Cell. Mol. Med.* **17**, 704–712.

Lachowski, D., Cortes, E., Pink, D., Chronopoulos, A., Karim, S. A., Morton, J. and Hernández, A. E. del R. (2017). Substrate rigidity controls activation and durotaxis in pancreatic stellate cells. *Sci. Rep.* **7**, 2506.

Lam, P. and Huttenlocher, A. (2013). Interstitial leukocyte migration in vivo. *Curr. Opin. Cell Biol.* **25**, 650–658.

Lauffenburger, D. A. and Horwitz, A. F. (1996). Cell migration: A physically integrated molecular process. *Cell* **84**, 359–369.

Lazopoulos, K. A. and Stamenović, D. (2008). Durotaxis as an elastic stability phenomenon. *J. Biomech.* **41**, 1289–1294.

Lee, J. and Jacobson, K. (1997). The composition and dynamics of cell-substratum adhesions in locomoting fish keratocytes. *J. Cell Sci.* **110**, 2833–2844.

Lee, J., Ishihara, A., Theriot, J. A. and Jacobson, K. (1993). Principles of locomotion for simple-shaped cells. *Nature* **362**, 167–171.

Lee, C.-F., Haase, C., Deguchi, S. and Kaunas, R. (2010). Cyclic stretch-induced stress fiber dynamics - Dependence on strain rate, Rho-kinase and MLCK. *Biochem. Biophys. Res. Commun.* **401**, 344–349.

Li, L., Nørrelykke, S. F. and Cox, E. C. (2008). Persistent cell motion in the absence of external signals: A search strategy for eukaryotic cells. *PLOS ONE* **3**, e2093.

Li, W., Yu, X., Xie, F., Zhang, B., Shao, S., Geng, C., Aziz, A. ur R., Liao, X. and Liu, B. (2018). A membrane-bound biosensor visualizes shear stress-induced inhomogeneous alteration of cell membrane tension. *iScience* **7**, 180–190.

Lieber, A. D., Yehudai-Resheff, S., Barnhart, E. L., Theriot, J. A. and Keren, K. (2013). Membrane tension in rapidly moving cells is determined by cytoskeletal forces. *Curr. Biol.* **23**, 1409–1417.

Lieber, A. D., Schweitzer, Y., Kozlov, M. M. and Keren, K. (2015). Front-to-rear membrane tension gradient in rapidly moving cells. *Biophys. J.* **108**, 1599–1603.

Liu, C., Baek, S., Kim, J., Vasko, E., Pyne, R. and Chan, C. (2014). Effect of static pre-stretch induced surface anisotropy on orientation of mesenchymal stem cells. *Cell. Mol. Bioeng.* **7**, 106–121.

Liu, Y., Galior, K., Ma, V. P.-Y. and Salaita, K. (2017). Molecular tension probes for imaging forces at the cell surface. *Acc. Chem. Res.* **50**, 2915–2924.

Lo, C.-M., Wang, H.-B., Dembo, M. and Wang, Y. (2000). Cell movement is guided by the rigidity of the substrate. *Biophys. J.* **79**, 144–152.

Luo, T., Mohan, K., Srivastava, V., Ren, Y., Iglesias, P. A. and Robinson, D. N. (2012). Understanding the cooperative interaction between myosin II and actin cross-linkers mediated by actin filaments during mechanosensation. *Biophys. J.* **102**, 238–247.

Ma, V. P.-Y. and Salaita, K. (2019). DNA nanotechnology as an emerging tool to study mechanotransduction in living systems. *Small* **15**, 1900961.

Maeda, Y. T., Inose, J., Matsuo, M. Y., Iwaya, S. and Sano, M. (2008). Ordered patterns of cell shape and orientational correlation during spontaneous cell migration. *PLoS One* **3**, e3734.

Mark, J. E. (1999). *Polymer data handbook*. Oxford University Press, New York.

Marshall A. Lichtman, P. J. W. (1984). Chemotactic peptide-induced changes in neutrophil actin conformation. *J. Cell Biol.* **99**, 1060–1065.

Martin, P. (1997). Wound healing--aiming for perfect skin regeneration. *Science* **276**, 75–81.

Matsumoto, R. and Sugimoto, M. (2007). Dermal matrix proteins initiate re-epithelialization but are not sufficient for coordinated epidermal outgrowth in a new fish skin culture model. *Cell Tissue Res.* **327**, 249–265.

Matsuoka, S., Shibata, T. and Ueda, M. (2013). Asymmetric PTEN distribution regulated by spatial

heterogeneity in membrane-binding state transitions. *PLoS Comput. Biol.* **9**, e1002862.

Matsusaka, S. and Wakabayashi, I. (2005). 5-Hydroxytryptamine as a potent migration enhancer of human aortic endothelial cells. *FEBS Lett.* **579**, 6721–6725.

McDonald, T. M., Pascual, A. S., Uppalapati, C. K., Cooper, K. E., Leyva, K. J. and Hull, E. E. (2013). Zebrafish keratocyte explant cultures as a wound healing model system: differential gene expression & morphological changes support epithelial-mesenchymal transition. *Exp. Cell Res.* **319**, 1815–1827.

Merkel, R., Simson, R., Simson, D. A., Hohenadl, M., Boulbitch, A., Wallraff, E. and Sackmann, E. (2000). A micromechanic study of cell polarity and plasma membrane cell body coupling in *Dictyostelium*. *Biophys. J.* **79**, 707–719.

Miyoshi, H. and Adachi, T. (2012). Spatiotemporal coordinated hierarchical properties of cellular protrusion revealed by multiscale analysis. *Integr. Biol. Quant. Biosci. Nano Macro* **4**, 875–888.

Mizuno, T. and Sekiguchi, Y. (2011). Staurosporine induces lamellipodial widening in locomoting fish keratocytes by abolishing the gradient from radial extension of leading edge. *Biophys. Nagoya-Shi Jpn.* **7**, 69–75.

Mogilner, A. and Oster, G. (1996). Cell motility driven by actin polymerization. *Biophys. J.* **71**, 3030–3045.

Mohammed, D., Versaevel, M., Bruyère, C., Alaimo, L., Luciano, M., Vercruysse, E., Procès, A. and Gabriele, S. (2019a). Innovative tools for mechanobiology: Unraveling outside-in and inside-out mechanotransduction. *Front. Bioeng. Biotechnol.* **7**,.

Mohammed, D., Charras, G., Vercruysse, E., Versaevel, M., Lantoine, J., Alaimo, A., Bruyere, C., Luciano, M., Glinel, K., Delhaye, G., et al. (2019b). Substrate area confinement is a key determinant of cell velocity in collective migration. *Nat. Phys.* **15**, 858.

Morin, T. R., Ghassem-Zadeh, S. A. and Lee, J. (2014). Traction force microscopy in rapidly moving cells reveals separate roles for ROCK and MLCK in the mechanics of retraction. *Exp. Cell Res.* **326**, 280–294.

Morioka, M., Parameswaran, H., Naruse, K., Kondo, M., Sokabe, M., Hasegawa, Y., Suki, B. and Ito, S. (2011). Microtubule dynamics regulate cyclic stretch-induced cell alignment in human airway smooth muscle cells. *PLOS ONE* **6**, e26384.

Morita, T., Tsuchiya, A. and Sugimoto, M. (2011). Myosin II activity is required for functional leading-edge cells and closure of epidermal sheets in fish skin ex vivo. *Cell Tissue Res.* **345**, 379–390.

Munevar, S., Wang, Y. and Dembo, M. (2001). Traction force microscopy of migrating normal and H-ras transformed 3T3 fibroblasts. *Biophys. J.* **80**, 1744–1757.

Nakashima, H., Okimura, C. and Iwadate, Y. (2015). The molecular dynamics of crawling migration in microtubule-disrupted keratocytes. *Biophys. Physicobiology* **12**, 21–29.

Nakata, T., Okimura, C., Mizuno, T. and Iwadate, Y. (2016). The role of stress fibers in the shape determination mechanism of fish keratocytes. *Biophys. J.* **110**, 481–492.

Naruse, K., Yamada, T. and Sokabe, M. (1998a). Involvement of SA channels in orienting response

of cultured endothelial cells to cyclic stretch. *Am. J. Physiol. - Heart Circ. Physiol.* **274**, H1532–H1538.

Naruse, K., Yamada, T. and Sokabe, M. (1998b). Involvement of SA channels of cultured endothelial cells. *Am. J. Physiol. - Heart Circ. Physiol.* **274**, H1532–H1538.

Naruse, K., Yamada, T., Sai, X. R., Hamaguchi, M. and Sokabe, M. (1998c). Pp125FAK is required for stretch dependent morphological response of endothelial cells. *Oncogene* **17**, 455–463.

Ni, Y. and Chiang, M. Y. M. (2007). Cell morphology and migration linked to substrate rigidity. *Soft Matter* **3**, 1285–1292.

Nichols, J. M., Veltman, D. and Kay, R. R. (2015). Chemotaxis of a model organism: progress with *Dictyostelium*. *Curr. Opin. Cell Biol.* **36**, 7–12.

Nishikawa, M., Hörning, M., Ueda, M. and Shibata, T. (2014). Excitable signal transduction induces both spontaneous and directional cell asymmetries in the phosphatidylinositol lipid signaling system for eukaryotic chemotaxis. *Biophys. J.* **106**, 723–734.

Okeyo, K. O., Adachi, T., Sunaga, J. and Hojo, M. (2009). Actomyosin contractility spatiotemporally regulates actin network dynamics in migrating cells. *J. Biomech.* **42**, 2540–2548.

Okimura, C. and Iwadate, Y. (2016). Hybrid mechanosensing system to generate the polarity needed for migration in fish keratocytes. *Cell Adhes. Migr.* **10**, 406–418.

Okimura, C. and Iwadate, Y. (2017). Directional Cell Migration in Response to Repeated Substratum Stretching. *J. Phys. Soc. Jpn.* **86**, 101002.

Okimura, C., Ueda, K., Sakumura, Y. and Iwadate, Y. (2016). Fast-crawling cell types migrate to avoid the direction of periodic substratum stretching. *Cell Adhes. Migr.* **10**, 331–341.

Pang, K. M., Lee, E. and Knecht, D. A. (1998). Use of a fusion protein between GFP and an actin-binding domain to visualize transient filamentous-actin structures. *Curr. Biol.* **8**, 405–408.

Parent, C. A. (2004). Making all the right moves: Chemotaxis in neutrophils and *Dictyostelium*. *Curr. Opin. Cell Biol.* **16**, 4–13.

Parsons, J. T., Horwitz, A. R. and Schwartz, M. A. (2010). Cell adhesion: integrating cytoskeletal dynamics and cellular tension. *Nat. Rev. Mol. Cell Biol.* **11**, 633–643.

Pellegrin, S. and Mellor, H. (2007). Actin stress fibres. *J. Cell Sci.* **120**, 3491–3499.

Pittenger, M. F., Mackay, A. M., Beck, S. C., Jaiswal, R. K., Douglas, R., Mosca, J. D., Moorman, M. A., Simonetti, D. W., Craig, S. and Marshak, D. R. (1999). Multilineage Potential of Adult Human Mesenchymal Stem Cells. *Science* **284**, 143–147.

Plotnikov, S. V., Pasapera, A. M., Sabass, B. and Waterman, C. M. (2012). Force fluctuations within focal adhesions mediate ECM-rigidity sensing to guide directed cell migration. *Cell* **151**, 1513–1527.

Pollard, T. D. and Borisy, G. G. (2003). Cellular motility driven by assembly and disassembly of actin filaments. *Cell* **112**, 453–465.

Pomorski, P., Krzemiński, P., Wasik, A., Wierzbicka, K., Barańska, J. and Kłopocka, W. (2007). Actin dynamics in *Amoeba proteus* motility. *Protoplasma* **231**, 31–41.

Popescu, G., Ikeda, T., Goda, K., Best-Popescu, C. A., Laposata, M., Manley, S., Dasari, R.

R.,Badizadegan, K. and Feld, M. S. (2006). Optical measurement of cell membrane tension. *Phys. Rev. Lett.* **97**, 218101.

Raab, M., Swift, J., Dingal, P. C. D. P., Shah, P., Shin, J.-W. and Discher, D. E. (2012). Crawling from soft to stiff matrix polarizes the cytoskeleton and phosphoregulates myosin-II heavy chain. *J. Cell Biol.* **199**, 669–683.

Raftopoulou, M. and Hall, A. (2004). Cell migration: Rho GTPases lead the way. *Dev. Biol.* **265**, 23–32.

Rapanan, J. L., Cooper, K. E., Leyva, K. J. and Hull, E. E. (2014). Collective cell migration of primary zebrafish keratocytes. *Exp. Cell Res.* **326**, 155–165.

Rapanan, J. L., Pascual, A. S., Uppalapati, C. K., Cooper, K. E., Leyva, K. J. and Hull, E. E. (2015). Zebrafish keratocyte explants to study collective cell migration and reepithelialization in cutaneous wound healing. *J. Vis. Exp. JoVE*.

Ream, R. A., Theriot, J. A. and Somero, G. N. (2003). Influences of thermal acclimation and acute temperature change on the motility of epithelial wound-healing cells (keratocytes) of tropical, temperate and Antarctic fish. *J. Exp. Biol.* **206**, 4539–4551.

Reid, B., Song, B., McCaig, C. D. and Zhao, M. (2005). Wound healing in rat cornea: the role of electric currents. *FASEB J.* **19**, 379–386.

Reinhart-King, C. A., Dembo, M. and Hammer, D. A. (2003). Endothelial Cell Traction Forces on RGD-Derivatized Polyacrylamide Substrata. *Langmuir* **19**, 1573–1579.

Ren, Y., Effler, J. C., Norstrom, M., Luo, T., Firtel, R. A., Iglesias, P. A., Rock, R. S. and Robinson, D. N. (2009). Mechanosensing through cooperative interactions between myosin II and the actin crosslinker cortexillin I. *Curr. Biol.* **19**, 1421–1428.

Ridley, A. J., Schwartz, M. A., Burridge, K., Firtel, R. A., Ginsberg, M. H., Borisy, G., Parsons, J. T. and Horwitz, A. R. (2003). Cell migration: Integrating signals from front to back. *Science* **302**, 1704–1709.

Roy, P., Rajfur, Z., Jones, D., Marriott, G., Loew, L. and Jacobson, K. (2001). Local photorelease of caged thymosin β4 in locomoting keratocytes causes cell turning. *J. Cell Biol.* **153**, 1035–1048.

Ruppel, K. M. and Spudich, J. A. (1996). Structure-function studies of the myosin motor domain: Importance of the 50-kDa cleft. *Mol. Biol. Cell* **7**, 1123–1136.

Ruppel, K. M., Uyeda, T. Q. and Spudich, J. A. (1994). Role of highly conserved lysine 130 of myosin motor domain. In vivo and in vitro characterization of site specifically mutated myosin. *J. Biol. Chem.* **269**, 18773–18780.

Sasaki, A. T., Janetopoulos, C., Lee, S., Charest, P. G., Takeda, K., Sundheimer, L. W., Meili, R., Devreotes, P. N. and Firtel, R. A. (2007). G protein-independent Ras/PI3K/F-actin circuit regulates basic cell motility. *J. Cell Biol.* **178**, 185–191.

Sato, K., Adachi, T., Matsuo, M. and Tomita, Y. (2005). Quantitative evaluation of threshold fiber strain that induces reorganization of cytoskeletal actin fiber structure in osteoblastic cells. *J. Biomech.* **38**, 1895–1901.

Sato, K., Kamada, S. and Minami, K. (2010). Development of microstretching device to evaluate cell

membrane strain field around sensing point of mechanical stimuli. *Int. J. Mech. Sci.* **52**, 251–256.

Sawada, Y., Tamada, M., Dubin-Thaler, B. J., Cherniavskaya, O., Sakai, R., Tanaka, S. and Sheetz, M. P. (2006). Force sensing by mechanical extension of the Src family kinase substrate p130Cas. *Cell* **127**, 1015–1026.

Schiffhauer, E. S., Luo, T., Mohan, K., Srivastava, V., Qian, X., Griffis, E. R., Iglesias, P. A. and Robinson, D. N. (2016). Mechanoaccumulative elements of the mammalian actin cytoskeleton. *Curr. Biol.* **26**, 1473–1479.

Schiffhauer, E. S., Ren, Y., Iglesias, V. A., Kothari, P., Iglesias, P. A. and Robinson, D. N. (2019). Myosin IIB assembly state determines its mechanosensitive dynamics. *J. Cell Biol.* **218**, 895–908.

Shibata, T., Nishikawa, M., Matsuoka, S. and Ueda, M. (2013). Intracellular encoding of spatiotemporal guidance cues in a self-organizing signaling system for chemotaxis in *Dictyostelium* cells. *Biophys. J.* **105**, 2199–2209.

Shin, M. E., He, Y., Li, D., Na, S., Chowdhury, F., Poh, Y.-C., Collin, O., Su, P., Lanerolle, P. de, Schwartz, M. A., et al. (2010). Spatiotemporal organization, regulation, and functions of tractions during neutrophil chemotaxis. *Blood* **116**, 3297–3310.

Small, J. V., Herzog, M. and Anderson, K. (1995). Actin filament organization in the fish keratocyte lamellipodium. *J. Cell Biol.* **129**, 1275–1286.

Smirnov, A. V., Nassonova, E. S., Chao, E. and Cavalier-Smith, T. (2007). Phylogeny, Evolution, and Taxonomy of Vannellid Amoebae. *Protist* **158**, 295–324.

Smirnov, A. V., Bondarenko, N., Glotova, A. and Nassonova, E. (2016). Morphology and phylogeny of *Vannella croatica* n. sp. (Amoebozoa, Discosea, Vannellida). *Eur. J. Protistol.* **52**, 65–72.

Sonoda, A., Okimura, C. and Iwadate, Y. (2016). Shape and area of keratocytes are related to the distribution and magnitude of their traction forces. *Cell Struct. Funct.* **41**, 33–43.

Sowers, A. E. (1984). Characterization of electric field-induced fusion in erythrocyte ghost membranes. *J. Cell Biol.* **99**, 1989–1996.

Stockem, W., Hoffmann, H.-U. and Gawlitta, W. (1982). Spatial organization and fine structure of the cortical filament layer in normal locomoting *Amoeba proteus*. *Cell Tissue Res.* **221**, 505–519.

Stroka, K. M. and Konstantopoulos, K. (2014). Physical biology in cancer. 4. Physical cues guide tumor cell adhesion and migration. *Am. J. Physiol. - Cell Physiol.* **306**, C98–C109.

Sun, Z., Guo, S. S. and Fässler, R. (2016). Integrin-mediated mechanotransduction. *J. Cell Biol.* **215**, 445–456.

Svitkina, T. M., Verkhovsky, A. B., McQuade, K. M. and Borisy, G. G. (1997). Analysis of the actin–myosin II system in fish epidermal keratocytes: Mechanism of cell body translocation. *J. Cell Biol.* **139**, 397–415.

Takao, D., Taniguchi, A., Takeda, T., Sonobe, S. and Nonaka, S. (2012). High-speed imaging of amoeboid movements using light-sheet microscopy. *PLOS ONE* **7**, e50846.

Tanimoto, H. and Sano, M. (2014). A simple force-motion relation for migrating cells revealed by multipole analysis of traction stress. *Biophys. J.* **106**, 16–25.

Tarantola, M., Bae, A., Fuller, D., Bodenschatz, E., Rappel, W.-J. and Loomis, W. F. (2014). Cell

substratum adhesion during early development of Dictyostelium discoideum. *PloS One* **9**, e106574.

Tee, Y. H., Shemesh, T., Thiagarajan, V., Hariadi, R. F., Anderson, K. L., Page, C., Volkmann, N., Hanein, D., Sivaramakrishnan, S., Kozlov, M. M., et al. (2015). Cellular chirality arising from the self-organization of the actin cytoskeleton. *Nat. Cell Biol.* **17**, 445–457.

Theriot, J. A. and Mitchison, T. J. (1991). Actin microfilament dynamics in locomoting cells. *Nature* **352**, 126–131.

Titus, M. A. (2017). Growing, splitting and stacking myosin II filaments. *Nat. Cell Biol.* **19**, 77–79.

Tondon, A., Hsu, H.-J. and Kaunas, R. (2012). Dependence of cyclic stretch-induced stress fiber reorientation on stretch waveform. *J. Biomech.* **45**, 728–735.

Torres, M. and Coates, T. D. (1999). Function of the cytoskeleton in human neutrophils and methods for evaluation. *J. Immunol. Methods* **232**, 89–109.

Trichet, L., Le Digabel, J., Hawkins, R. J., Vedula, S. R. K., Gupta, M., Ribrault, C., Hersen, P., Voituriez, R. and Ladoux, B. (2012). Evidence of a large-scale mechanosensing mechanism for cellular adaptation to substrate stiffness. *Proc. Natl. Acad. Sci. U. S. A.* **109**, 6933–6938.

Tse, J. R. and Engler, A. J. (2011). Stiffness gradients mimicking in vivo tissue variation regulate mesenchymal stem cell fate. *PloS One* **6**, e15978.

Tsugiyama, H., Okimura, C., Mizuno, T. and Iwadate, Y. (2013). Electroporation of adherent cells with low sample volumes on a microscope stage. *J. Exp. Biol.* **216**, 3591–3598.

Tsujioka, M., Yumura, S., Inouye, K., Patel, H., Ueda, M. and Yonemura, S. (2012). Talin couples the actomyosin cortex to the plasma membrane during rear retraction and cytokinesis. *Proc. Natl. Acad. Sci. U. S. A.* **109**, 12992–12997.

Ueki, A. and Kidoaki, S. (2015). Manipulation of cell mechanotaxis by designing curvature of the elasticity boundary on hydrogel matrix. *Biomaterials* **41**, 45–52.

Uyeda, T. Q. P., Iwadate, Y., Umeki, N., Nagasaki, A. and Yumura, S. (2011). Stretching actin filaments within cells enhances their affinity for the myosin II motor domain. *PLOS ONE* **6**, e26200.

Van Haastert, P. J. M. and Devreotes, P. N. (2004). Chemotaxis: signalling the way forward. *Nat. Rev. Mol. Cell Biol.* **5**, 626–634.

Vargas, P., Barbier, L., Sáez, P. J. and Piel, M. (2017). Mechanisms for fast cell migration in complex environments. *Curr. Opin. Cell Biol.* **48**, 72–78.

Verkhovsky, A. B., Svitkina, T. M. and Borisy, G. G. (1999). Self-polarization and directional motility of cytoplasm. *Curr. Biol.* **9**, 11-S1.

Vicente-Manzanares, M. (2013). Cell migration: cooperation between myosin II isoforms in durotaxis. *Curr. Biol.* **23**, R28–R29.

Vincent, L. G., Choi, Y. S., Alonso-Latorre, B., Álamo, D., C, J. and Engler, A. J. (2013). Mesenchymal stem cell durotaxis depends on substrate stiffness gradient strength. *Biotech J* **8**, 472–484.

Vogel, V. and Sheetz, M. (2006). Local force and geometry sensing regulate cell functions. *Nat. Rev. Mol. Cell Biol.* **7**, 265–275.

Wang, Y.-L. (1985). Exchange of actin subunits at the leading edge of living fibroblasts: Possible role

of treadmilling. *J. Cell Biol.* **101**, 597–602.

Wang, Y.-L. and Discher, D. E. (2007). *Cell Mechanics*. Academic Press.

Wang, H.-B., Dembo, M., Hanks, S. K. and Wang, Y.-L. (2001). Focal adhesion kinase is involved in mechanosensing during fibroblast migration. *Proc. Natl. Acad. Sci. U. S. A.* **98**, 11295–11300.

Wang, M.-J., Artemenko, Y., Cai, W.-J., Iglesias, P. A. and Devreotes, P. N. (2014). The directional response of chemotactic cells depends on a balance between cytoskeletal architecture and the external gradient. *Cell Rep.* **9**, 1110–1121.

Watanabe, N. and Mitchison, T. J. (2002). Single-molecule speckle analysis of actin filament turnover in lamellipodia. *Science* **295**, 1083–1086.

Weninger, W., Biro, M. and Jain, R. (2014). Leukocyte migration in the interstitial space of non-lymphoid organs. *Nat. Rev. Immunol.* **14**, 232–246.

Wessels, D., Soll, D. R., Knecht, D., Loomis, W. F., De, L. and Spudich, J. (1988). Cell motility and chemotaxis in *Dictyostelium* amebae lacking myosin heavy chain. *Dev. Biol.* **128**, 164–177.

Wilson, C. A., Tsuchida, M. A., Allen, G. M., Barnhart, E. L., Applegate, K. T., Yam, P. T., Ji, L., Keren, K., Danuser, G. and Theriot, J. A. (2010). Myosin II contributes to cell-scale actin network treadmilling through network disassembly. *Nature* **465**, 373–377.

Wong, J. Y., Velasco, A., Rajagopalan, P. and Pham, Q. (2003). Directed movement of vascular smooth muscle cells on gradient-compliant hydrogels. *Langmuir* **19**, 1908–1913.

Wu, J., Pipathsouk, A., Keizer-Gunnink, A., Fusetti, F., Alkema, W., Liu, S., Altschuler, S., Wu, L., Kortholt, A., Weiner, O. D., et al. (2015). Homer3 regulates the establishment of neutrophil polarity. *Mol. Biol. Cell* **26**, 1629–1639.

Xu, J., Wang, F., Van Keymeulen, A., Herzmark, P., Straight, A., Kelly, K., Takuwa, Y., Sugimoto, N., Mitchison, T. and Bourne, H. R. (2003). Divergent signals and cytoskeletal assemblies regulate self-organizing polarity in neutrophils. *Cell* **114**, 201–214.

Yam, P. T., Wilson, C. A., Ji, L., Hebert, B., Barnhart, E. L., Dye, N. A., Wiseman, P. W., Danuser, G. and Theriot, J. A. (2007). Actin–myosin network reorganization breaks symmetry at the cell rear to spontaneously initiate polarized cell motility. *J. Cell Biol.* **178**, 1207–1221.

Yang, T. D., Park, J.-S., Choi, Y., Choi, W., Ko, T.-W. and Lee, K. J. (2011). Zigzag turning preference of freely crawling cells. *PloS One* **6**, e20255.

Yumura, S. and Uyeda, T. Q. P. (1997). Transport of myosin II to the equatorial region without its own motor activity in mitotic *Dictyostelium* cells. *Mol. Biol. Cell* **8**, 2089–2099.

Zhao, M., Song, B., Pu, J., Wada, T., Reid, B., Tai, G., Wang, F., Guo, A., Walczysko, P., Gu, Y., et al. (2006). Electrical signals control wound healing through phosphatidylinositol-3-OH kinase-γ and PTEN. *Nature* **442**, 457–460.

Zhao, L., Sang, C., Yang, C. and Zhuang, F. (2011). Effects of stress fiber contractility on uniaxial stretch guiding mitosis orientation and stress fiber alignment. *J. Biomech.* **44**, 2388–2394.

早稲田大学　博士（理学）　学位申請　研究業績書

氏 名　　沖村　千夏　　印

（2019 年　10 月　現在）

種 類 別	題名、　発表・発行掲載誌名、　発表・発行年月、　連名者（申請者含む）
論文	○**Okimura, C.**, Taniguchi, A., Nonaka, S. and Iwadate, Y. (2018). Rotation of stress fibers as a single wheel in migrating fish keratocytes. ***Scientific Reports*** *8: 10615.* ○**Okimura, C.**, Sakumura, Y., Shimabukuro, K. and Iwadate, Y. (2018). Sensing of substrate rigidity and directional migration by fast-crawling cells. ***Physical Review E*** *97: 052401.* ○**Okimura, C.** and Iwadate, Y. (2016). Hybrid mechanosensing system to generate the polarity needed for migration in fish keratocytes. ***Cell Adhesion & Migration*** *10: 406-418.* ○**Okimura, C.**, Ueda, K., Sakumura, Y. and Iwadate, Y. (2016). Fast-crawling cell types migrate to avoid the direction of periodic substrate stretching. ***Cell Adhesion & Migration*** *10: 331-341.* ○Iwadate, Y., **Okimura, C.**, Sato, K., Nakashima, Y., Tsujioka, M. and Minami, K. (2013). Myosin-II-mediated directional migration of *Dictyostelium* cells in response to cyclic stretching of substrate. ***Biophysical Journal*** *104: 748-758.*
総説	**Okimura, C.** and Iwadate, Y. (2017). Directional cell migration in response to repeated substrate stretching. ***Journal of the Physical Society of Japan*** *86: 101002*.
講演 （演者に*）	（国際会議） ***Okimura, C.**, Taniguchi, A., Nonaka, S. and Iwadate, Y. A role of stress fibers in crawling migration of fish keratocytes. International Symposium on Fluctuation and Structure out of Equilibrium 2017. 2017 年 11 月 20 日-23 日 Sendai International Center. ***Okimura, C.** and Iwadate, Y. Control of directional migration of fast-crawling cells by the cyclic force application from the substrate. The 22nd International Congress of Zoology. 2016 年 11 月 14 日-18 日　Okinawa Institute of Science and Technology Graduate University. **Okimura, C.**, Ueda, K., Sakumura, Y. and *Iwadate, Y. Directional migration of neutrophil-like HL-60 cells by cyclic substrate stretching. International Symposium on Fluctuation and Structure out of Equilibrium 2015. 2015 年 8 月 20 日-23 日 Inamori Hall, Kyoto University. （招待講演） ***沖村千夏,** 魚類表皮の遊走細胞ケラトサイトのストレスファイバ車輪の回転　第５７回生物物理学会年会シンポジウム「生体運動の多様性と普遍性–細胞内ダイナミクスから集団運動まで–」2019 年 9 月 24 日-26 日　宮崎県シーガイア　コンベンションセンター

早稲田大学　博士（理学）　学位申請　研究業績書

種 類 別	題名、　　発表・発行掲載誌名、　　発表・発行年月、　　連名者（申請者含む）
	沖村千夏, 谷口篤史, 野中茂紀, *岩楯好昭. 魚類表皮の遊走細胞ケラトサイトの車輪 第６９回日本細胞生物学会大会シンポジウム「先端イメージングが解き明かす新しい細胞像」2017 年 6 月 13 日-15 日　仙台国際センター *Iwadate, Y., **Okimura, C.**, Mizuno, T. and Sakumura, Y. Directional migration of fast-crawling cells in response to cyclic stretching of substrate. Symposium on “Cell Proliferation, Differentiation, Migration, and Death” at International Symposium on Mechanobiology 2014　2014 年 5 月 20 日-23 日　岡山大学　（国際会議） *Sakumura, Y., **Okimura, C**. and Iwadate, Y. Computational model of directional migration of crawling cell on anisotropic substrate. Symposium on “Cell Proliferation, Differentiation, Migration, and Death” at International Symposium on Mechanobiology 2014　2014 年 5 月 20 日-23 日　岡山大学　（国際会議） *岩楯好昭, **沖村千夏**，佐藤克也，中島雄太，南和幸，水野敬文，作村諭一　細胞の基質牽引力に基づくアメーバ運動の前後極性　第３６回日本分子生物学会 ワークショップ：新しいメカノバイオロジーを目指す工学と生物学の融合　2013 年 12 月 3 日-6 日　神戸国際会議場　（国際会議）
その他	（論文） Sonoda, A., **Okimura, C.** and Iwadate, Y. (2016). Shape and area of keratocytes are related to the distribution and magnitude of their traction forces. ***Cell Structure and Function*** *41: 33-43.* Nakata, T., **Okimura, C.**, Mizuno, T. and Iwadate, Y. (2016). The role of stress fibers in the shape determination mechanism of fish keratocytes. ***Biophysical Journal*** *110: 481-492.* Nakashima, H., **Okimura, C.** and Iwadate, Y. (2015). The molecular dynamics of crawling migration in microtubule-disrupted keratocytes. ***Biophysics and Physicobiology*** *12: 21-29.* Tsugiyama, H., **Okimura, C.**, Mizuno, T. and Iwadate, Y. (2013). Electroporation of adherent cells with low sample volumes on a microscope stage. ***Journal of Experimental Biology*** *216: 3591-3598.* （日本語総説） **沖村千夏**, 谷口篤史, 野中茂紀, 岩楯好昭.（2019）車輪細胞見つけた！生物物理 Vol.59 No.2（通巻 342 号） （新聞掲載） **Okimura, C.** et. al. (2018) ***Scientific Reports*** *8: 10615.* の内容　2018 年 7 月 18 日 朝日新聞, 共同通信社, 日刊工業新聞 他, 2018 年 7 月 19 日 日経産業, 2018 年 9 月 14 日 文教速報